Summer 8-19-2016

The Pathogenesis of Natural Killer/T Cell Lymphoma

Bei Jiang
University of Nebraska Medical Center

THE PATHOGENESIS OF NATURAL KILLER/T CELL LYMPHOMA

By

Bei Jiang

A DISSERTATION

Presented to the Faculty of

The Graduate College in the University of Nebraska

In Partial Fulfillment of the Requirements

For the Degree of Doctor of Philosophy

Pathology & Microbiology Graduate Program

Under the Supervision of Professor Wing-Chung (John) Chan and Professor Kai Fu

University of Nebraska Medical Center

Omaha, Nebraska

May, 2016

Supervisory Committee:

Runqing Lu, Ph.D. Samuel J. Pirruccello, M.D. Kay-Uwe Wagner, Ph.D.

Acknowledgment

I would first like to acknowledge my advisor Dr. John Chan for continual support and guidance during my Ph.D. study. He has inspired me to think as a clinician and solve problems in a scientific way. His enthusiasm for research has always motivated me. I would like to extend special thanks to Dr. Kai Fu for advising me and arranging animal protocol changes after Dr. Chan moved to California, so that I could continue my study in Omaha. I would like to thank Dr. Timothy W. McKeithan for sharing his knowledge, insight and experience throughout my project, and also the joy we had as friends. I am especially grateful to Dr. Can Küçük and Dr. Xiaozhou Hu, as we worked as team and family together for 4 years. I also thank Dr. Chao Wang for being my best friend and lab mate during my entire graduate study. I would also like to thank the rest of my committee Dr, Runqing Lu, Dr. Samuel J. Pirruccello and Dr. Kay-Uwe Wagner for their valuable time and suggestions. I would like to thank every member in Dr. Chan's labpratory for making the lab a wonderful place to work every day.

I would like to thank my grandparents Xiuwen and Yongtao, who raised me and helped me realize the value of my life. I would like to thank my parents Wei and Huaizhou, who made me brave and independent. They have always believed in me and gave me tremendous support so that I could always pursuit my dream without worrying about anything. I would like to thank my friend Tony and his family Grace, Nancy and Tony, Sr who treated me like their family and help me adapt to the life in United States. I thank my friend Mike for always being there when I needed him and for helping me go though my bad days with his humor.

Molecular pathogenesis of natural killer/T-cell lymphomas

Bei Jiang, Ph.D.

University of Nebraska Medical Center, 2016

Supervisor: Wing-Chung (John) Chan, MD and Kai Fu, M.D., Ph.D.

Extranodal natural killer/T-cell lymphomas (NKTCL) are uncommon lymphomas with poor prognosis. In order to gain a better understanding of the molecular pathogenesis of NKTCL, we obtained and compared the global gene expression profile, global somatic mutation profile, and global methylation profile of normal NK cells, malignant NK cell lines, and NKTCL patient samples. We showed that the JAK-STAT pathway was constitutively activated in NKTCL through the cooperation between activation of signal transducer and activator of transcription proteins (STATs) via activating mutations and inactivation of STAT suppressor protein suppressor of cytokine signaling 6 (SOCS6) through promoter hypermethylation. Activating STAT3 and STAT5B mutations are associated with increased phosphorylated protein and a growth advantage to transduced cell lines or normal NK cells. Growth-promoting activity of the mutants can be partially inhibited by a JAK1/2 inhibitor or by expressing exogenous SOCS6. Molecular modelling and surface plasmon resonance measurements of the N642H STAT5B mutant indicate a marked increase in binding affinity of the phosphotyrosine-Y699 with the mutant protein. This is associated with the prolonged persistence of the mutant phosphoSTAT5B and marked increase of binding to target sites. We also showed that Blimp1, a tumor suppressor gene frequently inactivated in NKTCL by the combination of allelic deletion and promoter hypermethylation, has an effect on NK cell homeostasis, maturation and function using a NK-lineage specific Blimp1-knockout mouse model. Blimp1 knockout mice had a lower percentage of NK cells in peripheral lymphoid sites, such as spleen and peripheral blood, and higher percentage of NK cells in bone marrow when compared to wild-type mice. The maturation of NK cells was partially impaired in Blimp1

knockout mice. However, Blimp1-deficient NK cells proliferated better upon stimulation in vitro and in vivo, and had a potent cytotoxic ability. Together, these findings suggest potential pathways for therapeutic targeting in NKTCL patients.

List of figures

List of tables

List of abbreviations

6TM	Six-transmembrane domain
ABC-DLBCL	Activated B-cell type diffuse large B-cell lymphoma
aCGH	Array-comparative genomic hybridization
ADCC	Antibody-dependent cellular cytotoxicity
ANKL	Aggressive NK-cell leukemia
ANKL	Aggressive NK cell leukemia
AP1	Activating protein 1
APC	Antigen present cells
BCL6	B-cell lymphoma 6
Blimp1	Lymphocyte-induced maturation protein 1
CDS	Coding sequence
CFSE	Carboxyfluorescein succinimidyl ester
CGI	CpG island
Chip-q-PCR	Chromatin Immunoprecipitation quantitative PCR
CLP	Common lymphoid progenitor
CNA	Copy number alteration
DLBCL	Diffuse large B-cell lymphoma
DMEM	Dulbecco’s Modified Eagle Medium
EATL	Enteropathy associated T-cell lymphoma

EBV	Epstein–Barr virus
EDTA	Ethylenediaminetetraacetic acid
FACS	Fluorescence-activated cell sorting
FOXO1A	Forkhead box protein O1A
GEP	Gene expression profile
GFP	Green fluorescent protein
HMB-PP	(E)-4-hydroxy-3-methyl-but-2-enyl diphosphate
HS - γδ-PTCL	Hepatosplenic γδ -T cell lymphoma
IELs	Intraepithelial lymphocytes
IFN	Interferon
IL	Interleukin
IL2RB	IL2 receptor beta chain
IPP	Isopentenyl diphosphate
ITIM	Immunoreceptor tyrosin-based inhibitory motif
KIRs	Killer cell immunoglobulin-like receptors
LGL	Large granular leukemia
Lmp1	Latent membrane protein 1
Mac-1	Macrophage-1 antigen
MALT	Mucosa-associated lymphoid tissue
MAP2K4	Mitogen-activated protein kinase kinase 4

MEITL	Monomorphic epitheliotropic intestinal T-cell lymphoma
MHC	Major histocompatibility complex
MSCC	Methylation-sensitive cut counting
MSP	Methylation-specific PCR
MYC	Avian myelocytomatosis viral oncogene homolog
NFAT	Nuclear factor of activated T-cells
NF-Kb	Nuclear factor-κB
NKPs	NK cell progenitors
NKTCL	Extranodal natural killer/T-cell lymphomas
PAX5	Paired box 5
PB	Peripheral blood
PBL	Peripheral blood lymphocyte
PBMCs	Peripheral blood mononuclear cells
PBS	Phosphate buffered saline
PCR	Polymerase chain reaction
PDGFR	Platelet-derived growth factor receptor
PE	Phycoerythrin
PI3K	Phosphoinositide-3-kinase
PIAS	Protein inhibitor of activated stats
PolyIC	Polyinosinic-polycytidylic acid

PRDM1	PR domain-containing protein 1
PTPs	Protein inhibitor of activated stats
RAG2	Recombination activating gene 2
RIPA	Radioimmunoprecipitation assay buffer
RT-PCR	Reverse-transcriptase-polymerase chain reaction
SDS-PAGE	Sodium dodecyl sulfate polyacrylamide gel electrophoresis
SH2	Src homology 2
SHP1	Src homology region 2 domain-containing phosphatase-1
shRNA	Short hairpin RNA
siRNA	Short interfering RNA
SMILE	Dexamethasone, methotrexate, ifosfamide, l-asparaginase, and etoposide
SOCS	Suppressor of cytokine signaling
SPR	Surface plasmon resonance
STAT	Signal transducer and activator of transcription
TF	Transcription factor
TGF	Transforming growth factor
TSG	Tumor suppressor gene
TSS	Transcription start site
γδ T cells	Gamma delta T cells
γδ-TCL NHS	Non-hepatosplenic γδ -T cell lymphoma

List of Contents

Chapter I

Introduction

NK cell

The lymphocyte is a subtype of white blood cell in a vertebrate's immune system that plays an important role in immunosurveillance. Innate lymphoid cells (ILC) are group of innate immune cells that are derived from the lymphoid lineage but do not respond in an antigen-specific manner, as they lack somatic rearrangement of immunoglobulin and T cell receptor genes. There are three types of ILCs characterized based on cytokine secretion and transcriptional factor expression, NK cells are one of two group 1 ILC described to date. NK cells can kill pathogen-infected cells or malignant cells by releasing cytotoxic molecules such as perforin and granzymes. Upon degranulation, perforin can form pores on the target cell's plasma membrane. Granzymes then enter the target cell through the pore and cleave caspase-3 and Bid, which results in apoptosis (Buzza and Bird, 2006). NK cells can also protect the host by augmenting and recruiting other immune cells via secretion of cytokines, such as TNFα, TNFβ and IFNγ, and chemokines such as MIP-1α, MIP-1β and RANTES (Fauriat et al., 2010).

NK cell anatomical localization and maturation

NK cells localize throughout lymphoid and non-lymphoid tissues. In most tissues, NK cells comprise a small fraction of all lymphocytes (Gregoire et al., 2007). It is believed that NK cells develop from a common lymphoid progenitor (CLP) in the bone marrow(Kondo et al., 2001). However, studies show that NK cells in thymus and secondary lymphoid organs such as lymph nodes, have distinct phenotypic and functional features compared to those in the spleen and peripheral blood. Both CD34+ HPCs and downstream NK cell developmental intermediates have been identified in liver, uterus and mucosa-associated lymphoid tissue (MALT). Taken together, it is commonly accepted that NK cell developmental intermediates originate in the bone marrow then traffic to extramedullary tissues such as lymph nodes, liver, spleen and give

rise to functionally distinct mature NK cell subsets.(Res et al., 1996, Di Santo, 2006). CLPs can differentiate into NK cell progenitors (NKPs), marked by the expression of IL2/IL-15 receptor beta chain (IL2RB), also known as CD122 (Di Santo, 2006). IL-15 selectively promotes NK cell differentiation, proliferation and survival (Becknell and Caligiuri, 2005). The committed NKP then acquires functional receptors in an orderly fashion as they become functionally mature. In mice, NKPs first acquire NK1.1, CD94/NKG2A, and NKp46 followed by Ly49 receptors, DX5, and finally CD43 and Mac-1 (CD11b)(Kim et al., 2002). In human NK cells, receptors are expressed in the following order: CD161, CD56, CD94/NKG2A, NKp46, and NKG2D, killer immunoglobulin-like receptors (KIR) and CD16 (Freud et al., 2006, Perussia et al., 2005). Mature NK cells can be divided into different subsets based on the expression of surface molecules.

In mice, 4 populations of NK cells with different expression of CD11b and CD27 are present. NK cell differentiation is a 4-stage process following $CD11^{low}CD27^{low}$ to $CD11^{low}CD27^{high}$ to $CD11b^{high}CD27^{high}$ cells to the most mature $CD11^{bhigh}CD27^{high}$ cells (Chiossone et al., 2009). $CD11^{low}CD27^{low}$ double negative (DP) NK cells express low levels of NK maturation receptors and are considered to represent immature NK cells in various numbers in different lymphoid sites. $CD11^{low}CD27^{high}$ NK cells are the major NK –cell compartment in fetal and neonatal mice, whereas they are mainly found in bone marrow, lymph nodes and liver in the adult. $CD11^{low}$ NK cells have high proliferation ability compared to $CD11b^{high}$ NK cells. $CD11b^{high}$ NK cells are mostly present in peripheral sites such as peripheral blood, spleen and liver. $CD11b^{high}CD27^{high}$ NK cells have the greatest effector function. $CD11^{bhigh}CD27^{high}$ cells are also mostly found in peripheral sites, but these cells have greater restriction by self MHC (Hayakawa and Smyth, 2006)

In human, two subsets of NK cells are identified by expression of CD56 and CD16. $CD56^{high}$ $CD16^{dim}$ NK cells are the major component of the NK cell population in lymph nodes and tonsil; they secrete large quantities of cytokines upon stimulation, but they have low cytotoxic capacity. $CD56^{dim}CD16^{high}$ NK cells account for around 90% of NK cell population in peripheral blood and spleen. They have high cytotoxic capacity but have relatively lower capacity for cytokine production (Yu et al., 2013). Despite the differences in NK lineage markers between mouse NK cells and human cells, several experiments suggest that $CD56^{high}$ $CD16^{dim}$ human NK cells and $CD11^{low}$ mouse NK cells share similarities in localization (enrichment in lymph nodes), phenotype (expression of early NK markers such as IL7R and lack of effector markers such as Ly49 and KIR) and better proliferation ability.

NK cell activation

NK cells, as a member of the innate immune system, can recognize and kill transformed or virus-infected cells. Unlike cytotoxic T cells, which recognize target cells in a MHC-I-dependent manner, NK cells can response to cells that lack MHC-I through release from inhibitory receptors. Further studies show that besides inhibitory receptors, NK cell also process various activating receptors, and the interplay between inhibitory and activating receptors result in the proper response of NK cells to its targets.

NK cells express a repertoire of inhibitory receptors that have different structures and ligands (Long, 2008), and NK cells are heterogeneous in their expression of inhibitory receptors.The most common inhibitory receptors are belonged to three families: killer cell immunoglobulin-like receptors (KIRs), leukocyte immunoglobulin-like receptors (LILRs) and Ly49. Most KIRs are inhibitory and dominant but some are activating. They are present in human and nonhuman primates and are the main

receptor for MHC I molecules (HLA-A, HLA-B, HLA-C). KIRs are not present in mice, however Ly 49, which also have both activating and inhibitory isoforms, are the functional homologues of KIRs in mice. LILRs are recently discovered receptors, the inhibitory receptors are found on NK cells. KIRs and LILRs belong to the immunoglobulin superfamily which has Ig-like extracellular domains, whereas others, such as Ly49 and CD94-NKG2A receptors have a C-type lectin—like scaffold. The differences in their extracellular domains determin their ligand binding specificity. However, regardless the differences in their extracellular region, all the inhibitory receptors share a common immunoreceptor tyrosin-based inhibitory motif (ITIM) in their intracellular region. The inhibitory MHC I receptor interacts with MHC I molecules constitutively expressed on normal cells and suppress NK cell activation when engaged. Since MHC class I molecules are the main mechanism by which cells display viral or tumor antigens to cytotoxic T cells, some intracellular microbes and tumors cells adapt to downregulate their MHC I molecules on cell surface in order to avoid the killing by T cells. This causes NK cells losing the inhibitory signal and becoming more prone to activation. This "missing-self recognition" mechanism allows NK cells to be tolerant to self while able to kill stressed or infected cells (Yokoyama and Plougastel, 2003)

Unlike T and B cells, instead of having a dominant activation receptor, NK cells process different activating receptors. There are three major activating receptors in both human and mouse NK cells: the ITAM-bearing NK receptors such as CD16 (FCGR3A, which binds to the Fc portion of antibodies and allows NK cells to kill through antibody-dependent cellular cytotoxicity [ADCC]), the DAP10-associated NKG2D receptor, and the CD244 receptor(Moretta et al., 2001). Studies show that none of the activating receptor, except CD16, can activate NK cell alone. Only when the combination of several activating receptors transmit a activating signal that counterbalances the

inhibitory signal from inhibitory receptors, will the NK cell be activated (Lanier, 2008). NK cell's effector functions are also dependent on the cytokine microenvironment and interaction with other cells such as T cells and macrophages. IL-2 and IL15 are potent activators of human and mouse NK cells and have been used for NK cell culture (Sun et al., 2009).

γδT cell

Gamma delta T cells (γδ T cells) are a rare subset of T cells with a TCR composed of a γ chain and a δ chain, in contrast to the mainstream alpha beta T cells (αβ T cells), which have TCRs that is made up of α and β TCR chains. γδ T cells are considered to be a bridge between innate and adaptive immunity in that as they express both natural killer receptors such as NKG2D and γδ T cell receptors (Kong et al., 2009). On one hand, γδ T cells rearrange TCR genes to produce recombinatorial and junctional diversity and develop a memory phenotype as other adaptive immunity cells and interact with T and B cells in the adaptive immune system; on the other hand, they can recognize targets in a MHC-independent manner and they also have phagocytic and cytotoxic functions that are used by NK cells or macrophages in the innate immune system (Wu et al., 2014). Compare to αβ T cells, γδ T cells display more diverse functions. Similar to αβ T cells, they can provide help for B cells(Vantourout and Hayday, 2013), secrete cytokines such as IL10, IL17, IFN-γ and TNFα to activate or recruit other cells and kill malignant cells (Kong et al., 2009). In addition, they can present antigen to αβ T cells as antigen present cells (APC) (Brandes et al., 2005), and they play a role in maintaining epidermal integrity by secreting different kinds of growth factors (Schilbach et al., 2000).

γδ T cells cell anatomical localization and maturation

Both αβ and γδ T cells are developed from double negative (DN) CD3+ T cell precursors in the thymus. γδ T cells are mainly distributed in the skin and gut mucosa, within a population of lymphocytes known as intraepithelial lymphocytes (IELs)(Petermann et al., 2010). In human, there are three major γδ T cell subsets: Vδ1, Vδ2 and Vδ3 T cells. Vδ1 T cells are prominent in the intraepithelial location of mucosal surfaces. They maintain epithelial tissue integrity during damage, infection, or transformation by producing growth factors and cytokines. Vδ2 chain pairs almost exclusively with Vγ9 chain to form Vδ2 γ9 T cells. They comprise up to 50-90% of the peripheral γδ T-cell population and can serve as professional APCs, as they express MHC-II and costimulatory molecules such as CD80 and CD86 upon activation. Vδ3 T cells comprise only 0.2% of circulating T cells, but they are more frequent in patients with leukemia and chronic infections. They can express T cell and NK cell markers such as CD4, CD8, CD56, CD161 and NKG2D.

γδ T cells activation

Some γδ T cells recognize phosphoantigens such as (*E*)-4-hydroxy-3-methyl-but-2-enyl diphosphate (HMB-PP), an immediate upstream metabolite of isopentenyl diphosphate (IPP), in killed microorganisms including bacteria such as *Mycobacterium tuberculosis.* Human cells also produce IPP, but in physiologically concentration it is not sufficient to activate γδ T cells. However, certain tumor cells produce higher concentrations of IPP and activate γδ T cells. Cell-to-cell interaction with APC is required for the binding of γδ TCR and phosphoantigens, but antigen processing and MHC molecules are not required since γδ T cells use their TCR in a pattern recognition manner. Besides TCR signaling, activation of γδ T cells also requires other costimulatory molecules. Three major catergories of costimulatory molecules are used by γδ T cells: immunoglobulin (Ig)

superfamily coreceptors such as CD28, tumor necrosis factor receptor family members such as CD27 and atypical costimulatory molecules such as NKG2D. NKG2D is an important stimulatory molecule in other cytotoxic cells such as CD8+ T cells and NK cells. In γδ T cells, NKG2D can either directly activate γδ T cells, as in NK cells, or act as a co-receptor to the TCR as in $CD8^+$ T cells. Thus, γδ T cells share features and function with both NK cells and CD8+ T cells. This phenomenon is also observed in disease states, as NK/T cell lymphomas are derived from both NK cells and γδ T cells.

Extranodal natural killer/T-cell lymphoma

Extranodal natural killer/T-cell lymphomas (NKTCL) are uncommon lymphomas comprising about 1-2 % of all non-Hodgkin lymphoma (Vanherberghen et al., 2013). This disease has a high incidence in Asian and Central and South America. NKTCL is a group of diseases, caused by clonal proliferation of cytotoxic lymphocytes, with unique clinicopathologic features marked by a predilection to the nasal and paranasal areas with extensive necrosis and angioinvasion. Most of NKTCLs originate from NK cells, and the neoplasm cells are CD2+,CD56+,cCD3e+, CD7+,CD16+/-, cytotoxic granule-associated protein+, but TCR or immunoglobulin gene rearrangements are absent. A small fraction of NKTCL is of □ δT cell origin, and they share very similar clinical and pathological features with the NK cell derived lymphoma. Lesions most often present as tumor or destruction in extranodal sites, classically in nasal and paranasal areas but may also affect the upper respiratory tract, gastrointestinal tract and skin (Aozasa et al., 2008). NKTCL is an aggressive disease with poor prognosis for extranasal disease. Localized nasal and paranasal diseases are highly responsive to radiation therapy and have much better outcome.Traditional CHOP therapy showed little effect on NKTCL,

whereas an L-asparaginase- containing SMILE chemotherapy regimen (dexamethasone, methotrexate, ifosfamide, l-asparaginase, and etoposide) shows much better results (Jaccard et al., 2011). Although progress has been made in combining modified chemotherapy with radiotherapy and autologous bone marrow transplantation, many NKTCLs are not cured. Therefore, it is necessary to investigate the pathogenesis of NKTCL to discover new therapeutic targets.

Pathway alterations observed in NKTCL

NKTCL development is a multifactorial process. The high EBV infection rate and limited geographic distribution of this disease indicate an important role of EBV infection and genetic/environmental factors in the pathogenethsis of NKTCL. In addition, genetic alterations, including the activation of oncogenes and inactivation of tumor suppressor genes also contribute to NK/T cell malignant transformation. In our laboratory and others, studies were conducted at different levels aiming to decipher the genetic alterations in NKTCL. At the chromosome level, genome-wide array-based comparative genomic hybridization (aCGH) was used to identify chromosomal copy number abnormalities such as deletion, amplification and fusion associated with NKTCL. At the DNA level, global somatic mutation profiles are explored commonly by whole-exon sequencing, whereas epigenetic changes such as DNA methylation can be detected by DNA methylation assays. At the RNA level, the gene expression profiles (GEP) of NKTCL were analyzed and compared to those of normal NK cells or other leukemia/lymphoma by microarray-based methods and more recently by RNA-sequencing. However, there is no proteomics study on NKTCL.

Genome-wide profiling studies described above identified several potential molecular pathways that might play an important role in pathogenesis of NKTCL. *Gene*

expression profile studies shown that several pathways such as JAK-STAT, Angiogenesis, platelet-derived growth factor receptor (PDGFR), NOTCH, WNT, and NF*κ*B signaling pathways are activated in NKTCL(Huang et al., 2010, Iqbal et al., Ng et al.). The activation of oncogenic pathways was usually due to activation of oncogens through amplification or activating mutation and/or inactivation of tumor suppressor genes by mechanisms like allele deletion, missense/nonsense mutations or DNA methylation. Some important pathways related to this study are described below.

EBV infection and Lmp1expression

A distinctive feature of NKTCL is the strong association with Epstein–Barr virus infection; EBV is positive in 100% of NKTCL cases by in situ hybridization(Chiang et al., 1996). EBV undergoes latency II infection in NK cells, in which they only express a restricted pattern of viral proteins limiting to EBNA1, LMP1, and LMP2 (Xu et al., 2001). EBNA1 is required for the maintenance of viral episomes and expressed in all latency phases. LMP2B can promote cell proliferation and survival. LMP1 is the main transforming protein of EBV. The N-terminal six-transmembrane domain (6TM) of Lmp1 regulates its own transcription and degradation through its activation of unfolded protein response and autophagy. Its C-terminal domain activate several downstream molecules such as nuclear factor-κB (NF-*κ*B) and activating protein 1 (AP-1) and signal transducer and activator of transcription (STAT) , leading to NK/T-cell activation and proliferation(Chen, 2012).Thus Lmp1 acts like a constitutively activated tumor necrosis factor receptor family member, in fact in B cell Lmp1 can substitute for the signaling of CD40(Graham et al., 2010), another member of TNF family. In vitro study shown that Lmp1 silencing in EBV+ NK cell line resulted in decreased cell proliferation and survival and a reduction in cell invasion and migration, suggesting the oncogenic role of Lmp1 in NKTCL(Sun et al., 2015).

Activation of JAK-STAT pathway

The JAK/STAT pathway is the principal signaling mechanism for a wide array of cytokines and growth factors. To simplify the process, JAK activation occurs opon ligand-mediated receptor dimerization or multimerization which allowed the trans-phosphoralation of JAKs. The activated JAKs subsequently phosphorylate additional target including the major substrate STATs. The phosphotyrosine of STATs permits the dimerization of STATS. The dimerizaed STATs then enter nucleus and binds specific sequence to activate or repress transcription of target gene. In addition to those effectors, there are three major classes of negative regulator: SOCS (suppressor of cytokine signaling), PIAS(protein inhibitor of activated stats) and PTPs(protein tyrosine phosphotases). The SOCSs complete a negative feedback loop in the JAK/STAT circuitry: activated STATs stimulate transcription of the SOCS genes and the resulting SOCS protein bind phosphorylated JAKs and their receptors to turn off the pathway.

Constitutive activation of STAT3 and STAT5 are known to increase tumor cell proliferation, survival and invasion(Yu et al., 2009). Aberrant STAT3 and STAT5B activation were shown in activated B-cell type Diffuse Large B-cell lymphomas (ABC-DLBCL) (Lam et al., 2008) and CD8+ Lymphoblastic Lymphoma (Bessette et al., 2008), respectively. Recently, activating mutations were identified in *STAT3* (Jerez et al., 2012, Koskela et al.) and *STAT5B(Rajala et al.)* in NK-LGL and T-LGL cases suggesting an oncogenic role for these mutations. On the other hand, SOCSs the negative regulator of JAKs are silenced in different tumors. Promoter methylation mediated silencing of *SOCS1* were shown in hepatocellular carcinoma (Yoshikawa et al., 2001) and multiple myeloma(Galm et al., 2003) , *SOCS3* in lung cancer (He et al., 2003) and in myeloproliferative disorders(Fourouclas et al., 2008) and *SOCS6* in gastric cancer(Lai et al.). It is possible that accumulation of the oncogenic mutations and/ or silencing of the

negative regulators in JAK-STAT pathway contribute to the neoplastic transformation of NK cells.

Loss function of Blimp1

According to our study, 6q21 deletion is a frequent chromosomal abnormality observed in 44% of NKCL cases. PR domain zinc finger protein 1 (PRDM1) is an important transcriptional regulator within this deleted region. We later found that PRDM1 was inactivated in NKTCL by the combination of allelic deletion and promoter hypermethylation. Blimp1 is a transcription suppressor; it binds to its target genes in the promoter region though zinc-finger motifs, and suppresses transcription by recruiting proteins such as histonedeacetylase1 and 2, G9a histone methyl transferases that modified histones to create a more inactive structure. PRDM1, also known as B lymphocyte-induced maturation protein 1(Blimp1), has various effects on the function and homeostasis of B cells and T cells(Martins and Calame, 2008). In B cells, Blimp1 is a master regulator of B cell maturation and immunoglobulin secretion(Savitsky and Calame, 2006). In T cells, Blimp1 regulate cell proliferation and effector functions[50,51]. In activation of Blimp1 was observed in several malignancies. Blimp1 was silenced through hypermethylation in EBV-positive Burkitt lymphoma(Zhang et al., 2014), and in another study investigators shown that Blimp1 inactivated by multiple mechanisms, including homozygous deletions, truncating or missense mutations and transcriptional repression by constitutively active BCL6, in difuse large B cell lymphoma(DLBCL) (Mandelbaum et al., 2010). In our previous study, knocking down PRDM1 resulted in a positive selection of NK cells. Whereas ectopic PRDM1 expression in PRDM1-null NK cell lines resulted in G2/M cell cycle arrest, increased apoptosis, and a strong negative selection. These finding, along with the observation that PRDM1 was inactivated in NKTCL, indicated that PRDM1 is a potential tumor suppressor gene in NKTCL.

Aim of the dissertation

In order to gain a better understanding of the molecular pathogenesis of NKTCL, we obtained and compared the global gene expression profile, global somatic mutation profile, and global methylation profile of normal NK cells, malignant NK cell lines as well as NKTCL patients, and identified potential tumor suppresser genes and oncogenes. Our previous GEP study shown JAK-STAT pathway was activated in NKTCL. It is important to investigate the underlining mechanism as this will give us an insight in potential therapeutic targets. This dissertation explores the underline mechanism of constitutive JAK-STAT actication in NKTCL and the effect of JAK-STAT activation on NK cell behaviors. In addition, this study compares the mutation profile of NKTCL and other γδ-T derived lymphoma; this will give us a better understanding of the ambiguous relationship between NK cells and γδ-T. Our previous study shown Blimp1 was frequently inactivated in NKTCL and in vitro experiments in normal malignant human NK cells indicated Blimp1 as a tumor suppressor gene in NKTCL. Explore the role of Blimp1 in NK cells in mouse model will give us a better understanding as how Blimp1 affects NK cells in vivo and whether Blimp1 deletion alone or combine with other oncogenic alternations can lead to malignancies development in vivo.

Group	Cell type	Mediators produced	Function
Group 1 ILCs	NK cell	IFNγ, Perforin, granzymes	Immunity to virus and intracellular pathologens Tumor surveillance
	ILC1	IFNγ	Inflammation?
Group 2 ILC	ILC2	IL5,IL9,IL13 amphiregulin	Immunity to helminthes Wound healing
Group 3 ILCs	LTi cell	IL17,IL22, lymphotoxin	Lymphoid tissue development Intestinal homeostasis Immunity to extracellular bacteria
	Ncr+ ILC3	IL22	Homeostasis of epithelia Immunity to extracellular bacteria
	Ncr-ILC3	IL17, IFNγ	Immunity to extracellular bacteria

Table 1-1: Summary of innate lymphoid cell subsets, mediators production and functions

ILCs are further divided into three groups: group 1 ILCs, group 2 ILCs and group 3 ILCs, based on their ability to produce type 1, type 2 and T_H17 cell-associated cytokines, respectively. LTi: Lymphoid tissue inducer cell

Chapter II

Material and method

Patient samples and cell lines

The phenotypic characteristics of all NKTCL, δγ-PTCL and EATL type II cases (n=94), NK- and δγ T-cell lines (n= 9) used in this study are summarized in Table 2-1 and Table 2-2. Culture conditions of NK and γδ-T cell lines were as described previously(Iqbal et al., 2009, Nagata et al., 2001). The DHL16 cell line was cultured in RPMI-1640 (Gibco-Invitrogen) including 10% FBS; penicillin G (100 units/mL) and streptomycin (100 µg/mL) at 37 °C in 5% CO_2.

DNA and RNA extraction

Extraction and purification of DNA and RNA from tumor cases were performed simultaneously using AllPrep DNA/RNA Mini Kit (Qiagen Inc., Valencia, CA) or ALLPrep DNA/RNA FFPE Kit (Qiagen Inc). Genomic DNA was isolated from NK or γδ T-cell lines using DNeasy Blood and Tissue Kit (Qiagen Inc.).

Whole transcriptome sequencing and data analysis

RNA-sequencing was performed on resting NK cells, NK-cells activated by IL2 or by K562-Clone9-mb21, 17 NKTCL cases and 3 NK-cell lines. Briefly, 100-bp paired-end libraries were prepared with the TrueSeq RNA preparation kit (Illumina Inc., San Diego, CA), and high-throughput sequencing was performed at the UNMC Next Generation Sequencing Core facility and Tufts University (TUCF) Genomics Core Facility using Illumina Genome Analyzer IIX or HiSeq 2000 Sequencing systems. FASTQC reports were evaluated for each sample to evaluate the quality of basic statistics. Two different pipelines were used to generate the SNVs. The main pipeline used for SNV detection was described previously (Schmitz et al., 2012) with the following addition. In addition to the NCBI SNP database (dbSNP) and 1000 Genomes project (Abecasis et al., 2012), three normal NK samples were used to filter out the SNPs. The presence of the SNVs

was evaluated by visualizing the SNVs using Integrative Genomics Viewer software (IGV) (http://www.broadinstitute.org/igv). Finally, the Cosmic release v69 (http://cancer.sanger.ac.uk/cancergenome/projects/cosmic/) was used to annotate the variants observed in previous studies. The secondary pipeline used for SNV detection is as follows: The read were aligned to the human reference genome (NCBI GRCh37) using the BWA aligner(Li and Durbin, 2009) with paired-end (sample) mode and with default options. After merging BAM files, PCR duplications were also removed. Then, GATK tool (DePristo et al., 2011) was used to realign indel-containing reads to the reference genome. After realignment, GATK UnifiedGenotyper was used to generate SNP and indel callsets for 24 (21 malignant and 3 normal NK samples) RNA-Seq samples, using a merged BAM file including all 24 datasets with specific IDs. Variant Quality Score Recalibration filter was applied using the GATK resource bundle 1.2 to help minimize false positives. Then, ANNOVAR tool(Wang et al., 2010), version 2013-02-11, was used to annotate the detected SNPs and indels. For gene and filter annotation, the April 2012 version of the annotation database (hg191000g2012apr) and dbSNP version 137 was used. For comparison against the 1000 Genomes Project, the data 1000g2012apr was used. Lastly, the SNVs present in three normal NK samples were filtered out. The basic statistics of RNA-Seq are shown in Table 2-2. Furthermore, the number of SNVs and their annotations identified by the primary RNA-Seq pipeline for 17 NKTCL cases are shown in Fig. 2-1. The RNA-sequencing data will be deposited into dbGaP (http://www.ncbi.nlm.nih.gov/gap/) database.

Whole exome-sequencing and data analysis

Trueseq DNA library kit (FC-121-2001, Illumina) was used to prepare libraries of a NKTCL case DNA and DNA from the peripheral blood of the same patient. Rapid 100-bp paired-end sequencing was performed with Hiseq2500 (Illumina) at the UNMC Next

Generation Sequencing Core facility. Raw sequencing reads were mapped to the human reference genome hg19 using BWA. GATK was used for local realignment and base quality recalibration. Picard (http://picard.sourceforge.net) was used to mark duplicates. VarScan(Koboldt et al., 2009) called variants for paired NKTCL and the corresponding normal sample. In this study, only *STAT3* and *STAT5B* mutation status was evaluated; the whole sequencing profile will be reported later.

Whole genome amplification

Whole genome amplification (WGA) of the NKTCL (n=20) or γδ-PTCL (n=4) and KAI3 cell line was performed using the Repli-g kit (Qiagen Inc., Valencia, CA). 50 ng of tissue material was used as a template for amplification. The sensitivity of mutation detection was evaluated by applying Sanger sequencing on the G to A mutation detected in the intron4/exon5 splice junction of *PRDM1* detected previously (Fig. 2-2A)(Iqbal et al., 2009). Uniform linear amplification of genomic DNA from each NK sample was tested with PCR, which generated ~ 3 kb amplicons using KAI3 cell line or NKTCL cases (Fig. 2-2B,C).In addition, WGA DNA from NKTCL cases was run on TAE-agarose gels, which showed that WGA DNA contains large fragments (>10kb) (Fig. 2-2D).

Compilation of the list of JAK/STAT pathway genes

The list of genes in the JAK/STAT pathway was compiled using the following resources: 1) The genes screened in NK or T-LGL cases in a recent report (Jerez et. al. *Blood* 2012).2) The JAK-STAT pathway genes defined in Ingeniuty pathway analysis (IPA) program Ingenuity Systems [http:// www.ingeniuty.com], 3) JAK/STAT pathway genes shown in Cell Signaling Technology website (http://www.cellsignal.com/pathways/jak-stat.jsp). 4) The genes shown to play a role in JAK-STAT pathway based on the literature.

Mutation validation by Sanger sequencing

Sanger sequencing was performed on DNA from cryopreserved or FFPE tissues, or cDNA if only RNA was available. Sequencing was focused on the SH2 domain of *STAT3* and *STAT5B* and the previously reported mutation hotspots for *JAK3*. The genomic DNA sequences around the *JAK3* A572V, A573V and V722I SNVs was obtained using UCSC (http: //genome. ucsc. edu/) genome browser. PCR primers covering SNVs were designed with the PrimerQuest software (IDT DNA technologies, Coralville, IA). The primers were optimized with gradient PCR, and the forward and reverse primers used for PCR amplification of WGA or FFPE gDNA or cDNA samples were used for Sanger sequencing. Analysis of the sequences was performed using Vector NTI 10.3.0 (Invitrogen, Carlsbad, CA, USA) and Sequence Scanner Software v1.0 (Applied Biosystems Inc.).

Promoter methylation analysis of SOCS6

Methylation specific cut counting (MSCC) procedure was employed to determine the methylation level of SOCS6 as described earlier (Ball et al., 2009) in NKTCL cases (n= 12) and malignant NK cell lines (n=2). We specifically concentrated on the HpaII sites in the promoter of SOCS6 (+/- 1 kb of TSS) whereas the complete methylation profile by MSCC will be published later. The library preparation and high throughput sequencing was performed at the epigenetic core facility by Illumina Genome Analyzer II X. R program scripts (http://www.R-project.org) were used to identify the average promoter MSCC cut count data. To determine the significance of change in count data, an analysis for fit based on the Poisson distribution at the p=0.05 level was employed. Based on this analysis, a significant change was determined to be a four-fold or greater difference between two samples. 48h IL2 activated NK-cells were used as the standard to evaluate promoter methylation**.**

NK-cell isolation and activation for RNA-Seq

Primary human NK cells were isolated from peripheral blood lymphocytes (PBL) using a human NK-cell isolation kit (Miltenyi Biotec, Auburn, CA) as described previously(Meinhardt et al., 2012). The purity of NK cells was evaluated by CD56-APC and CD3-PE double staining, and samples with >95% $CD56^{+}CD3^{-}$ cells were used for RNA-Seq. Resting NK cells were cultured in the presence of 100 IU of IL2 for 48h to obtain activated NK cells. Higher levels of NK-cell activation were achieved by coculturing freshly isolated PBLs with engineered K562 cells, K562-Clone9-mb21, as described in detail before(Somanchi et al., 2011, Kucuk et al., 2013).

q-RT-PCR

Real-time PCR was performed using DyNAmo HS SYBR Green qPCR Kit (Thermo Scientific Inc) with CFX Connect (Bio-Rad, Hercules, CA) real time thermocycler. Melting curve analysis was performed to ensure amplification specificity. The ΔΔCt method was used to calculate the relative mRNA expression level. Human *RPL13A* and mouse eEF2 were used for normalization of gene expression in human and mouse samples respectively.

STAT3 shRNA transfection in 293T cells

The STAT3 shRNA was transfected into 293T cells as follows: 150,000 cells were seeded in 2 ml using 6-well plates in triplicate 24 h before transfection. 3 µg of PLVTH or PLVTH-S3S (STAT3 shRNA)(Piva et al., 2010) was transfected into 293T cells using Turbofect (Thermo Scientific,Waltham, MA) according to the manufacturer's recommendations. 51 h post-transfection, cells were harvested for q-RT-PCR.

Western Blot

Western blot was performed as described previously with the following modifications (Iqbal et al., 2009). RIPA buffer supplemented with a protease inhibitor cocktail (Sigma Aldrich, St Louis, MO) and phosphatase inhibitor cocktails 2 and 3 (Sigma Aldrich, St Louis, MO) was used to prepare the whole cell lysate. 20 µg protein/sample was used for Western blot. BSA (Sigma-Aldrich, St Louis, MO) was used instead of non-fat dry milk during blocking. The primary antibodies used for Western blotting are as follows: STAT3 (Cell Signaling, Danvers, MA), STAT5 (3H7) Rabbit mAb #9358 (Cell Signaling Inc.,Danvers, MA) ,phospho-STAT5 D47E7 Rabbit mAb # 4322 (Cell Signaling), phospho-STAT3 (Cell Signaling, Danvers, MA) and α-Tubulin (Sigma-Aldrich).

STAT3 shRNA expression in NK-cell lines

The lentiviral construct used for *STAT3* knock-down was described previously (Piva et al., 2010). Lentiviral transduction of NK-cell lines or DHL16 was performed following the protocol used for retroviral transduction(Kucuk et al., 2013) with the following modifications: 4 µg PLVTH or PLVTH-S3S was cotransfected with 2 µg of PMD2G and 2 µg psPAX2 packaging constructs into the 293T cell line to generate lentiviral particles. Transduction was performed once rather than twice. Transduction efficiency was determined with fluorescence-activated cell sorting (FACS) 3 days post-transduction.

Generation and expression of the STAT3 or STAT5B mutant constructs

Wild type (WT) STAT5B was PCR-cloned with the high-fidelity PfuUltra II Fusion HS DNA Polymerase (Agilent Technologies, Palo Alto, CA) using NK92 cell line cDNA as the template and then cloned into the multiple cloning site (MCS) of the pMIG expression vector using NotI and SalI restriction sites. Similarly, WT STAT3 was PCR-cloned into pMIG from KAI3 cell line cDNA using NotI and SalI sites. Diagnostic mapping and full

insert sequencing was performed. These WT STAT3 or STAT5B constructs were used as templates for site-directed mutagenesis to generate the STAT3 or STAT5B mutants used for functional studies as described below apart from the STAT3-Y640F-pMIG construct, which was PCR-cloned with PfuUltra II Fusion HS DNA Polymerase using the cDNA from NKYS cells, which have the STAT3 Y640F mutation.

STAT3 or STAT5B SNVs observed in NKTCL, γδ-PTCL or EATL type II samples (patient samples or cell lines) were generated using the Quick-Change Site-Directed Mutagenesis Kit (Agilent technologies, Santa Clara, CA) according to the manufacturer's instructions using WT STAT3 or STAT5B-pMIG vectors. Diagnostic restriction mapping and full sequencing of the inserts were performed to ensure the presence of introduced mutation and absence of another SNV. The primers used for site-directed mutagenesis (SDM) are as follows:

STAT3-S614R-SDM-F: GAAAGCAGCAAAGAAGGACGCGTCACTTTCACTTGG

STAT3-S614R-SDM-R: GTGACGCCTCCTTCTTTGCGGCTTTCACTGAATCTT

STAT3-G618R-SDM-F: GAAAGCAGCAAAGAAGGACGCGTCACTTTCACTTGG

STAT3-G618R-SDM-R: CCAAGTGAAAGTGACGCGTCCTTCTTTGCTGCTTTC-3

STAT3- D661Y-SDM-F: TGGGCTATAAGATCATGTATGCTACCAATATCCTGG

STAT3- D661Y-SDM-R: CCAGGATATTGGTAGCATACATGATCTTATAGCCCA

STAT3- A702T-SDM-F: AGCTGACCCAGGTAGCACTGCCCCATACCTGAAG

STAT3- A702T-SDM-R: CTTCAGGTATGGGGCAGTGCTACCTGGGTCAGCT

STAT5B-E579K-SDM-F: GGTTTGACGGTGTGATGAAAGTGTTAAAAAAACATC

STAT5B-E579K-SDM-R: GATGTTTTTTTAACACTTTCATCACACCGTCAAACC

STAT5B-N642H-SDM-F: GGAAAGAATGTTTTGGCATCTGATGCCTTTTACC

STAT5B-N642H-SDM-R: GGTAAAAGGCATCAGATGCCAAAACATTCTTTCC

STAT5B-Y665F-SDM-F: GCTTGGGAGACTTGAATTTCCTTATCTACGTGTTTC

STAT5B- Y665F-SDM-R: GAAACACGTAGATAAGGAAATTCAAGTCTCCCAAGC

STAT5B-I704L-SDM-F: GGATACGTGAAGCCACAGCTCAAGCAAGTGGTCCCTG

STAT5B-I704L-SDM-R: CAGGGACCACTTGCTTGAGCTGTGGCTTCACGTATCC

Retroviral transduction of NK-cell lines was performed as previously described(Kucuk et al., 2011) with the following modifications: 4 µg of pMIG or pMIG vectors expressing WT or mutated STAT3/STAT5B gene was cotransfected with 4 µg of the packaging construct PCL-Ampho into the 293T cell line. A single transduction was performed. Transduction efficiency was determined with flow cytometry on GFP^+ cells 2-4 days post-transduction. KAI3 cells were cultured in the presence of 20% FBS to increase transduction efficiency.

SOCS6 cloning and expression in NK-cell lines

The *SOCS6* coding sequence (NCBI accession number: NM_004232.3) was PCR-amplified with the high-fidelity *PfuUltra* II Fusion HS DNA Polymerase (Agilent Technologies, Palo Alto, CA) from 48h IL2 activated human NK cell cDNA and cloned into the pMIG expression plasmid upstream of the internal ribosomal entry site using NotI and SalI sites. The construct was validated by diagnostic restriction mapping and Sanger sequencing of the inserts. Retroviral transduction of NK-cell lines was performed as previously described with the following modifications: 4 µg of pMIG or pMIG-SOCS6 vector was cotransfected with 4 µg of the packaging construct PCL-Ampho into the 293T cell line. Single transduction was performed. Transduction efficiency was determined with flow cytometry on GFP positive cells 2-4 days post-transduction. YT cells were cultured in the presence of IL2 during transduction to increase transduction efficiency.

Conditioning primary human NK cells for retroviral transduction

Primary human NK cells were expanded using a special *ex vivo* system that involves coculturing primary human NK cells with an engineered NK-cell target, K562-Cl9-mb21, which activates and induces proliferation of NK cells robustly as described before(Kucuk et al., 2013, Kucuk et al., 2011). The expansion procedure is briefly as follows: First, primary human NK cells were isolated by negative selection using EasySep^{TM} Human NK cell enrichment kit (Stemcell technologies,Vancouver ,Canada). Then, primary NK cells were admixed in a 1:2 ratio with 100 Gr irradiated K562-Cl9-mb21cells, which express CD86, 4-1BBL and mIL21 on their surface, and cultured in NK-cell expansion medium (NKEM) (Somanchi et al., 2011). Cells were spun down at 400 g for 5 min, and the culture medium was renewed every three days with fresh culture medium, keeping the cell density at 250,000 cells/ml after every subculture. 9 days after coculture started, cells were immunostained with CD56-PE (Biolegend, San Diego, CA) and CD3-FITC (Biolegend) antibodies to determine the NK-cell purity by FACS. On the same day purity was determined, primary NK cells were transduced with WT or mutant STAT5B retroviral constructs.

Determination of positive/negative selection of transduced cells using FACS

STAT3 shRNA or STAT3/STAT5B mutant transduced NK cell lines were tracked by quantification of the GFP^{+} cells using flow cytometry after transduction to determine negative or positive selection of cells, respectively, because GFP was used as the marker of transduction. The following flow cytometers were used for determination of GFP^{+} cells: FACS Calibure (BD Biosciences), BD LSRFortessa (BD Biosciences) and Gallious (Beckman Coulter Inc.) Autofluorescent cells, which emit both green and orange, represent false positive, untransduced cells, were filtered out through proper gating. During quantification of GFP^{+} cells in transduced primary NK cells, dead cells

were labeled and filtered out by staining the cells with 0.5ug/ml DAPI (Biolegend, cat.no: 422801) for 10 min before flow cytometry.

ChIP-q-PCR

10 million cells isolated from GFP-sorted, empty vector, STAT5B-WT or N642H-mutant transduced KAI3 cells were used for chromatin immunoprecipitation using ChIP-IT Express Enzymatic (Active Motif, Carlsbad, CA) following the manufacturer's recommendations.The procedure is briefy as follows: The enzymatic digestion time was optimized as 10 min based on the TAE-agarose gel image. $10*10^6$ cells /sample were fixed with 1% formaldehyde. After enzymatic fragmentation, STAT5 (3H7) Rabbit mAb #9358 (Cell Signaling Inc.,Danvers, MA) and rabbit anti-IgG Control (Abcam Inc., Cambridge, MA) antibodies were used side-by-side for immunoprecipitations. 20 µg of chromatin/reaction was immunoprecipitated using dilutions of STAT5 or IgG antibody based on manufacturers' recommendations. After elution of DNA , reversal of DNA crosslinks, and proteinase K treatment, q-PCR was performed using 2 µl of gDNA in replicate. STAT5 immunoprecipated DNA levels were normalized to the levels of IgG immunoprecipitated DNA for each sample. STAT5 binding sites reported before for *IL2Ra(Kanai et al., 2014)*, *BCL2(Li et al., 2010)*,BCL-XL(Kanai et al., 2014), *HIF2α(Fatrai et al., 2011)* and *MIR155HG*(Kopp et al., 2013) were evaluated. The sequences of ChIP-q-PCR primers used in this study are as follows:

lL2Rα-ChIP-q-PCR-F: AAAACCAATTTCTTGGGATGG-3

lL2Rα-ChIP-q-PCR-R: AGGGGAAATTCCGTTGAGTT

BCL2 ChIP-q-PCR-F: ACTTTACATTTCTGTTGTGTTTACAGC

BCL2 ChIP-q-PCR-R: ATTCATACATATGCACACGCACA

BCL-XL ChIP-q-PCR F: AATTCAGCTGCCAGCCTCT

BCL-XL ChIP-q-PCR R: CAACCGCTTCCTTTTCTGAG

HIF2α (EPAS1) ChIP-q-PCR F: CAGTGTCCTGAGACTGTATG-

HIF2α (EPAS1) ChIP-q-PCR R: CTGTCAGACCCGAAAAGA

AZD1480 treatment of mutant STAT3 or STAT5B transduced KAI3 cells

25,000 KAI3 cells were seeded in 2 ml inside 24-well plates in replicates or triplicates and treated with 0, 0.5 µM, 1 µM or 2 µM of AZD1480 for 72 h. 72 h post-treatment, the total viable cell number in each well was quantified using a Vi-cell XR Cell Viability Analyzer (Beckman Coulter Inc.) according to the manufacturer's instructions. Total cell number in each treated sample was normalized to that of the untreated control cells.

Three-dimensional structural modeling of the STAT5B-N642H mutant

The STAT5B structure was modeled on the available STAT5A structure (PDB ID: 1Y1U) using the program MODELLER(Sali and Blundell, 1993). There was little difference in the SH2 domains as these two proteins have extremely similar primary sequences. Then, the modeled STAT5B SH2 domain was compared to other proteins containing SH2 domains that had been co-crystallized with peptides (v-SRC, GRB2, SH2B, NCK2) which showed the site of the N642H was directly located in the key binding pocket of the phosphorylated tyrosine. Phosphorylated self-peptide (STAT5B: VDG-PTR-VKPQ) was docked into the SH2 domain of WT-STAT5B or N642H-STAT5B, respectively. Protein-protein docking was done with the FFT-based docking tool ClusPro(Comeau et al., 2004) on a dedicated server. Key binding residues (STAT5B: R618, S620, N621, K600, N642) were specified based on previous peptide-SH2 domains co-crystallized structures (PDB ID: 2HDX, 1SHA, 2CIA, 1TZE). The best docking results were selected based on an electrostatically favored scoring function. ClusPro docking server first clustered 1000 ligand positions with the lowest energy score according to the 9 angstrom C-alpha

RMSD radius and then ranked the best model. With the energy-minimized protein-peptide docked model, the binding energy of the complex was calculated with MolDock (Thomsen and Christensen, 2006).

Wild-type and N642H mutant STAT5B cloning, expression and purification for surface plasmon resonance (SPR)

For surface plasmon resonance, wild-type (WT) and N642H-mutant STAT5B [residues between 128aa-717aa, NM_012448] was PCR-cloned into the SMT3-pET28b+ plasmid using the BamHI and XhoI cloning sites. BclI instead of BamHI restriction site was used in the forward primer to prevent digestion of STAT5B due to the presence of an internal BamHI site. A TGA stop codon was included in the reverse primer so that C-term His was not expressed. High-fidelity *PfuUltra* II Fusion HS DNA Polymerase (Agilent Technologies, Palo Alto, CA) was used to amplify STAT5B insert from STAT5B-WT-pMIG vector. Diagnostic mapping and Sanger sequencing of the inserts and the integration sites were performed to check the quality of the clones.

WT and mutant STAT5B expression was performed as follows: Plasmid DNA was transformed into BL21 (DE3) Codon Plus RIL competent cells (Agilent Technologies) and plated on LB agar plates with chloramphenicol (Cam) and kanamycin (Kan). Single colonies were selected and grown in LB media with Cam and Kan overnight at 37 °C. 6 X 6 mL of overnight culture was used to inoculate 6 X 1L LB media with Kan and Cam. Cultures were grown at 37 °C to an optical density of 0.6, then flasks were moved to a pre-cooled shaker at 18 °C. Cultures were grown at 18 °C until they reached an optical density between 0.9-1.1. Protein expression was induced with a final concentration of 500 µM IPTG, and cells were allowed to grow 16-20 hrs at 18 °C with continued shaking. Cells were harvested by centrifugation, resuspended in PBS and frozen at -20 °C until purification.

His6-SMT fusions of both WT and N642 mutant STAT5B were purified as previously published (Donaldson et al., 2013). Briefly, cells were thawed and lysed by French pressure cell with DNase I and PMSF. Lysates were clarified by centrifugation and filtration. Lysates were applied to Ni-NTA (Thermo Scientific HisPur) and washed with a PBS/ imidazole gradient. Eluted protein was dialyzed overnight at 4 °C into PBS in the presence of His6-ULP1 enzyme with 1 mM DTT. The dialyzed protein was incubated with Ni-NTA beads prior to concentration to remove uncleaved material, His6-SMT and His6-ULP1. The unbound material was then loaded onto the preparative grade superdex G200 gel filtration column (GE lifesciences) and exchanged into 50 mM Tris pH 8.0, 100 mM NaCl, 1 mM EDTA, and 1 mM DTT on column. The peak eluting at ~190 mL was concentrated, aliquotted into small volumes, and stored at -80 °C.

Surface plasmon resonance binding assay

SPR studies were carried out with the GE Lifesciences Biacore T100 instrument at 25 °C. STAT5B WT and N642H variant ligands were thawed and extensively dialyzed into HBS-N buffer (GE lifesciences). 50 µg/mL samples of protein were made by diluting the dialyzed stock samples into acetate pH 5.0 buffer immediately before immobilization. Both STAT5B proteins were coupled using EDC/NHS amine coupling chemistry with final immobilization levels of 5345.6 RU for WT and 5433.9 RU for N642H variant. Reference channels received a blank amine coupling protocol. The analyte, phosphopeptide (KAVDG (p) YVKPQI) (Anaspec, Fremont, CA) was prepared by dissolution in water and extensive dialysis into water. The peptide stock solution was stored at 4 °C prior to analysis. 2-fold dilutions of the phosphopeptide stock were prepared in HBS-EP+ (GE lifesciences) ranging from 100 µM to 0.78 µM immediately prior to analysis. Peptide samples were flowed over the immobilized ligand at a rate of 30 µL/min with each concentration being run in duplicate. HBS-EP+ was used both as

running and regeneration buffer. K_D values were calculated using BiaEvaluation software (Biacore AS, Uppsala, Sweeden) by fitting the binding isotherms to a 1:1 Langmuir model.

STAT5B Triple flag tag vector construction

A triple flag tag sequence was fused to C terminal of wild-type and mutant STAT5B and inserted into PMIG vector. For regulated STAT5B expression, triple flag STAT5 sequence were inserted into pBMN-DHFR-YFP vector so that the sequence was fused with DHFR on its C terminal. The triple flag tag sequence used in the experiment is:GAC TAC AAGGAC CACGAC GGTGAC TAC AAGGAC CACGACATCGACTAC AAGGACGACGACGACAAGTGA (D Y K D H D G D Y K D H D I D Y K D D D D K Stop)

CHIP-Seq assay

10 million cells isolated from GFP-sorted, empty PMIG vector, STAT5B-WT-3xFlag or STAT5B-N642H-3xFlag-PMIG transduced KAI3 cells were used for chromatin immunoprecipitation using ChIP-IT Express Enzymatic (Active Motif, Carlsbad, CA) following the manufacturer's recommendations. The procedure is briefy as follows: The enzymatic digestion time was optimized as 10 min based on the TAE-agarose gel image. $10*10^6$ cells /sample were fixed with 1% formaldehyde. After enzymatic fragmentation, Anti-Flag mAb () #9358 (Cell Signaling Inc.,Danvers, MA) and rabbit anti-IgG Control (Abcam Inc., Cambridge, MA) antibodies were used side-by-side for immunoprecipitations. 20 µg of chromatin/reaction was immunoprecipitated using dilutions of STAT5 or IgG antibody based on manufacturers' recommendations. After elution of DNA, reversal of DNA crosslinks, and proteinase K treatment, q-PCR was performed using 2 µl of gDNA in replicate. STAT5 immunoprecipated DNA levels were normalized to the levels of IgG immunoprecipitated DNA for each sample. STAT5

binding sites reported before for KAI3 cells were transduced with empty PMIG vector, wild-type STAT55-Flag-PMIG and STAT5B-N642H-Flag-PMIG. GFP positive cells were sorted 4 days after transduction. 1 x 10^{7} cells were used for Immune-precipitation.

Donor vector and sgRNA generation for STAT5B mouse

The loxp flanked wild type STAT5B- STAT5B N642H construct was inserted into Bluescript vector by Gibson assembly. Primers with 20bp overhang were used to amplify each sequence. 5' homology arm, mouse wild type STAT5B exon16, 3' homology arm were amplified from mouse genome. Huamn N642H STAT5B exon 16 was amplified from patient sample. Sequence containing two paired of loxP sites were amplified from vector MSCV- FLIPi-P2G-Thy1.1-PTEN vector (Addgene). Primers for Gibson assembly are as follows:

STAT5BMM5'FLANK-F:,CCGGGCTGCAGGAATTCGATGGACGGAATTACACTTTCTG

STAT5BMM5'FLANK-R:
GTTATAGACTAAGGAAGGAATGGTCATTCTTAGGTGGCAATGTTAGCAGCAACACC
TGCCATTAATTAGAG

5'2XLOXP-SPACER-F:
TTCCTTCCTTAGTCTATAACTTCGTATAGGATACCTTATACGAAGTTATGGTGAACC
GCATCGAGCTGAAG

5'2XLOXP-SPACER-R:
GTAAACCTTGATAACTTCGTATAATGTGTACTATACGAAGTTATCACGAACTCCAGC
AGGACCATGTG

STAT5BHU-EX16-FLANKS-F: ACGAAGTTATCAAGGTTTACATCTGCCC

STAT5BHU-EX16-FLANKS-R:

GGACTTCTTGGGTTATTTTTAAATGGAGATTTCTATTG STAT5BMU-EX16-FLANK-F:

AAAAATAACCCAAGAAGTCCCCGTTGGC

STAT5BMU-EX16-FLANK-R : CCCAGCCATCGCCCTGGGTATTGCCTGA

3'2XLOXP-F: TACCCAGGGCGATGGCTGGGTTCATGGTG

3'2XLOXP-F:

ACGAATTTGTGTATTTCCTAAGAATTTTACGACAATATGATAAGCTTGGCTGCAGG

STAT5BMU3'FLANK-F:

TAGGAAATACACAAATTCGTGAGAAAGAAAGACTTCACACACATCTTGATGCTGGCT

CTG

STAT5BMU3'FLANK-R: ACGGTATCGATAAGCTTGATGGATACTCTAGGAAACTCAG

sgRNA sequence was cloned into T7-promoter containing pUC57-sgRNA expression vector using BsaI sites as described previously(Shen et al., 2014). Vector were linearized DraI and in vitro–transcribed using the MEGAshortscript Kit (Ambion, AM1354). sgRNAs were purified by MEGAclear Kit (Ambion, AM1908). To test sgNRA efficiency, sgRNA sequence were cloned into CAS9 expressing vector pSpCas9 (BB)-2A-GFP. 3T3 cells were transfected with sgRNA containing pSpCas9(BB)-2A-GFP plasmid, DNA were isolated 2 days posttransfection and Cas9 mediated edition was tested with SURVEYOR assay (Invitrogen) (Cong and Zhang, 2015) STAT5B sgRNA sequence are as follows:

STAT5B-CRISPR1-SENSE: GCAATGTTAGCAGCAACACC

STAT5B-CRISPR1I-ANTISENSE: GGTGTTGCTGCTAACATTG

STAT5B-CRISPR2- SENSE: TGACCATTCCTTCCTTAGTC

STAT5B-CRISPR2- ANTISENSE: GACTAAGGAAGGAATGGTCA

STAT5B-CRISPR3- SENSE: CTAAGAATTTTACGACAATA

STAT5B-CRISPR3- ANTISENSE: TATTGTCGTAAAATTCTTAG

STAT5B-CRISPR4- SENSE: AAGACTTCACACACATCTTG

STAT5B-CRISPR4- ANTISENSE: CAAGATGTGTGTGAAGTCTT

Mice

LMP1^{flSTOP} mice on a BALB/c background, Ncr1-cre mouse strains on the C57BL/6 background were purchased from the Jackson Laboratory. Blimp1f/f mice on C57/b6 background were kindly given to us by Dr. Alexander Tarakhovsky, Cre reporter mice on BALBc background by Dr. Kay-Uwe Wagner. To test Cre mediated recombination in vivo, Ncr1-cre mice crossed with GFP $^{stopf/f}$ mice to generate Ncr1-cre, GFP $^{stopf/-}$ mice and mice in first generation were used for experiment. Ncr1-cre mice were crossed with Blimp1f/f or Blimp1f/- to generate Ncr1-cre, Blimpf/-mice in first generation. Ncr1-cre; Blimpf/- mice were crossed with Blimp1f/f to generate Ncr1-cre; Blimpf/f mice. LMP1^{flSTOP} mice were crossed with Blimpf/f or Ncr1-cre,Blimpf/f for at least 5 generation to generate Blimpf/f,LMP1^{flSTOP} and Ncr1-cre,Blimpf/f,LMP1^{flSTOP} mice.

Antibodies for flow cytometry

The following antibodies were purchased from BD Biosciences: NK-1.1 (PK136), CD3e (145-2C11), CD4 (RM4-5), CD8a (53-6.7), CD45R/B220 (RA3-6B2), CD19 (1D3),TCRβ (H57-597), CD27 (LG3A10), CD11b (M1/70), NKp46 (29A1.4), CD69(H1.2F3). For flow cytometry, single-cell suspensions were prepared from PBMC, lymph nodes, spleen, bone marrow followed by red blood cell lysis. Purified rat anti–mouse CD16/CD32 (2.4G2; BD Pharmingen) was added to avoid nonspecific binding. Stained samples were

fixed with 0.5% paraformaldehyde 4 °C overnight. Stained samples were analyzed using FACSCantoII and FACSDiva software Version 6.1.2 (BD Biosciences). Cell number were counted using BD Accur C6 Cytometer (BD Biosciences)

NK-cell purification, expansion, and function

Single-cell suspensions were prepared from 3-4 spleens/genotype. NK cells were isolated using negative seletion NK cell isolation kit (Miltenyi Biotec) as unwanted cells were labeled with magnetic beads and attached to the magnetic column while untouched NK cells were collected. NK cells were expanded for 6-12 days in RPMI 1640 medium containing 10% fetal calf serum (FCS), β-2ME, L-glutamine, and penicillin/streptomycin supplemented with rhIL2 1000U/mL The purity as assessed by flow cytometry was > 90%-95%. For in vitro proliferation assays, freshly purified NK cells or NK cells at day 6 were seeded in 24-well plates under IL2 or IL15. Cells were stained with 0.4% trypan blue and counted using automated cell counter (Invitrogen).

NK-cell cytotoxicity was analyzed by flow cytometry. Briefly, target YAC-1 cells were labeled with carboxyfluorescein diacetate succinimidyl ester (CFSE; Invitrogen) in 37°C for 1 hour. 1×10^3 target cells/well was incubated expanded NK cells at day 10 at the indicated E:T ratios for 4 hours at 37°C. Propidium iodide (Sigma-Aldrich) was added to each well immediately before flow cytometry. The percentage of specific lysis was determined as CFSE+PI+.

In vivo T cell depletion

For antibody-mediated T cell depletion, 40 ug anti-CD3 antibodies (145-2C11) were injected intraperitoneally (i.p.) everyday for 5 days every other week. In another experiment, 30mg/kg body weight Cyclosporin A (Selleckchem) were injected intraperitoneally daily along with 200ug anti-CD3 antibodies every 3-4 days.

In vivo PolyIC stimulation

For acute poly IC stimulation, mice were injected i.p. with 20ug poly IC (Invivogen), blood were collected retro-obitally on day 1 and day 3. For chronic poly IC stimulation, mice were injected i.p. with 200ug polyIC every other day for 4 weeks. Lymphocyte profile was analysis in different organs.

Statistical analysis

Mean and SEM were calculated using Microsoft Office Excel (Microsoft), two-tailed unpaired t-test was applied, $p<0.05$ was considered statistically significant.

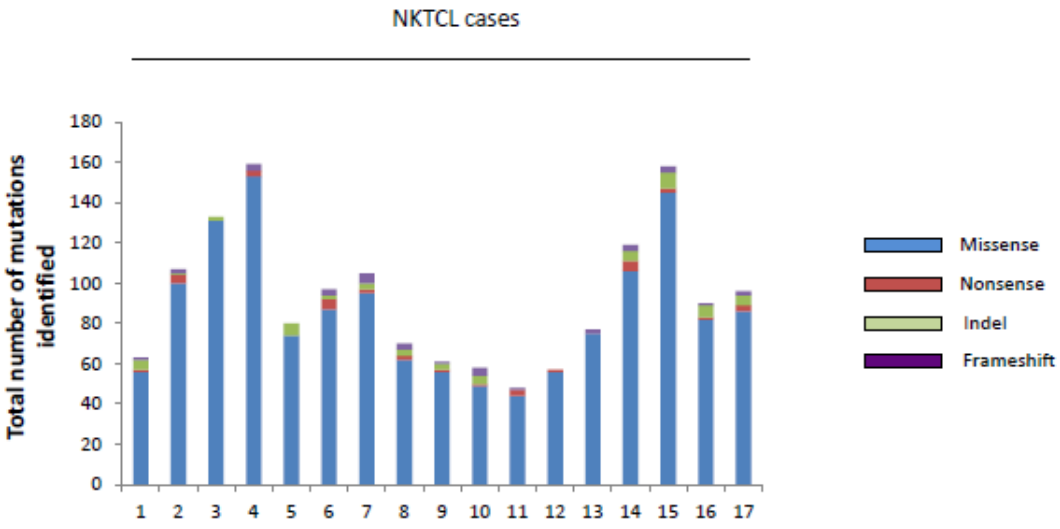
NKTCL cases
Total number of mutations identified
180
160
140
120
100
80
60
40
20
0
1
2
3
4
5
6
7
8
9
10
11
12
13
14
15
16
17
Missense
Nonsense
Indel
Frameshift

Figure 2-1:Total number of mutations identified by RNA-Seq in each NKTCL cases.

The number of missense, indel, nonsense and frameshift mutations are shown for 17 NKTCL cases as column percase based on the primary RNA-Seq pipeline.

A

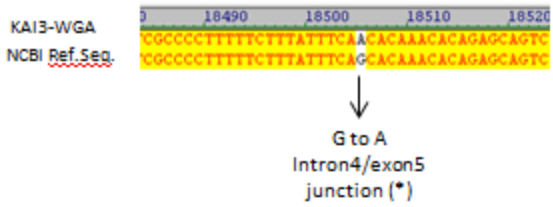

B

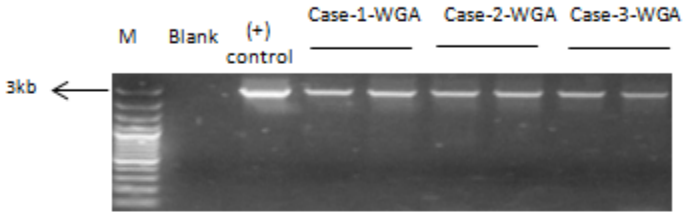

* = Iqbal,Kucuk et. al. Leukemia 2009.

C

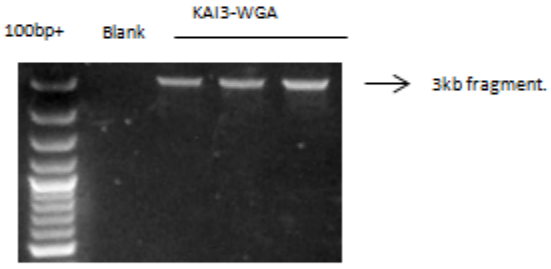

D

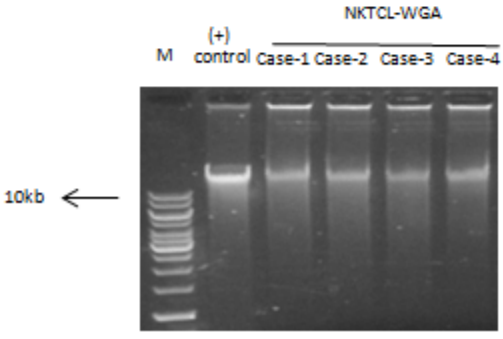

Figure 2-2: The quality control of whole genome amplification procedure using NK samples

(A) The reported PRDM1 mutation was detected by Sanger-PCR using whole genome amplified (WGA) DNA from KAI3 cell line. (B) ~3kb DNA amplicon generated with PCR using WGA DNA as a template from the KAI3 cell line. *RPL13A* specific primers were used. (C)~3 kb fragment was generated using the WGA DNA from NKCL cases (n=3) as in B. TAE-Agarose gel results of the PCR amplicons from three representative NKCL cases were shown in duplicate. (D) 1ug of WGA genomic DNA from 4 representative NKCL cases was run on 0.8% TAE-agarose gel to show the relatively large size of the amplified genomic DNA.

A

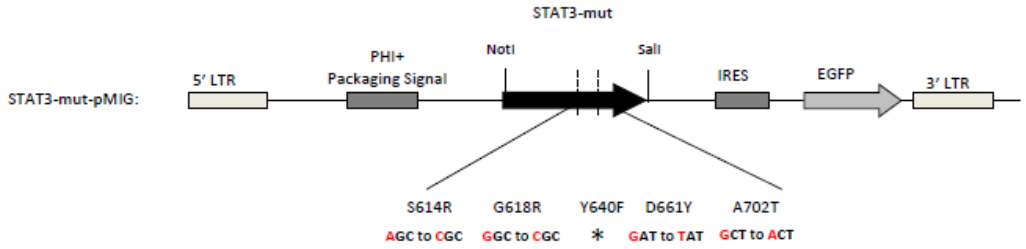
STAT3-mut
PHI+
Packaging Signal
NotI
SalI
5′ LTR
IRES
EGFP
3′ LTR
STAT3-mut-pMIG:
S614R
AGC to CGC
G618R
GGC to CGC
Y640F
*
D661Y
GAT to TAT
A702T
GCT to ACT

B

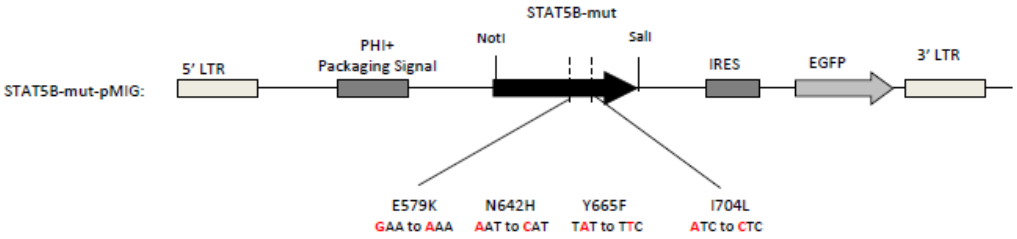
STAT5B-mut
PHI+
Packaging Signal
NotI
SalI
5′ LTR
IRES
EGFP
3′ LTR
STAT5B-mut-pMIG:
E579K
GAA to AAA
N642H
AAT to CAT
Y665F
TAT to TTC
I704L
ATC to CTC

Figure 2-3: Generation of the mutated STAT3 or STAT5B expression construct

The STAT3 (A) and STAT5B (B) mutant expression construct generated and used in functional studies are shown. The nucleotide changes and their corresponding effects on the targeted residues are indicated. The altered nucleotides are shown in red color inside the context of the amino acid codon affected. * NKYS cDNA, which has Y640F mutation, was used as a template during cloning.

Disease Category		Case number	Number of cases with STAT3 mutation	STAT3 mutation type	Number of cases with STAT5B mutation	STAT5B mutation type
Gamma-delta T cell lymphoma	Hepatosplenic	9	0	-	3	N642H
					1	I704L
	Primary cutaneous	15	1	G618R*	3	N642H
			1	Y640F	1	E579K
Enteropathy-associated T-cell lymphoma (EATL), type II	γδ-TCR expression	16	0	-	7	N642H
	Others **	3	0	-	0	-
NK/T cell lymphoma #		51	1	D661Y	0	-
			1	S614R	1	N642H
			1	A702T	2	Y665F

*: One case initially diagnosed as NKTCL and with a STAT3 mutation (G618R) was reclassified as primary cutaneous γδ –PTCL category due to clonality of γδ gene rearrangement.

#: For the cases with no TCR rearrangement data available or TCR with germline configuration, they were classified under NK/T cell lymphoma category as they may have derived from NK or T cells. γδ –PTCL had demonstrable clonal rearrangement of the TCR γ gene and the expression of γδTCR by immunostaining and/or gene expression signature indicative of γδ-T-cell derivation.

**: Three of 19 EATL type II cases have only αβ-TCR expression (n=2) or they are TCR silent (n=1).

Table 2-1: The STAT3/STAT5B mutations observed in γδ-PTCL, EATL, NKCL or NKTCL cases and cell lines

Cell line	Original description of disease	CD56	T-cell receptor	EBV	IL2 dependence	STAT3 mutation
KHYG1	Aggressive NK-cell leukemia	+	germline	-	IL-2	-
NK-92	Aggressive NK-cell leukemia	+	germline	+	IL-2	-
YT	"ALL with thymoma"	+	germline	+	No	+
SNK-6	Nasal- NK-cell lymphoma	+	germline	+	IL-2	+
NKYS	Nasal- NK-cell lymphoma	+	germline	+	IL-2	+
KAI3	severe chronic active EBV infection	+	germline	+	IL-2	-
SNT-8	Nasal T-cell lymphoma	+	TCR γ/δ+	+	IL-2	+
SNT-13	severe chronic active EBV infection	+	TCR γ/δ+	+	IL-2	-
SNT-15	severe chronic active EBV infection	+	TCR γ/δ+	+	IL-2	+

Table 2-2: Characteristics of NK and γδ- T cell lines used in the study and STAT3 mutation status

Chapter III

Identification of mutations of JAK-STAT pathway genes in natural killer and peripheral γδ T-cell lymphomas

Introduction

Mature NK cell malignancies are classified under two major categories by the current WHO classification(Jaffe, 2009): Aggressive NK cell leukemia (ANKL) and extra-nodal NK/T cell lymphoma of nasal type (NKTCL). NKTCLs can be clinically classified as nasal or extra-nasal lymphomas based on the primary site of the tumor (Au et al., 2009). NKTCLs are rare malignancies with poor prognosis, particularly in advanced stage or with extranasal presentation (Kwong, 2005). NKTCL shows marked geographic differences in incidence with much higher frequency in East Asia and Central/South America (Au et al., 2009). NKTCLs are frequently associated with EBV infections(Kwong, 2005); however, the role of EBV in the pathogenesis of NKTCLs is not well understood despite two studies suggesting an oncogenic role for *EBNA1(Ian et al., 2008)* and *LMP1(Komabayashi et al.) ,* genes encoded by EBV. Interestingly, non-hepatosplenic γδ -TCL (γδ-TCL NHS) showed a very similar gene expression profile to NKTCL (Iqbal et al.) suggesting that these two diseases are highly similar and may use the same oncogenic mechanisms during neoplastic transformation. There is little insight into the aberrant pathways operative in γδ –TCLs.

Based on gene expression profile (GEP) differences between malignant and normal NK cells (Huang et al., 2010, Iqbal et al., Ng et al.), constitutive activation of the JAK-STAT, NF-kB, AKT and MYC pathways in NKTCL cases have been demonstrated. Given that the activation of these pathways is a part of the normal NK cell activation process (Dybkaer et al., 2007), it is possible that accumulation of oncogenic mutations in genes affecting these pathways contributes to the neoplastic transformation of NK cells by aberrantly promoting proliferation and survival. However, there is still limited information regarding the mechanistic basis for the constitutive activation of these growth promoting pathways. Recently, two groups reported activating JAK3 mutations in

NKTCL cases(Koo et al., Bouchekioua et al.) but a recent report showed that JAK3 mutations are not frequent in NKTCLs at least in Japan (Kimura et al., 2014). This marked difference in mutation frequency requires additional investigation.

The JAK-STAT pathway plays a key role in mediating cytokine signaling in NK cells (Dybkaer et al., 2007). This role has recently been underscored by phosphorylation of STAT1, STAT3 and STAT4 in mouse NK cells in response to MCMV infection (Bezman et al., 2012). Constitutive activation of STAT3 and STAT5 is known to increase tumor cell proliferation, survival and invasion(Yu et al., 2009). Aberrant STAT3 and STAT5B activation has been shown in activated B-cell type diffuse large B-cell lymphomas (ABC-DLBCL) (Lam et al., 2008) and CD8+ lymphoblastic lymphoma (Bessette et al., 2008), respectively. Recently, activating mutations were identified in *STAT3* (Jerez et al., 2012, Koskela et al.) and *STAT5B(Rajala et al.)* in NK-large granular leukemia (LGL) and T-LGL cases suggesting an oncogenic role for these mutations. These mutations were located in the Src homology 2 (SH2) domain which is essential for homodimerization and activation of STATs (O'Shea et al., 2002).

SOCS family proteins are induced in response to cytokine signaling and they have been known to act as the negative regulators of the JAK-STAT pathway (Krebs and Hilton, 2001). Promoter methylation-mediated silencing of *SOCS* gene expression was shown for *SOCS1* in hepatocellular carcinoma (Yoshikawa et al., 2001) and multiple myeloma(Galm et al., 2003) , for *SOCS3* in lung cancer (He et al., 2003) and in myeloproliferative disorders(Fourouclas et al., 2008) and for *SOCS6* in gastric cancer(Lai et al.). These studies showed that the JAK-STAT pathway may be constitutively activated by hypermethylation-mediated silencing of the negative regulators of the pathway in addition to activating mutations of the mediators of the pathway.

In this study, we investigated the genome-wide driver mutations in NKTCLs using a combination of RNA sequencing, whole-exome sequencing (WES) and Sanger sequencing, and identified activating mutations of *STAT3* and *STAT5B* in the SH2 domain. STAT5B mutations were also observed at a high frequency in γδ-T-cell-derived lymphomas (γδ-PTCLs). The mutatant proteins were more resistant to inactivation and promoted cell growth and survival by binding to their direct targets. The JAK-STAT activation could be partially inhibited by JAK1/2 inhibitors and expression of the negative regulator SOCS6, suggesting a potential therapeutic option for these patients.

Results

Frequent STAT3 and STAT5B mutations are identified by WTS in NKTCL cases

WTS was performed on resting NK cells, NK cells activated by IL2 or by K562-Clone9-mb21, 17 NKTCL cases and 3 NK cell lines. Totally 9424 annotated SNVs were identified in NKTCL cases and NK cell lines (Table 3-1). First, we validated the mutations detected from our WTS data that may be functionally significant including the mutations in FAS, TP53, BRAF, MAP2K1, CREBBP, EP300 and MLL2 genes, by Sanger sequencing on the corresponding genomic DNA. The BRAF (G469A) and MAP2K1 (K57N) SNVs have been detected frequently in epithelial tumors(Paik et al., 2011, Marks et al., 2008, Shukla et al.) and have been shown to be oncogenic(Roring et al., Wan et al., 2004, Marks et al., 2008). Of note, FAS and TP53mutations were identified in NKTCLs by traditional Sanger sequencing in previous studies.

WTS identified a number of mutations that may affect the JAK/STAT pathway including one STAT3 missense SNV (S614R, G618R and A702T) in each of three NKTCL cases (3 of 17, 18%). Interestingly, all of the STAT3 SNVs were located in the SH2 domain, a domain critical for STAT3 activation (Fig. 3-1A left). STAT3 S614R and STAT3 G618R mutations were recently reported in NK-LGL or T-LGL leukemia cases (Jerez et al., 2012). The third STAT3 mutation, STAT3 A702T was predicted to be benign by Polyphen-2; however, this residue is located close to a phosphorylated residue 705 raising the possibility that the mutation may alter the phosphorylation of residue 705. *STAT5B* missense mutation (STAT5B N642H) was present in one of 17 (6%) NKTCL cases (Fig. 3-1B). STAT5A and STAT5B are highly conserved in this residue and introduction of STAT5A N642H was reported previously to confer growth factor independent growth in leukemic cell lines(Ariyoshi et al., 2000). In total, STAT3 and STAT5B mutations were observed in 4 of 17 (23.5%) NKTCL cases with WTS data.

Targeted resequencing of STAT3 and STAT5B in NKTCL,γδ-PTCL and enteropathy associated T-cell lymphoma (EATL) type II patient cohort and cell lines

NK cell and γδT cell share similar properties and functions, and our gene expression profiling studies found that NKTCL and γδ-PTCL cases share a very similar profile with each other and with normal NK cells. These observations suggest that NK cell and γδT cell derived lymphoma may use similar oncogenic mechanisms. To compare the role of *STAT3/STAT5B* SH2 domain mutations in NK cell and γδT cell derived lymphoma, we screened the SH2 domains of *STAT3* and *STAT5B* in additional NKCL and γδ-T cell lines, as well as NKTCL, γδ-PTCL and enteropathy associated T-cell lymphoma (EATL) type II patient cohort (Fig. 3-2A).

Since all observed SNVs were located in the SH2 domain, we sequenced the SH2 domains of *STAT3* and *STAT5B* by targeted Sanger sequencing in 35 additional NKTCK cases collected in China (Fig. 3-3). One *STAT3* D661Y mutation was observed in 35 cases (2.9%) and two *STAT5B* mutations (Y665F and N642H) was observed in two of these 35 screened cases (5.7%) (Fig. 3-2B, C). Frequency of both STAT3 and STAT5B mutations was lower in Chinese NKTCL cases. These analyses yielded a *STAT3* and *STAT5B* mutation frequency of 5.9% in all NKTCL patients screened by WTS, WES and/or Sanger sequencing (Fig. 3-2D, left).

RNA-Seq analysis on 3 NK-cell lines revealed an activating mutation, Y640F, in the SH2 domain of STAT3 in NKYS cells, which was validated by Sanger sequencing (Fig. 3-2B). Interestingly, 2 out of 3 additional NK-cell lines (SNK6 and YT) showed *STAT3* mutations when screened by Sanger sequencing, raising the *STAT3* mutation frequency to 50% of the 6 NK-cell lines studied (Fig. 3-2B). However, Sanger

sequencing of the SH2 domain (exon14-exon18) of *STAT5B* in these NK-cell lines did not reveal any *STAT5B* mutations.

Two recent studies reported the presence of *JAK3* A572V, A573V or V722I mutations in NKTCL (Koo et al., 2012, Jiang et al., 2015). However, neither WTS nor hotspot sequencing of 40 NKTCL cases revealed these SNVs, consistent with a recent report(Kimura et al., 2014). The discrepancy may be due to a variety of factors including the genetic composition of the populations and different stimuli that initiate and sustain the initial phase of NK-cell proliferation.

We also screened the SH2 domains of *STAT3* and *STAT5B* in 3 γδ T-cell lines and 24 γδ-PTCL cases [15 primary cutaneous (PC)-γδ-PTCL and 9 hepatosplenic (HS) - γδ-PTCL cases]. Among the three γδ T-cell lines, we observed a *STAT3* Y640F mutation (SNT-15) and a *STAT3* D661Y mutation (SNT-8), but no *STAT5B* mutation (Fig. 3-2B). We identified only a *STAT3* Y640F mutation in 1 of 24 γδ-PTCL cases (Fig. 3-2B). On the other hand, 8 of 24 (33.3%) cases (4 PC and 4 HS) showed activating *STAT5B* mutations in the SH2 domain (Fig. 3-2C, D).

Enteropathy associated T-cell lymphoma (EATL) is an aggressive PTCL with higher incidence in Europe and USA (Delabie et al., 2011). The disease is now classified into two subtypes: Type I is the classical type expressing TCR-αβ and is associated with celiac disease and gluten-sensitive enteropathy. EATL type II cases have been shown to frequently express TCR-γδ ~ 78% in one study (Chan et al., 2011)), and they are not associated with gluten-sensitive enteropathy. Targeted sequencing revealed *STAT5B* N642H mutations in 7 of 19 EATL type II cases (36.8%) (Fig. 3-2C, D). Intriguingly, all mutated EATL type II cases have γδ-T cell receptor expression (7/16 of TCR-γδ positive cases) underscoring the significance of STAT5B mutations in the neoplastic transformation of γδ-T cells giving rise to different subtypes of γδ-PTCL.

STAT3 is constitutively activated in NK cell lines with STAT3 mutations

To address whether STAT3 mutations activate the STAT3 pathway, we performed western bloting on 6 NK cell lines using STAT3 and phospho-STAT3 antibodies. Consistent with the targeted sequencing results, we observed high phospho-STAT3 expression in SNK6, NKYS and YT cell lines (Fig. 3-4). The three NK cell lines without STAT3 mutations (NK92, KHYG1 and KAI3) express phospho-STAT3 at much lower levels suggesting that STAT3 is highly activated in 3 of 6 (50%) of NK cell lines due to the presence of activating mutations in the SH2 domain.

NK-cell lines with STAT3 mutations show high pY-STAT3 expression and shRNA-mediated knock-down of STAT3 inhibits NK-cell line growth

Next, we transduced the NKYS and YT cell lines, which have the activating STAT3-Y640F mutation, with empty vector or STAT3 shRNA with confirmed activity (Fig. 3-5) to evaluate whether STAT3 silencing inhibits growth of NK cells. We quantified the percentage of GFP positivity of STAT3 shRNA transduced cells at regular time intervals starting 3 days post-transduction, and observed a markedly reduced percentage of GFP^+ cells compared to vector-only transduced cells, suggesting a strong negative selection pressure after STAT3 knock-down (Fig. 3-6A-D). We did not observe a decrease in the percentage of GFP^+ population in STAT3 shRNA-transduced KAI3 cells, which express wild-type STAT3 (Fig. 3-6E, F). STAT3 protein knockdown efficiency was ~72%, ~78% and ~39% in NKYS, KAI3 and YT cell lines, respectively (Fig. 3-6G, H), which may account for the more moderate decrease in growth observed in YT cells after STAT3 knock-down.

Ectopic expression of STAT3 or STAT5B mutants promotes growth in KAI3 cells under limiting IL2 concentrations.

Some of the STAT3/STAT5B mutations have been reported in other tumors and are likely oncogenic, but other mutations have not been previously identified. We used several approaches to confirm that these mutations are functionally significant and not passenger mutations or uncommon SNPs. We performed site directed mutagenesis of each of the mutants and transduced KAI3 cells, which lack STAT3 or STAT5B mutations, with retroviruses expressing each of the STAT3 and STAT5B mutants and determined the % of GFP^+ cells post-transduction in regular time intervals. With only two exceptions, all STAT5B- or STAT3-mutant transduced KAI3 cells showed significant progressive positive selection under limiting IL2 concentrations compared with WT-transduced cells (Fig. 3-7A, B). STAT3 A702T mutant showed only modest positive selection when compared with WT transduced cells.

Western blot analysis in cell lines clearly demonstrated an association of STAT3 mutations with increased phosphorylation. As there are no cell lines with STAT5B mutations, we measured the phosphorylation of STAT5B proteins in STAT5B-mutant transduced KAI3 cells and found it to be clearly increased compared with WT transduced cells (Fig. 3-7C).

Ectopic expression of STAT5B I704L or N642H mutants promotes growth of primary human NK cells

We transduced STAT5B mutants (N642H and I704L) into primary human NK cells obtained through coculture with engineered K562 cells, K562-Cl9-mb21, and observed robust promotion of cell growth in mutant compared to WT transduced cells (Fig. 3-8).

Intriguingly, the effect of STAT5B N642H was prominent and the strongest among all mutants tested in KAI3 cells or normal NK cells.

STAT5B target genes are transcriptionally upregulated in STAT5B-mutant transduced cells through direct binding to conserved STAT5 binding sites

We evaluated the expression of known STAT5B targets, IL2Rα(Kanai et al., 2014), BCL-XL(Silva et al., 1999), BCL2(Li et al., 2010), MIR155HG(Kopp et al., 2013) and HIF2α(Fatrai et al., 2011) in KAI3 cells transduced with STAT5B mutants (N642H and I704L) and observed significantly higher expression compared to WT or empty vector transduced cells (Fig. 3-9A-E), indicating that the mutants are functionally active and upregulate oncogenic STAT5B targets, which in part accounts for better promotion of survival/growth in NK cells. Next, we performed ChIP-q-PCR on STAT5 binding sites for these genes. Compared to KAI3 cells transduced with empty vector or wild- type STAT5B, a robust increase in occupancy of STAT5 binding sites was observed in STAT5B-N642H transduced KAI3 cells (Fig. 3-9F-J), indicating that increased STAT5B binding due to the mutation, upregulates the expression of the target genes. Altogether, these results suggest that the STAT3 and STAT5B mutations are oncogenic, driver mutations.

Three-dimensional modeling and surface plasmon resonance (SPR) analysis of the N642H mutant shows stronger affinity for the phosphorylated tyrosine Y699

STAT5B N642H is the most frequent mutation identified in γδ-PTCLs and appears to have the highest functional potency. Hence, we sought to determine the molecular basis of the functional alterations resulting from this mutation through structural analysis. To

mimic homodimerization, we docked a tyrosine-phosphorylated STAT5B peptide into the WT and mutant SH2 domains (Fig. 3-10A-C). Molecular docking showed that the peptide has a significantly higher binding affinity to the N642H mutant than the WT (Fig. 3-10D) largely due to the direct electrostatic interaction of the mutant histidine with the phosphotyrosine. To confirm these modeling studies, we produced nonphosphorylated wild-type and N642H STAT5B (residues 128 to 717), purified each to homogeneity, and performed surface plasma resonance (SPR) studies. The wild-type and mutant STAT5B proteins were coupled to individual channels of a CM5 SPR chip, and the phosphopeptide KAVDG(p)YVKPQI was passed over each channel at increasing concentrations (0.8 to 100 μM) in duplicates. The binding affinity of the peptide to the wild-type and N642H mutant was determined by fitting the equilibrium saturation point as a function of peptide concentration. The dissociation constants for the N642H mutant and wild-type STAT5B were 2.9 μM and 14 μM, respectively (Fig.3-10E). While these measurements represent a ~5 fold difference for the peptide to the monomeric STAT5B-WT compared to N642H mutant, it is important to note that phosphoSTAT5B forms a homodimer and thus there are two phosphotyrosine binding sites. Consequently, $K_{Dimer} = K_{Monomer1} \bullet K_{Monomer2}$ which translates to a 25-fold increase in association constant for the dimer. Hence, the homodimeric N642H mutant is substantially more stable than the wild-type. This finding supports the molecular model and the *in vitro* cell based assay observations.

To address whether the STAT5B-N642H mutation is associated with prolonged STAT5B activation in the presence of acute JAK-STAT5 pathway activation, we performed western blot analysis on IL2-activated YT cells in a time-course experiment to evaluate P-STAT5 expression. The JAK-STAT5 pathway is known to be inducible in this cell line (Nagy et al., 2009) and we observed P-STAT5 expression only in the presence

of IL2 (data not shown). We incubated empty vector, STAT5B-WT or N642H-mutant transduced YT cells with IL2 for 30 minutes, and evaluated P-STAT5 expression up to 6 h after IL2 withdrawal. P-STAT5 expression disappeared 1 h after transient IL2 stimulation in empty vector (EV) or STAT5B-WT transduced cells whereas it persisted for more than 6 h in N642H-transduced cells (Fig.3-10F). These results suggest that the N642H mutation increases affinity of the phospho-STAT5B dimer and thereby resulting in far more persistent activation.

AZD1480 inhibits STAT3/STAT5B mutant transduced NK cells

Most NKCL and γδ-PTCL cell lines are still dependent on IL2 which signals mainly through JAK1/2 to activate STAT3 and STAT5 (Johnston et al., 1996, Johnston et al., 1995). JAK inhibitors are expected to be effective in interrupting this signaling pathway in cells with wild-type STAT3 and STAT5. However, it is unclear whether the inhibitor would effectively inhibit this pathway at a tolerable dosage in cells harboring the mutants. We treated STAT3 or STAT5B-mutant and WT transduced KAI3 cells with 0.5 μM AZD1480, a selective JAK1/2 inhibitor(Derenzini et al., 2011). We quantified viable cells at 72 h post-treatment and observed inhibition of growth in all the mutant STAT3 and STAT5B transduced cells (Fig. 3-11A, B). With higher concentrations of AZD1480, we observed up to 60% inhibition in STAT5B N642H-mutant transduced cells (Fig. 3-11C, right), associated with reduced STAT5 phosphorylation in a dose-dependent manner (Fig. 3-11D). Next, we treated YT and NKYS cells, which have STAT3 mutations, with the JAK1/2 inhibitor and observed dose-dependent inhibition of cell growth (Fig.3-11E). These data suggest that JAK1/2 inhibitors may have therapeutic efficacy for NKTCL and γδ-PTCL patients with the mutations. This may have immediate clinical application as JAK1/2 inhibitors are already approved for myeloproliferative

disorders (Pardanani, 2008, Sonbol et al., 2013). Thus they are available for trials in NKTCL or γδ-PTCL patients while STAT3 and STAT5B inhibitors are still not clinically available. Further development of small-molecule inhibitors targeting STAT3 or STAT5B dimerization or DNA binding or siRNA approaches may synergize with JAK1/2 inhibitors to improve the outcome in these diseases with currently dismal prognosis.

Activating *STAT3* mutations coordinated with silencing of *SOCS6* in NKTCLs

In our previous study we showed that SOCS6 was silenced through promoter methylation in NKCL cases and NK cells lines. The SOCS6 mRNA was expressed at low level in 5 out of 6 NK cell lines compared to resting or activated NK cells and intriguingly all NK cell lines with activating STAT3 mutations had low SOCS6 expression based on q-RT-PCR (Fig. 3-12). To address whether there is cooperation between activating *STAT3* mutations and silencing of *SOCS6* in NKCL samples in establishing constitutive activation of STAT3, we transduced the NKYS cell line which harbors a STAT3 Y640F activating mutation with the empty vector or retrovirus expressing SOCS6 and quantified the % of GFP+ cells in regular time intervals. The YT cell line is partially IL2 dependent so IL2 was removed from cell culture medium 3 days post-transduction. We observed a significant reduction of SOCS6 transduced YT cells when we compared the percentage of GFP+ cells 4 days and 8 days post-transduction whereas no change was observed for empty vector transduced cells and similarly transduced control DHL16 cells, a malignant B cell line that does not have STAT mutations (Fig. 3-13B). Next we tested the effect of SOCS6 on apoptosis by staining the empty vector or SOCS6 transduced YT cell line with early apoptotic marker Annexin V. We observed significantly higher % of AnnexinV+/GFP+ cells in SOCS6 transduced YT cells compared with empty vector transduced cells (4.5% vs 12.5% in empty vector or SOCS6 transduced cells,

respectively) (Figure 3-14A,B). To address whether SOCS6 mediated negative selection pressure is due to inhibition of the JAK-STAT3 pathway, we performed western blot analysis to evaluate P-STAT3 levels. P-STAT3 protein expression in SOCS6 transduced NKYS cells was lower compared with empty vector transduced cells (Fig 3-14C). These finding indicated that activating *STAT3* mutations cooperated with silencing of *SOCS6* in NKCL samples, resulting in enhanced activation of STAT3.

Discussion

Identification of possible oncogenic signaling pathways in malignant NK cells could give us an insight on the mechanism of the pathogenesis of NKTCL as well as suggesting potential therapeutic strategies. Previous GEP-based studies reported several aberrant activated pathway in NKTCL such as the MYC, WNT, NF-□B and TGFb pathways(Iqbal et al.). The constitutive activation of different pathways is often due to the accumulation of multiple genomic imbalances or mutations that cause the activation of oncogenes or inactivation of tumor suppressor genes. In our study, we investigated the genomic abnormalities occurring in NKTCL and γδT derived lymphoma at different levels. At the chromosomal level, we identified chromosomal copy number abnormalities such as gain/loss by aCGH. We found 6q22 loss was the most frequent abnormality in NKTCL samples. At the DNA level, we investigated epigenetic changes by analyzing global methylation profile using the "methylation-sensitive cut counting" (MSCC) assay. We identified 95 genes with strong evidence for being silenced though promoter methylation, including BCL2L11 (BIM), PTPN6 (SHP1), TET2, SOCS6, and ASNS.In this study, we investigated and compared the somatic mutation profile of NKTCL and other γδT derived lymphomas using next generation sequencing (NGS). NGS study of NKTCL and γδT should enable the identification of the full spectra of oncogenic mutations contributing to the aberrant activation of oncogenic pathways or inactivating of JAK-STAT pathways leading to the transformation of NK cells. This knowledge will aid in the development of the targeted therapies with better efficacy and less cytotoxicity.

Although *STAT3* or rarely *STAT5B* mutations have been reported in malignancies such as B-cell lymphomas(Ohgami et al., 2014), angioimmunoblastic T-cell lymphoma(Odejide et al., 2014) , $CD30^+$ T-cell lymphoma(Ohgami et al., 2013) and the indolent LGLL disease(Qiu and Fan, 2016), our study describes prevalent activating

STAT5B and STAT3 mutations in aggressive lymphomas of NK and γδ-T cell of origin. The frequency of activating *STAT3* mutations was much higher in NK (50%) and γδ-T-cell lines (67%) compared with NKTCL (5.9%) or γδ-PTCL patient samples (8.3%). This suggests that JAK-STAT3 pathway activation may be more critical in cell survival independent of stromal components and that consequently the activating mutations are selectively enriched in cell lines.

Intriguingly, *STAT5B* mutations were far more frequent in γδ T-cell lymphomas including multiple subtypes: hepatosplenic, EATL type II and other mucocutaneous γδ-PTCL (34.9%) than in NKTCL cases (5.9%). It is worth mentioning that in the 2016 revision of the World Health Organization (WHO) classification of lymphoid neoplasms, EATL type II s formally renamed as monomorphic epitheliotropic intestinal T-cell lymphoma (MEITL) due to its distinctive features. Our study showed that the STAT5B mutations were highly associated with γδMEITL. All these observations imply a pivotal role of STAT5B in γδ-PTCL pathogenesis.

Two groups reported frequent activating JAK mutations in NKTCL. In our study and other recent studies(Kimura et al., 2014), we failed to detect the JAK3 mutations in NKCLs, an in some studies JAK3 mutations were observed in a low frequency. This suggests that *JAK3* mutations may not be frequent in NKTCLs, at least in the population that we studied. This discrepancy may be due to a variety of factors including but not limited to the characterization of malignant NK samples.

Importantly, our *in vitro* functional data suggested that mutant STAT3/STAT5B, act as transcriptional activators, which contribute to the potent proliferative and survival ability of NK cells under limited IL2 condition by directly binding and upregulating genes involved in cell proliferation and cell cycle. Even though mutant STAT3/STAT5B had a higher binding potency to their target, their activation still required the phosphorylation by

upstream JAK kinase as withdrawal of IL2 result in a decrease in mutant p-STAT3/STAT5B level. However, mutant STAT3/STAT5B can form a tightly associated dimer that is resistant to inactivation by phosphatases which results in a prolonged activation of JAK-STAT pathway. Although the mutant p- STAT3/STAT5B dimers were resistant to inactivation, the activation of JAK-STAT pathway still could be regulated through upstream sites. Both JAK kinase inhibitor and ectopic expression of STAT inhibitor SOCS disrupt the positive selection effect of mutant STATs. Therefore drugs that target JAK-STAT pathway or reactivation of SOCS6 could be effective in treating NKTCL or other γδ T cell derived lymphomas. Genomic-based strategies for cancer therapy such as small interference RNA (siRNA) based therapy promise potent gene inhibition with selectivity, even down to the level of single-nucleotide variant. Therefore, mutant STATs-specific siRNA therapy may benefit NKTCL patients with particular mutations, as this approach only target tumor cells results in less potential toxicity.

A

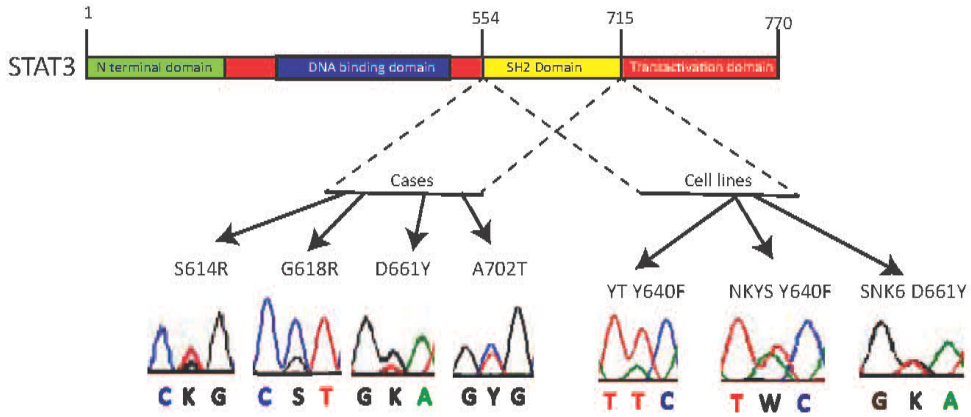
1
554
715
770
STAT3
N terminal domain
DNA binding domain
SH2 Domain
Transactivation domain
Cases
Cell lines
S614R
G618R
D661Y
A702T
YT Y640F
NKYS Y640F
SNK6 D661Y
C K G
C S T
G K A
G Y G
T T C
T W C
G K A

B

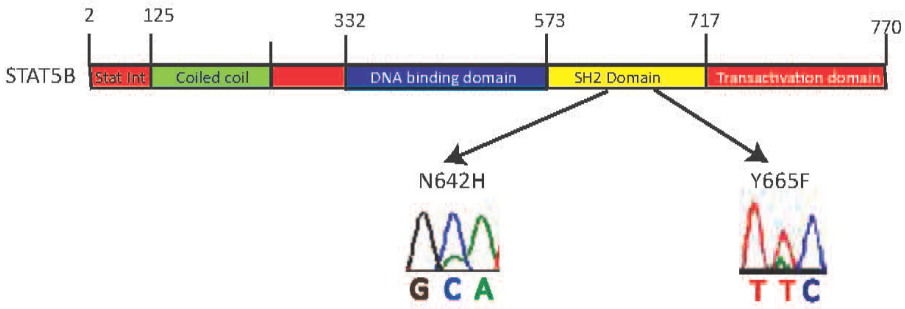
2
125
332
573
717
770
STAT5B
Stat Int
Coiled coil
DNA binding domain
SH2 Domain
Transactivation domain
N642H
Y665F
G C A
T T C

C

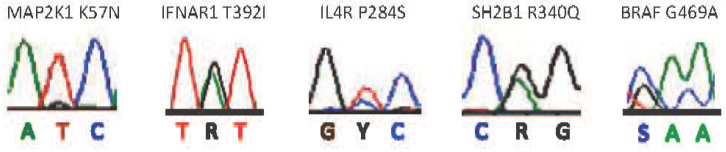
MAP2K1 K57N
IFNAR1 T392I
IL4R P284S
SH2B1 R340Q
BRAF G469A
A T C
T R T
G Y C
C R G
S A A

Figure 3-1: Activating JAK-STAT pathway mutations are frequent in NKTCL cases.

The location of the mutated residues in the SH2 domain of STAT3 (A) and STAT5B (B) and the type of residues mutated in other members of the JAK-STAT pathway genes (C) in NK-cell lines and/or NKTCL cases are shown. The chromatograms show the relative height of the sequencing peak for the mutations compared with the WT allele.

A

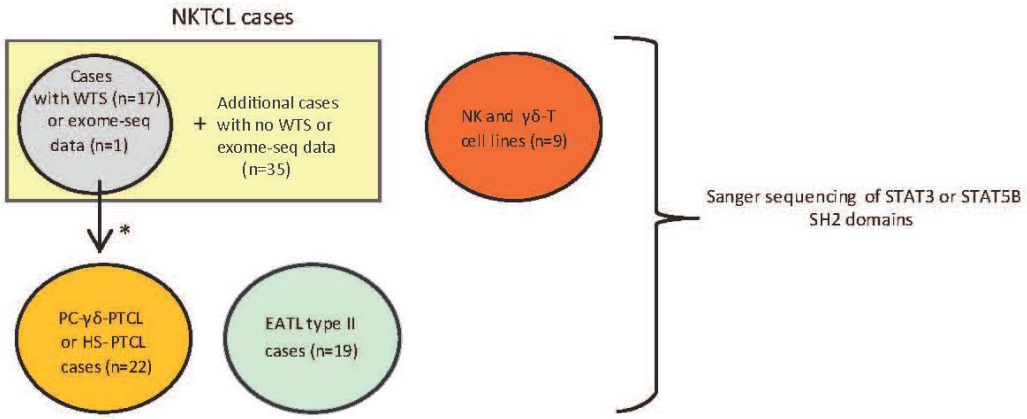
NKTCL cases
Cases with WTS (n=17) or exome-seq data (n=1)
+ Additional cases with no WTS or exome-seq data (n=35)
*
PC-γδ-PTCL or HS-PTCL cases (n=22)
EATL type II cases (n=19)
NK and γδ-T cell lines (n=9)
Sanger sequencing of STAT3 or STAT5B SH2 domains

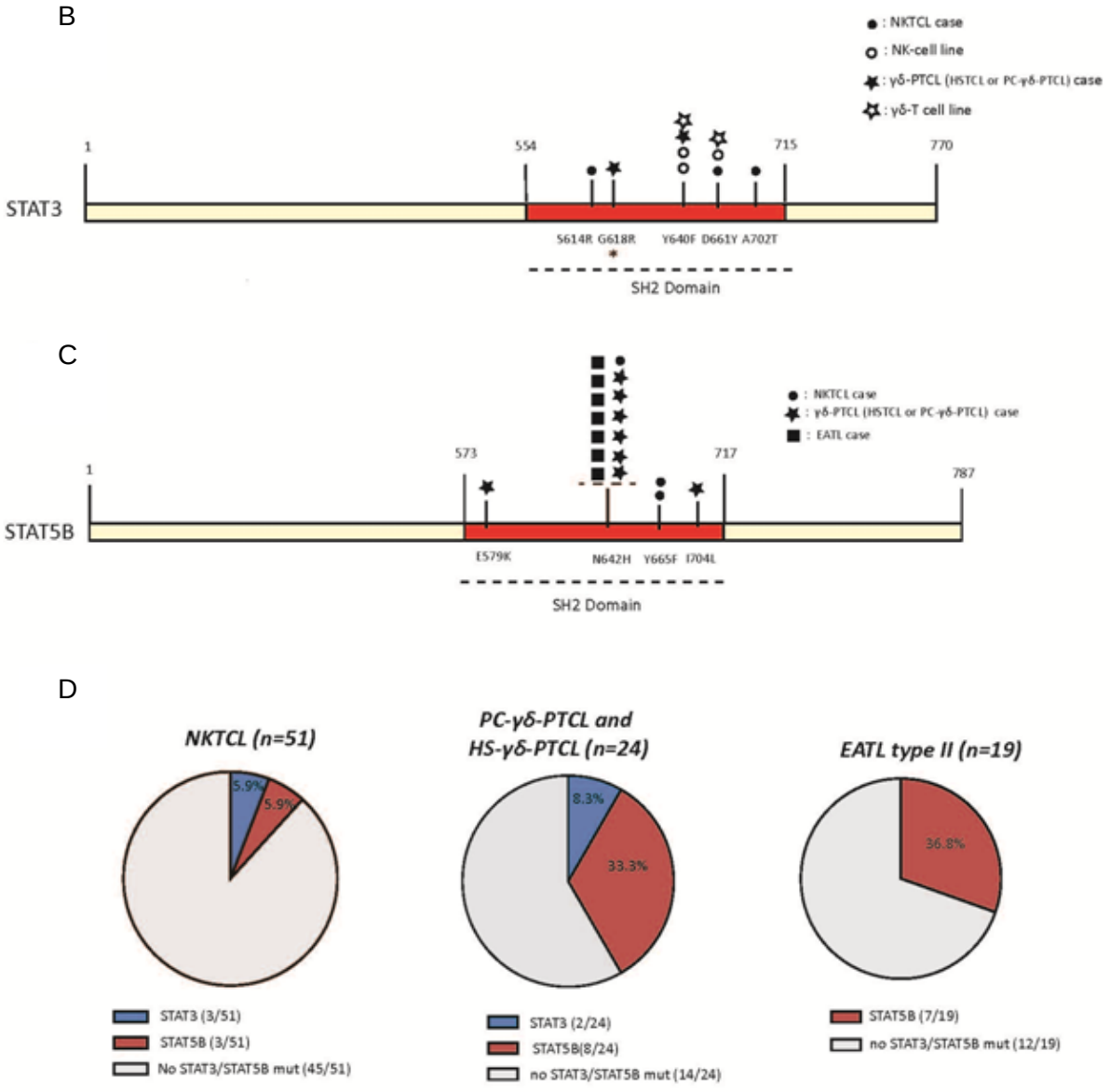
B
● : NKTCL case
○ : NK-cell line
★ : γδ-PTCL (HSTCL or PC-γδ-PTCL) case
☆ : γδ-T cell line
1
554
715
770
STAT3
S614R G618R
Y640F D661Y A702T
SH2 Domain
C
● : NKTCL case
★ : γδ-PTCL (HSTCL or PC-γδ-PTCL) case
■ : EATL case
573
717
787
1
STAT5B
E579K
N642H Y665F I704L
SH2 Domain
D
NKTCL (n=51)
5.9%
5.9%
STAT3 (3/51)
STAT5B (3/51)
No STAT3/STAT5B mut (45/51)
PC-γδ-PTCL and
HS-γδ-PTCL (n=24)
8.3%
33.3%
STAT3 (2/24)
STAT5B(8/24)
no STAT3/STAT5B mut (14/24)
EATL type II (n=19)
36.8%
STAT5B (7/19)
no STAT3/STAT5B mut (12/19)

Figure 3-2: Activating STAT3 and STAT5B mutations are frequent in lymphomas of NK or γδ-T cell of origin.

(A) The diagram shows the type of mutation analyses performed and the number of tumour samples used for each analysis. The locations of the primers used for PCR and Sanger sequencing of the *STAT3* and*STAT5B* SH2 domains are shown in. The location of the mutated nucleotides found in the SH2 domains of *STAT3* (B) and *STAT5B* (C) in tumour cases (NKTCL, γδ-PTCL (PC-γδ-PTCL and HS-γδ-PTCL) or EATL type II) and cell lines (NK and γδ-T cell lines) are shown (not to scale). Mutations of different tumour cases or cell lines are indicated with different symbols over the SH2 domains, and the disease types to which these symbols refer are shown in the upper right corner of the panels. Other than A702T, all *STAT3* mutations were reported in LGLL by Koskela *et al* and Jerez *et al* STAT5B N642H and Y665F mutations were rarely (~1%) observed in LGLL by Rajala *et al*. (D) the percentages of STAT3 and STAT5B mutations in NKTCL (*n*=51), γδ-PTCL (*n*=24) or EATL type II cases (*n*=19) are shown with pie charts. Apart from the STAT5B Y665F mutation identified using WES; all SNVs identified in this study have been cross-validated on genomic DNA with Sanger sequencing using both forward and reverse primers. *: two NKTCL tumour samples with WTS data was re-classified later as PC-γδ-PTCL due to γδ-TCR expression. One of these two reclassified cases is the sample with the STAT3-G618R mutation.

A

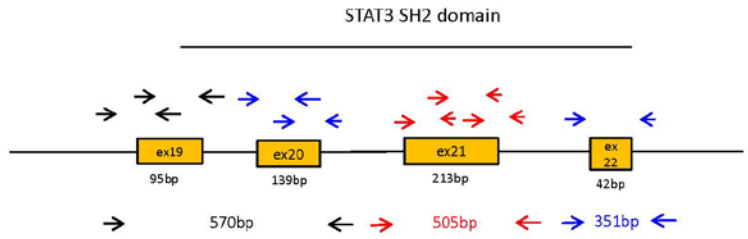
STAT3 SH2 domain
ex19
ex20
ex21
ex 22
95bp
139bp
213bp
42bp
570bp
505bp
351bp

B

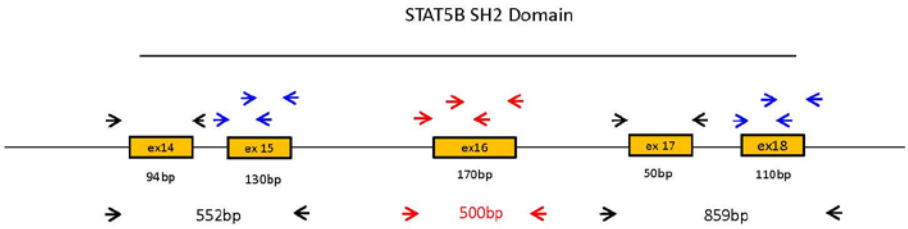
STAT5B SH2 Domain
ex14
ex 15
ex16
ex 17
ex18
94bp
130bp
170bp
50bp
110bp
552bp
500bp
859bp

Figure 3-3: The locations and amplicon sizes of Sanger primers for the exons in the SH2 domain of STAT3 and STAT5B.

(A) Primer pairs generating small size amplicons for STAT3 Sanger sequencing of FFPE tumor samples are shown as arrows above the diagram. Primer pairs generating larger size (>350 bp) amplicons used for samples with high molecular weight DNA are shown with arrows below the diagram. The colors of the arrow correspond to different exons. (B) The locations of the primer pairs used for Sanger sequencing of the STAT5B SH2 domain in FFPE tumor samples are shown as arrows above the diagram. The locations of the primer pairs generating >500bp size amplicons used for Sanger sequencing STAT5B SH2 domain in cyropreserved NKTCL or γδ-PTCL samples are shown as arrows below the diagram.

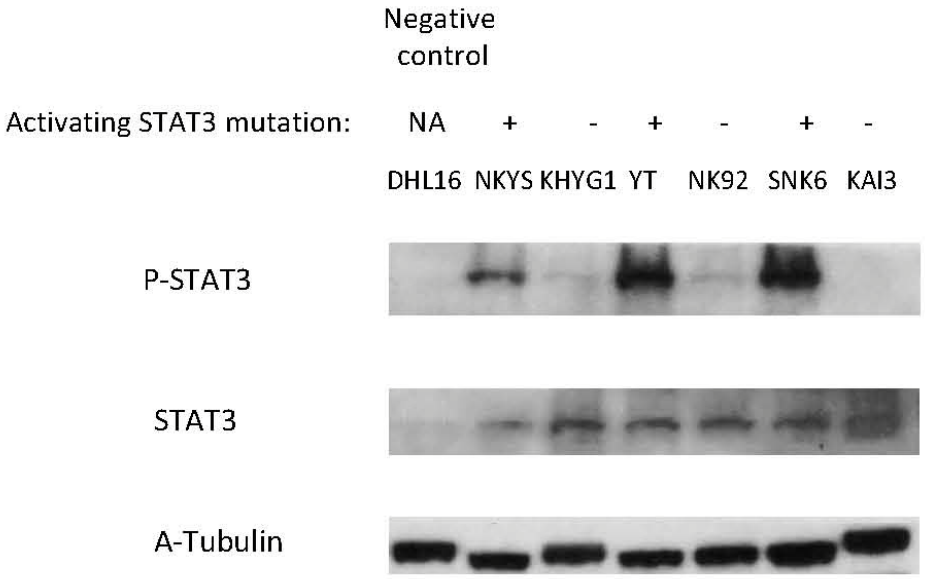
Negative control
Activating STAT3 mutation:
NA + - + - + -
DHL16 NKYS KHYG1 YT NK92 SNK6 KAI3
P-STAT3
STAT3
A-Tubulin

Figure 3-4: NK cell lines with STAT3 mutations show high STAT3 activation.

Western blot was performed on whole cell lysates (WCL) from 6 NK cell lines using phospho tyrosine (Y705)-STAT3 and STAT3 antibodies. The germinal center B cell line, DHL16, which does not have STAT3 activation was used as a negative control. α-Tubulin was used to ensure equal loading of the samples. The name of the cell lines used is indicated on top of the gel image. The presence or absence of activating STAT3 mutations is shown with (+) or (-) signs, respectively. NA: Not available.

A

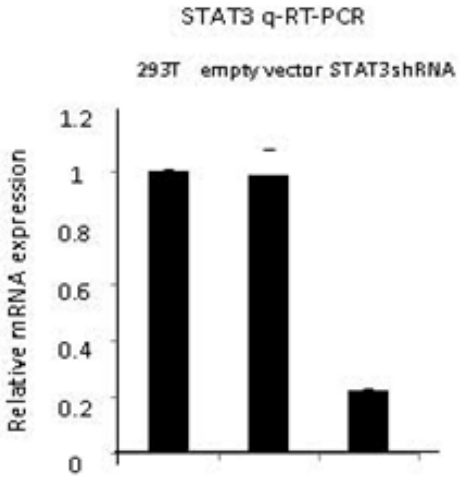
STAT3 q-RT-PCR
293T empty vector STAT3shRNA
Relative mRNA expression
1.2
1
0.8
0.6
0.4
0.2
0

B

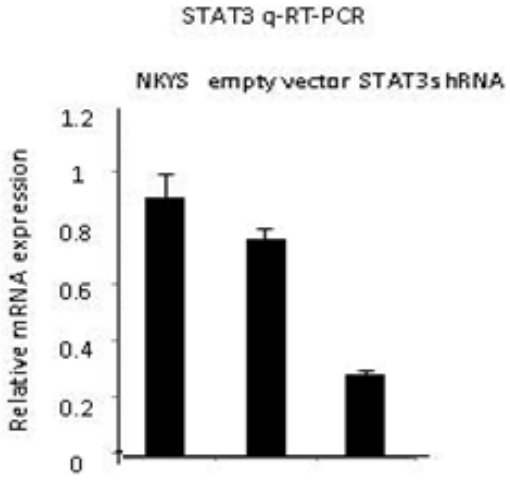
STAT3 q-RT-PCR
NKYS empty vector STAT3shRNA
Relative mRNA expression
1.2
1
0.8
0.6
0.4
0.2
0

Figure 3-5: STAT3 knock-down efficiency in 293T and NKYS cells

(A) STAT3 knock-down efficiency was evaluated with q-RT-PCR on STAT3 shRNA transfected 293T cells. STAT3 mRNA levels in STAT3 shRNA transfected 293T cells were normalized to STAT3 expression in untrasnfected cells and compared with empty vector transfected cells 51 h after transfection. (B) Evaluation of the STAT3 knock-down efficiency in NKYS cells transduced with empty vector or STAT3 shRNA. STAT3 shRNA transduced NKYS cells were purified by FACS sorting 3 days post-transduction to enrich GFP+ cells. STAT3 mRNA expression was determined using FACS sorted NKYS cells transduced with empty vector or STAT3 shRNA. Unsorted NKYS cells were used to normalize STAT3 expression.

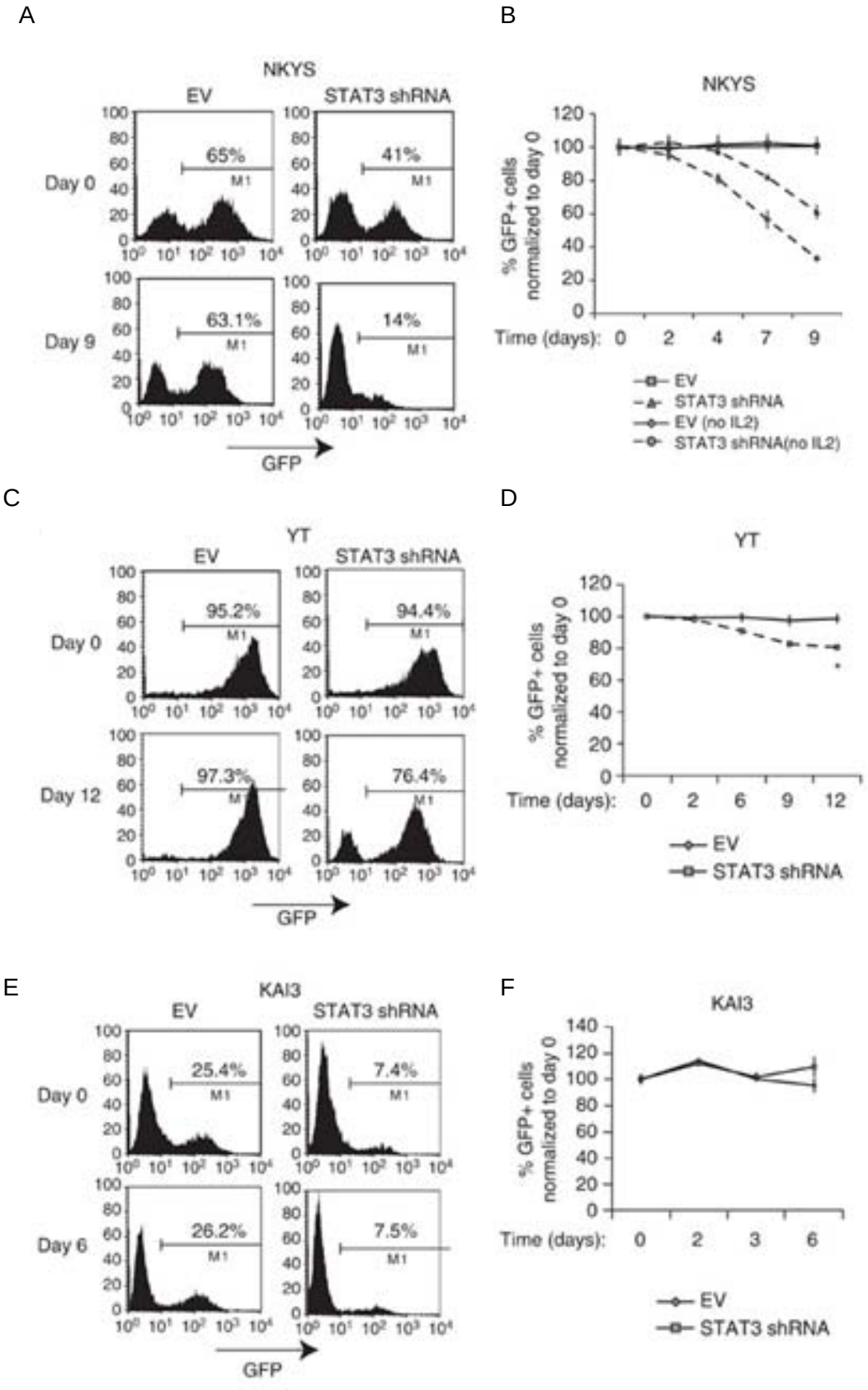
A
NKYS
EV
STAT3 shRNA
Day 0
Day 9
65%
41%
63.1%
14%
M1
GFP
B
NKYS
% GFP+ cells normalized to day 0
Time (days): 0 2 4 7 9
EV
STAT3 shRNA
EV (no IL2)
STAT3 shRNA(no IL2)
C
YT
EV
STAT3 shRNA
Day 0
Day 12
95.2%
94.4%
97.3%
76.4%
M1
GFP
D
YT
% GFP+ cells normalized to day 0
Time (days): 0 2 6 9 12
EV
STAT3 shRNA
E
KAI3
EV
STAT3 shRNA
Day 0
Day 6
25.4%
7.4%
26.2%
7.5%
M1
GFP
F
KAI3
% GFP+ cells normalized to day 0
Time (days): 0 2 3 6
EV
STAT3 shRNA

G


NKYS
YT
KAI3
PLVTH S3S
PLVTH S3S
PLVTH S3S
STAT3
— 80 kDa
α-Tubulin
— 50 kDa

H

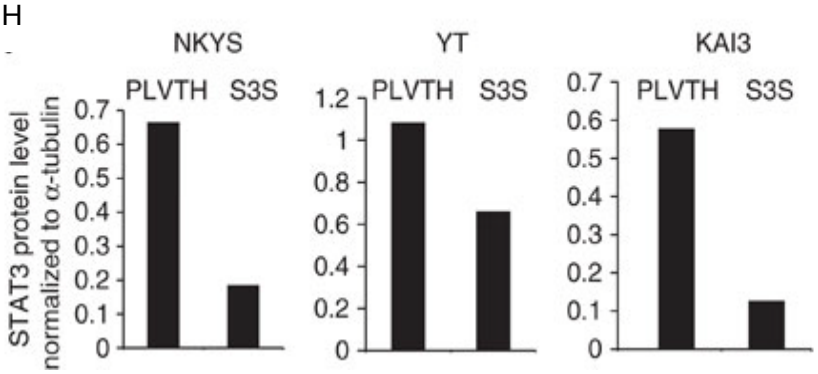
NKYS
YT
KAI3
PLVTH S3S
PLVTH S3S
PLVTH S3S
STAT3 protein level normalized to α-tubulin
0.7
0.6
0.5
0.4
0.3
0.2
0.1
0
1.2
1
0.8
0.6
0.4
0.2
0

Figure 3-6: NK-cell lines with STAT3 mutations show high pY-STAT3 expression and shRNA- mediated knock-down of STAT3 inhibits NK-cell line growth

(A) Representative flow cytometric plots showing the percentage of GFP^+ cells 3 days (day 0) and 12 days (day 9) post-transduction of NKYS cells with empty vector (EV) or STAT3 shRNA after removing IL2 from the culture medium at day 0. (B) Quantification of the percentage of GFP^+ cells post-transduction of NKYS cells with empty vector or STAT3 shRNA at regular time intervals. In one experiment, cells were cultured in the presence of IL2 (5-7 ng/ml) until 3 days (day 0) post-transduction and then IL2 was removed from the culture medium. In the second experiment, IL2 was always included post-transduction of NKYS cells. Each data point is representative of two biological replicates. (C) Representative FACS plots showing the percentage of GFP^+ cells of YT cell line transduced with empty vector or STAT3 shRNA 3 days (day 0) or 15 days (day 12) post-transduction. (D) Quantification of the percentage of GFP^+ cells by FACS between 3 and 15 days post-transduction with empty vector or STAT3 shRNA. For one week before transduction, YT cells were cultured in the presence of IL2. Three days post-transduction (day 0), cells were transferred to medium lacking IL2. (E) Representative FACS plots showing the percentage of GFP^+ cells in empty vector or STAT3 shRNA transduced KAI3 cells. (F) Quantification of the percentage of GFP^+ cells after transduction of KAI3 cells with empty vector or STAT3 shRNA. 3 days post-transduction (day 0), the percentage of GFP^+ cells was determined by flow cytometry, and cells were switched to NK culture medium with reduced IL2 (25 IU/ml).

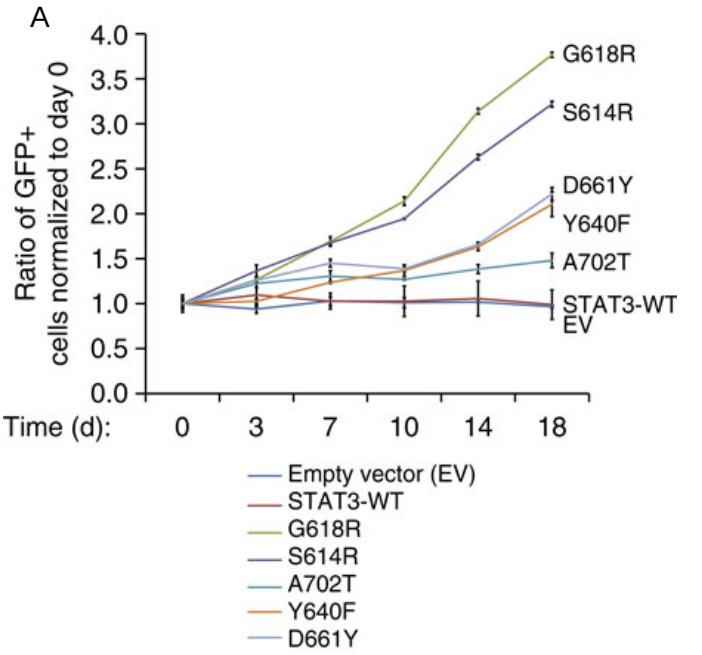
A
Ratio of GFP+ cells normalized to day 0
4.0
3.5
3.0
2.5
2.0
1.5
1.0
0.5
0.0
Time (d):
0
3
7
10
14
18
G618R
S614R
D661Y
Y640F
A702T
STAT3-WT
EV
Empty vector (EV)
STAT3-WT
G618R
S614R
A702T
Y640F
D661Y

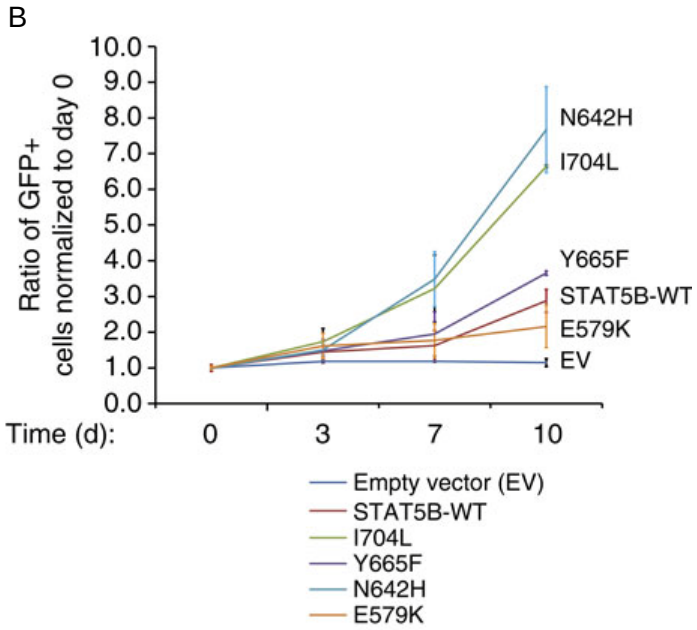
B
Ratio of GFP+ cells normalized to day 0
10.0
9.0
8.0
7.0
6.0
5.0
4.0
3.0
2.0
1.0
0.0
Time (d):
0
3
7
10
N642H
I704L
Y665F
STAT5B-WT
E579K
EV
Empty vector (EV)
STAT5B-WT
I704L
Y665F
N642H
E579K

C

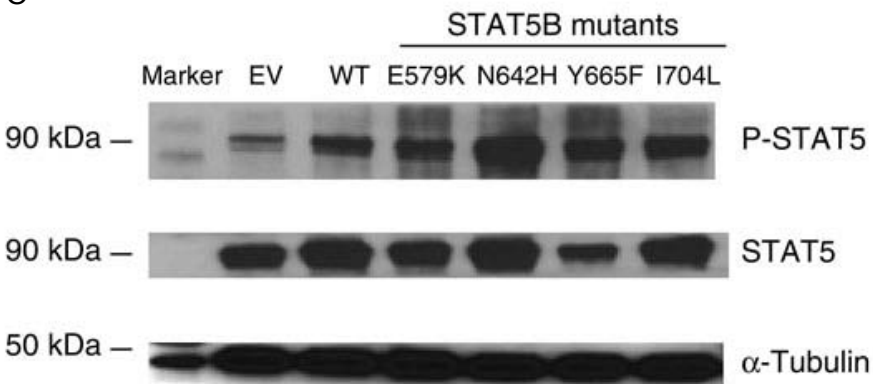
STAT5B mutants
Marker
EV
WT
E579K
N642H
Y665F
I704L
90 kDa —
P-STAT5
90 kDa —
STAT5
50 kDa —
α-Tubulin

Figure 3-7: Ectopic expression of STAT3 or STAT5B mutants promotes growth in KAI3 cells under limiting IL2 concentrations.

(A) Quantification of the percentage of GFP^+ cells post-transduction of KAI3 cells with each STAT3 mutant observed in tumor samples. Transduced cells were cultured in regular IL2 concentrations for 4 days, then switched to limiting (25 IU) IL2 concentrations. Day 0 = 4 days post-transduction. Each data point shows the mean of biological replicates. The average values for the % of GFP^+ cells at day 0 were 6.9%, 3.2%, 6.0%, 2.8%, 4.1%, 4.3% and 3.2% for EV, STAT3-WT, S614R, G618R, Y640F, D661Y or A702T transduced cells, respectively. (B) Quantification of the percentage of GFP^+ cells post-transduction of KAI3 cells with each STAT5B mutant observed in tumor samples as in A. Means ±SD of 2 independent experiments with replicates are shown (n=4). The average values for the % of GFP^+ cells at day 0 were 4.8% ,6.8% , 5.9%, 5.7%, 8.2%, 6.7% for EV, STAT5B-WT, E579K, N642H, Y665F or I704L-mutant transduced cells, respectively. The percentage of GFP^+ cells for each sample is normalized to day 0 in both A and B. (C) P-STAT5 (Y699) and STAT5 protein expression levels in KAI3 cells transduced with STAT5B mutants are shown by western blot. Six days post-transduction, the GFP^+ population of STAT5B-mutant transduced cells was isolated by FACS, and then placed into culture medium with limiting (25 IU/ml) concentrations. Whole cell lysates were collected 11 days post-transduction. One experiment representative of three experiments is shown.

A

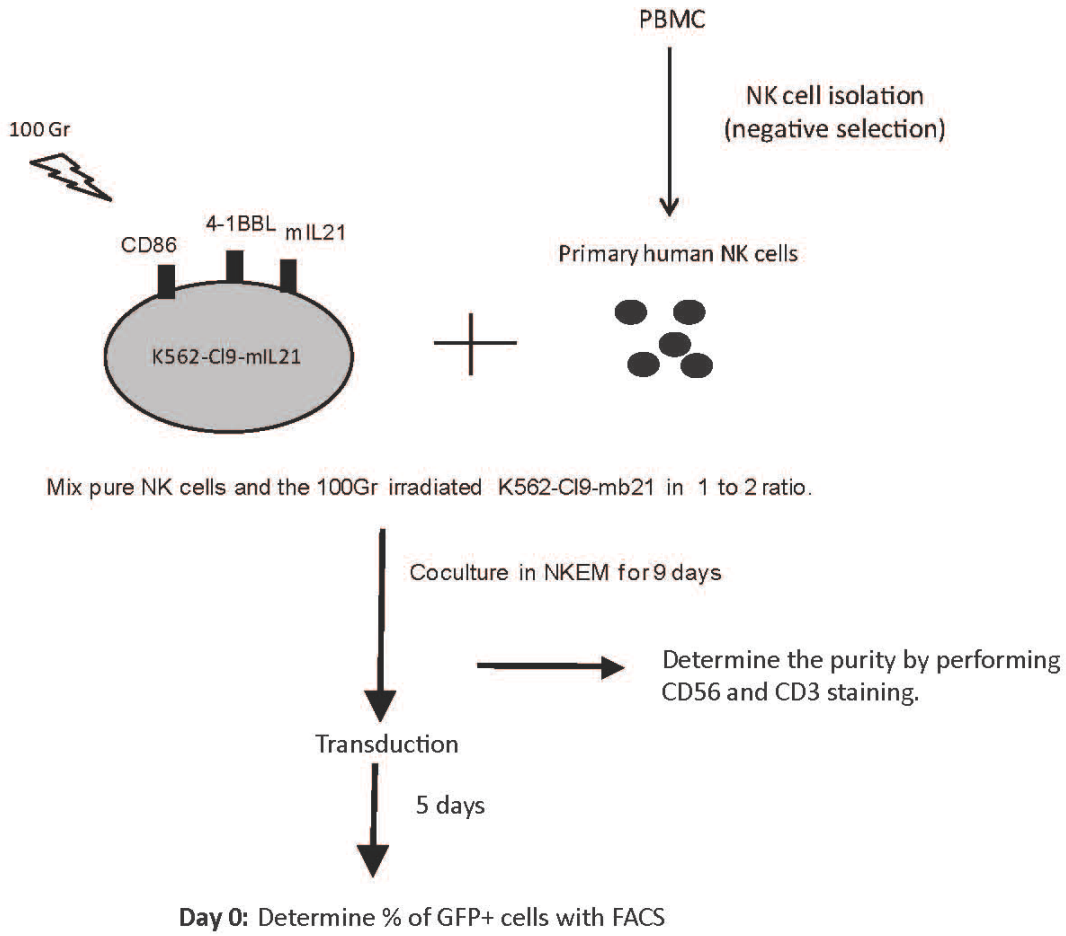
PBMC
NK cell isolation
(negative selection)
100 Gr
4-1BBL
mIL21
CD86
Primary human NK cells
K562-Cl9-mIL21
Mix pure NK cells and the 100Gr irradiated K562-Cl9-mb21 in 1 to 2 ratio.
Coculture in NKEM for 9 days
Determine the purity by performing
CD56 and CD3 staining.
Transduction
5 days
Day 0: Determine % of GFP+ cells with FACS

B

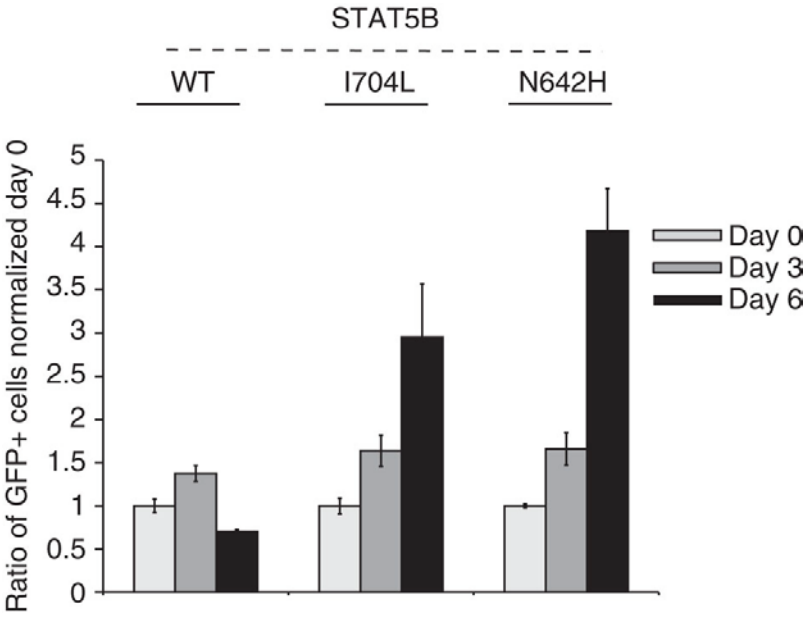
STAT5B
WT
I704L
N642H
Ratio of GFP+ cells normalized day 0
5
4.5
4
3.5
3
2.5
2
1.5
1
0.5
0
Day 0
Day 3
Day 6

Figure 3-8: Ectopic expression of STAT5B I704L or N642H mutants promotes growth of primary human NK cells

(A) Schematic representation of the coculture system used to activate and condition NK-cells for retroviral transduction with N642H or I704L mutant forms of STAT5B. Pure NK cells isolated from PBMCs were admixed with 100 Gr-irradiated engineered K562 cells, K562-Cl9-mb21, as shown. Characterization of K562-Cl9-mb21 cells used to induce proliferation of primary human NK cells was performed before(Somanchi et al., 2011). The purity of NK cells ($CD56^+/CD3^-$ cells) was ~94%. (B) Quantification of the percentage of GFP^+ cells post-transduction of primary NK cells with STAT5B-WT or each of two STAT5B mutants (I704L or N642H) at three-day intervals. The percentage of GFP^+ cells for each sample is normalized to day 0. Day 0 indicates 5 days post-transduction. The average % of GFP^+ cells at day 0 was 4.6%, 4.9% and 4.8% for STAT5B-WT, N642H or I704L-transduced cells, respectively. Data are means ±SD of biological replicates. Dead cells were stained with 0.5 µM of DAPI (Biolegend, cat.no: 422801) to exclude them from quantification.

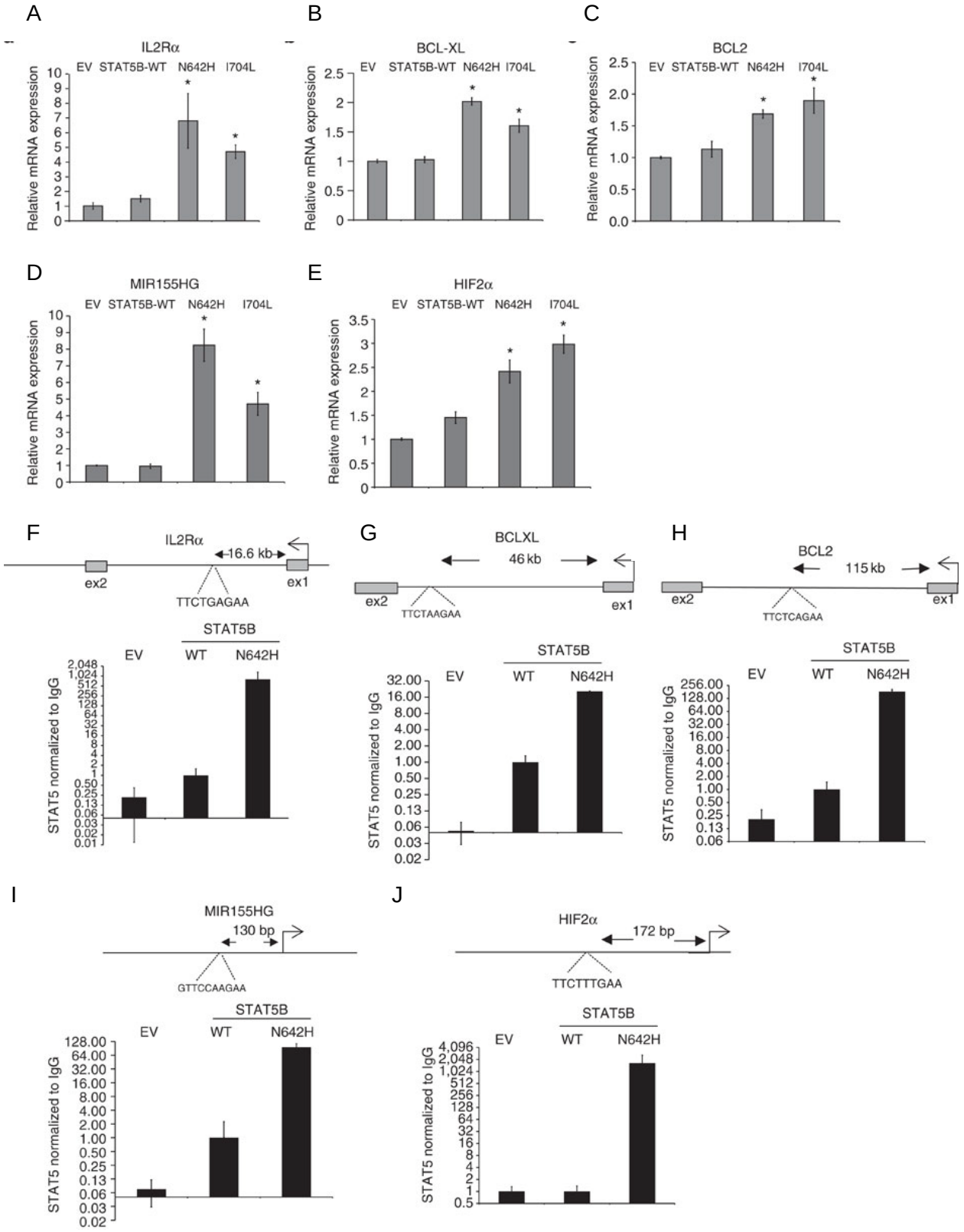
A
IL2Rα
EV STAT5B-WT N642H I704L
Relative mRNA expression
B
BCL-XL
EV STAT5B-WT N642H I704L
Relative mRNA expression
C
BCL2
EV STAT5B-WT N642H I704L
Relative mRNA expression
D
MIR155HG
EV STAT5B-WT N642H I704L
Relative mRNA expression
E
HIF2α
EV STAT5B-WT N642H I704L
Relative mRNA expression
F
IL2Rα
16.6 kb
ex2
ex1
TTCTGAGAA
STAT5B
EV WT N642H
STAT5 normalized to IgG
G
BCLXL
46 kb
ex2
ex1
TTCTAAGAA
STAT5B
EV WT N642H
STAT5 normalized to IgG
H
BCL2
115 kb
ex2
ex1
TTCTCAGAA
STAT5B
EV WT N642H
STAT5 normalized to IgG
I
MIR155HG
130 bp
GTTCCAAGAA
STAT5B
EV WT N642H
STAT5 normalized to IgG
J
HIF2α
172 bp
TTCTTTGAA
STAT5B
EV WT N642H
STAT5 normalized to IgG

Figure 3-9: STAT5B target genes are transcriptionally upregulated in STAT5B-mutant transduced cells through direct binding to conserved STAT5 binding sites

Relative mRNA expression of *IL2Rα* (A), *BCL-XL* (B), *BCL2* (C), *MIR155HG* (D) and, *HIF2α* (E) is shown in control vector or STAT5B-mut transduced cells prepared as described in A. Means ± SD of two independent experiments (total combined samples = 4) are shown. * = $p<0.01$ and ** = $p<0.05$ compared to WT. ChIP-q-PCR results for known STAT5 binding sites are shown for *IL2Rα (*F*), BCL-XL* (G), *BCL2* (H), *MIR155HG* (I) *and HIF2α* (J) in EV, STAT5B-WT or STAT5B-N642H transduced KAI3 cells. STAT5 pull-down normalized to IgG control as a fold difference compared with the STAT5B-WT sample is shown in the y-axis using a log scale. STAT5B consensus sites and their approximate distance to the TSS sites are indicated.

A B C

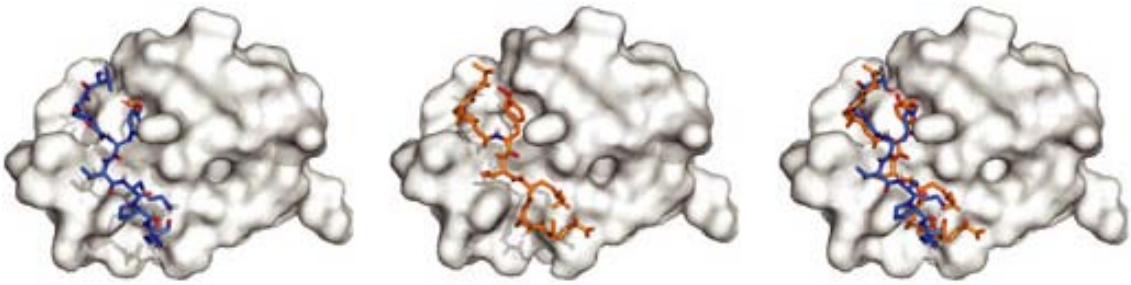

D

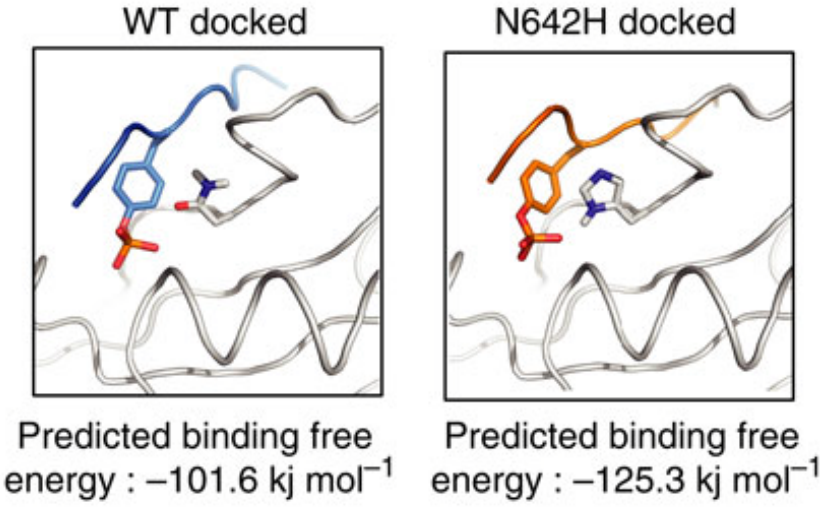
WT docked
N642H docked
Predicted binding free energy : –101.6 kj mol^{-1}
Predicted binding free energy : –125.3 kj mol^{-1}

E

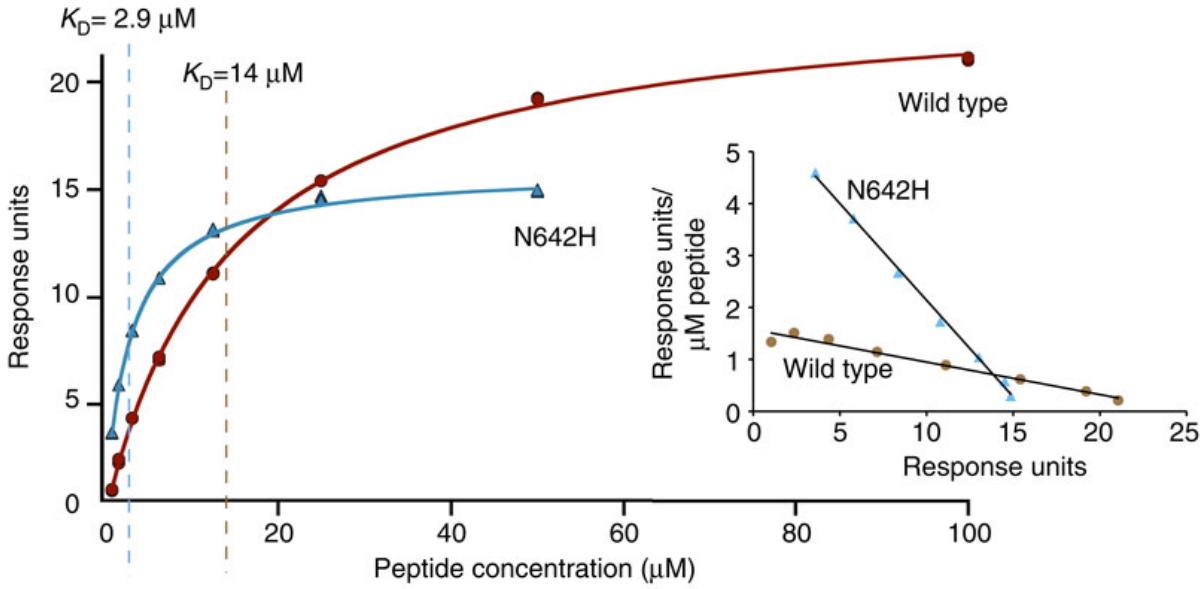
K_D= 2.9 µM
K_D=14 µM
Wild type
N642H
Response units
Peptide concentration (µM)
0
5
10
15
20
0
20
40
60
80
100
Response units/ µM peptide
N642H
Wild type
0
1
2
3
4
5
0
5
10
15
20
25
Response units

F

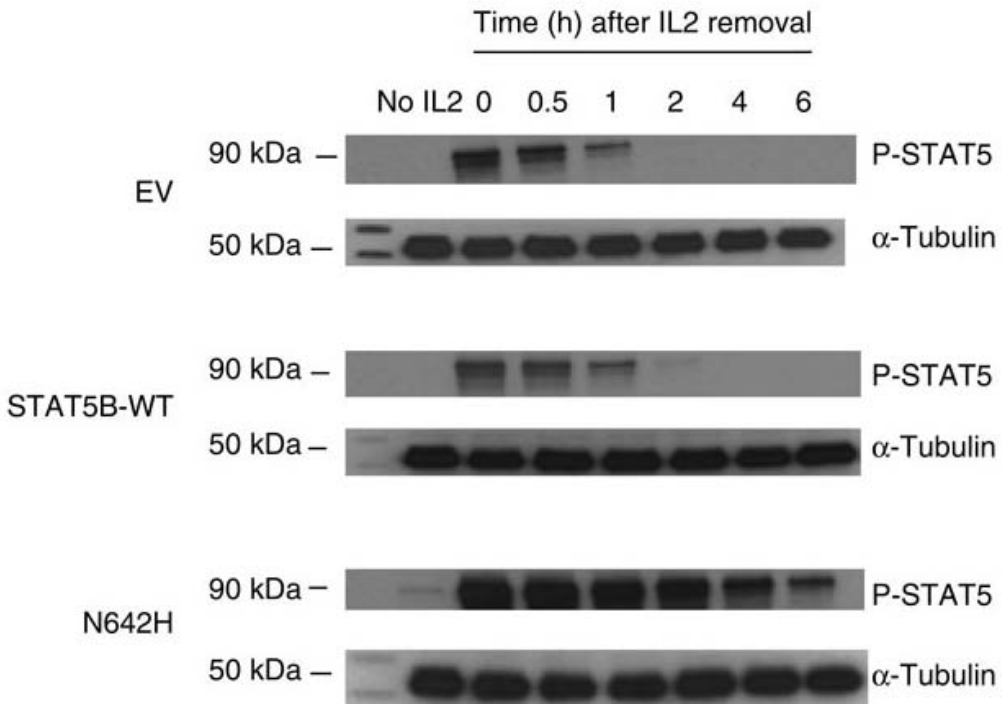
Time (h) after IL2 removal
No IL2 0 0.5 1 2 4 6
EV
90 kDa
P-STAT5
50 kDa
α-Tubulin
STAT5B-WT
90 kDa
P-STAT5
50 kDa
α-Tubulin
N642H
90 kDa
P-STAT5
50 kDa
α-Tubulin

Figure 3-10: Three-dimensional modeling and SPR analysis of the N642H mutant shows stronger affinity for the phosphorylated tyrosine Y699

The phosphorylated STAT5B peptide involved in homodimerization was docked into the SH2 domain of either WT (A) or N642H (B) STAT5B. The overlay of these structures (C) shows little difference in the docking poses. In both cases, the N642 or H642 residue was found to be in close proximity to the phosphorylated tyrosine on the STAT5B peptide (D). The binding energy of these docked structures was calculated for both the WT (-101.5 kj/mol) and N642H (-125.3 kj/mol). (E) SPR binding isotherms of phosphopeptide with STAT5B WT (brown circles) and N642 mutant (blue triangles). Calculated K_D values of 14 µM and 2.9 µM for STAT5B WT and N642H mutant, respectively, are indicated by vertical lines. An inset shows the Scatchard plot of the same data (F) Western blot image showing P-STAT5(Y699) and STAT5 levels before or after culturing empty vector (EV), STAT5B-WT or N642H mutant transduced, GFP-sorted YT cells in the absence (no IL2) or the presence of IL2. YT cells were cultured in the absence of IL2 in each stage of the experiment including one week before transduction. The image is representative of two independent western blots.

A

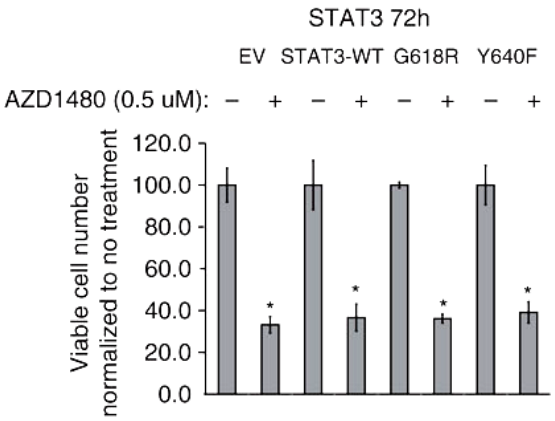
STAT3 72h
EV STAT3-WT G618R Y640F
AZD1480 (0.5 uM): – + – + – + – +
Viable cell number normalized to no treatment
120.0
100.0
80.0
60.0
40.0
20.0
0.0
*

B

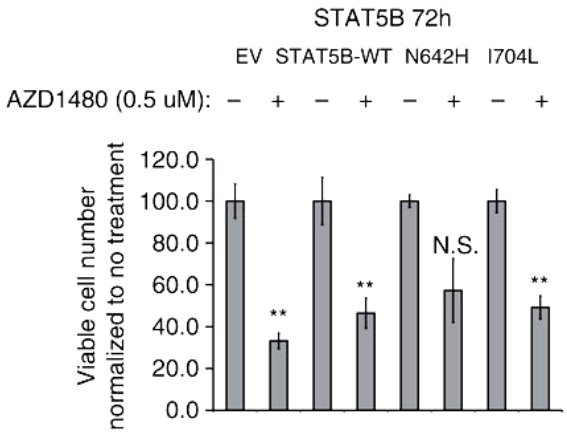
STAT5B 72h
EV STAT5B-WT N642H I704L
AZD1480 (0.5 uM): – + – + – + – +
Viable cell number normalized to no treatment
120.0
100.0
80.0
60.0
40.0
20.0
0.0
**
N.S.

C

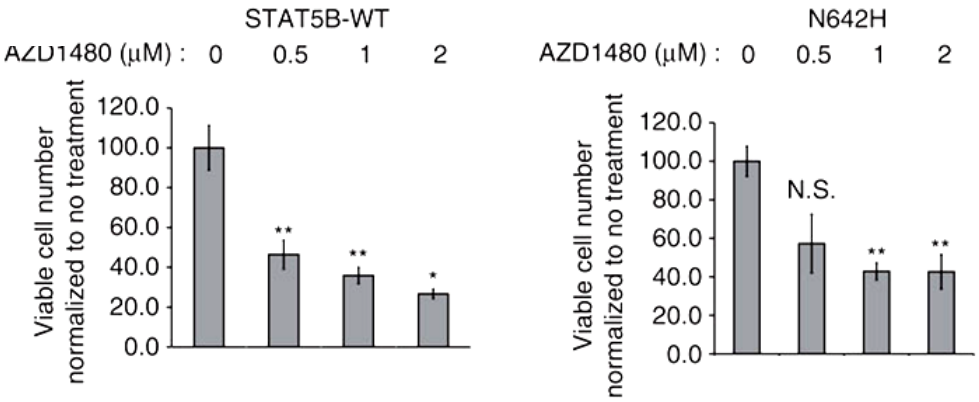
STAT5B-WT
AZD1480 (μM) : 0 0.5 1 2
Viable cell number normalized to no treatment
120.0
100.0
80.0
60.0
40.0
20.0
0.0
**
**
*
N642H
AZD1480 (μM) : 0 0.5 1 2
Viable cell number normalized to no treatment
120.0
100.0
80.0
60.0
40.0
20.0
0.0
N.S.
**
**

D

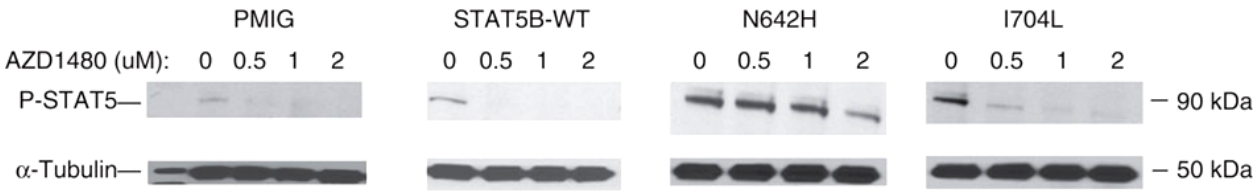
PMIG
STAT5B-WT
N642H
I704L
AZD1480 (uM): 0 0.5 1 2
0 0.5 1 2
0 0.5 1 2
0 0.5 1 2
P-STAT5—
— 90 kDa
α-Tubulin—
— 50 kDa

E

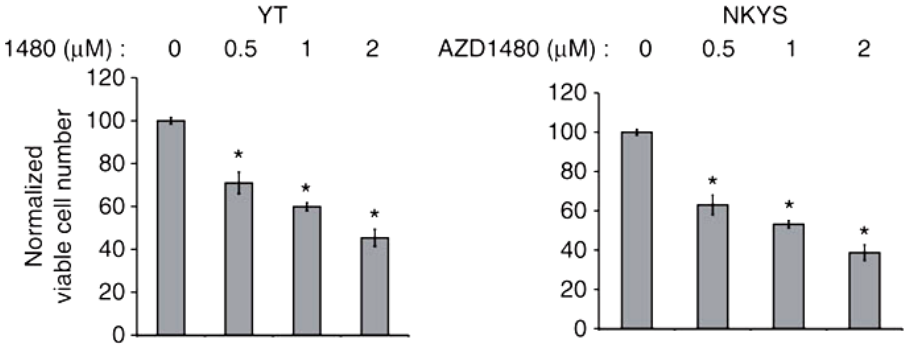
YT
1480 (μM) : 0 0.5 1 2
Normalized viable cell number
120
100
80
60
40
20
0
*
*
*
NKYS
AZD1480 (μM) : 0 0.5 1 2
120
100
80
60
40
20
0
*
*
*

Figure 3-11: AZD1480 inhibits STAT3/STAT5B mutant transduced NK cells

25,000 STAT3-mutant (A) or STAT5B-mutant (B) transduced, GFP^+-sorted KAI3 cells were treated with 0.5 µM AZD1480 in 2ml medium for 72 h. Dead cells were stained with trypan blue , viable cell number was determined using Vi-cell XR cell viability analyzer (Beckman Coulter Inc.) and normalized to the corresponding untreated sample. Means ± SD of two biological replicates are shown. (C) Normalized viable cell number of STAT5B-WT (left) or N642H mutant (right) transduced KAI3 cells treated with progressively increasing doses of AZD1480 for 72 h. Each column represents mean ± SD of three biological replicates. (D) P-STAT5 (Y699) levels were analyzed by western blot on empty vector (EV), STAT5B-WT, N642H or I704L transduced KAI3 cells treated with progressively increasing doses (0.5 µM,1 µM or 2 µM) of AZD1480 for 4h (E) Normalized numbers of viable STAT3-mutated NKYS and YT cells treated as in (C) are shown *: $P<0.01$ vs no treatment; **: $p<0.05$ vs no treatment. N.S.: Not significant.

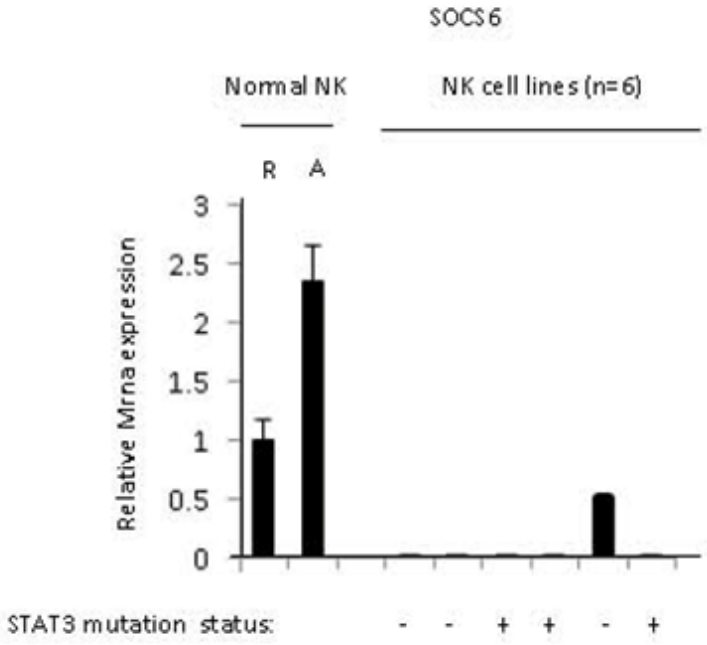

R: Resting NK cells

A: 48h IL2 activated NK cells

Figure 3-12: q-RT-PCR shows *SOCS6* silencing in 5 of 6 NK cell lines.

R: Resting NK cells, A: 48h IL2 activated normal NK cells. The STAT3 mutation status is indicated with a (+) or (-) sign for each NK cell line. A (+) sign indicates the presence of the mutation.

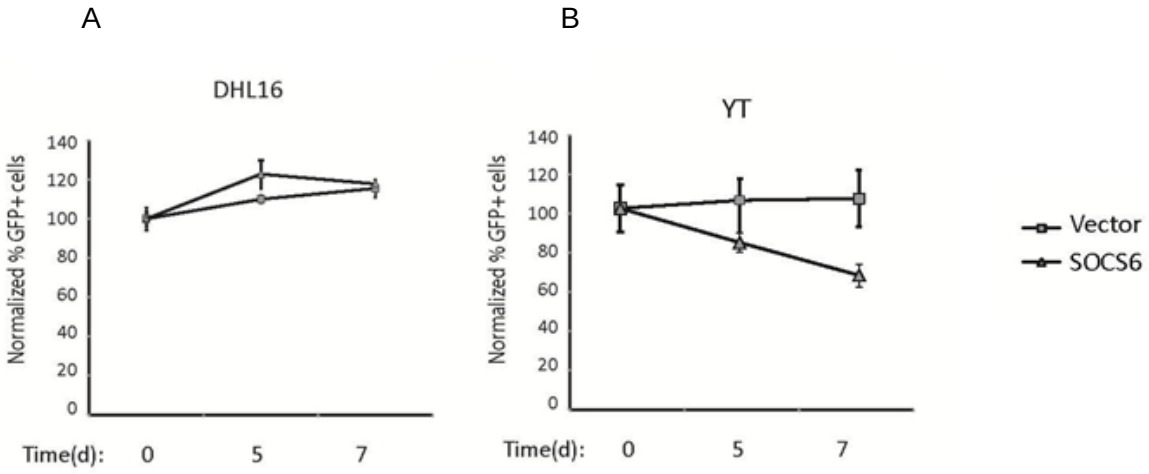
A
B
DHL16
YT
Normalized % GFP+ cells
140
120
100
80
60
40
20
0
Time(d): 0 5 7
Vector
SOCS6

Figure 3-13: Ectopic expression of SOCS6 is associated with negative selection pressure in NK cell lines with STAT3 mutations.

(A) Quantification of the % of GFP+ population in empty vector or SOCS6 transduced YT cells at 2 day intervals for 4 days. Mean (+/- SD) was shown. Each data point represents 2-4 biological replicates. (B) Quantification of the % of GFP+ population in empty vector or SOCS6 transduced DHL16 cells at 5 days and 7 days post transduction. Mean (+/- SD) was shown. Each data point represents 2-4 biological replicates.

A

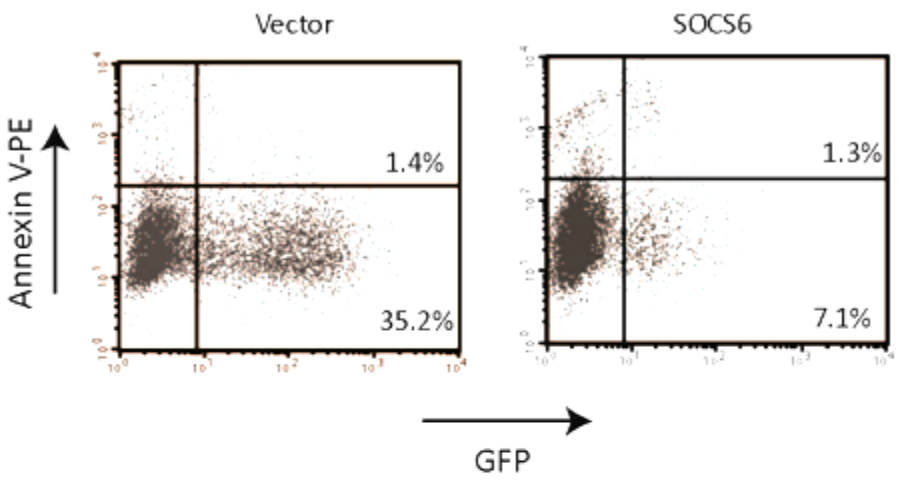
Vector
SOCS6
Annexin V-PE
1.4%
35.2%
1.3%
7.1%
GFP

B

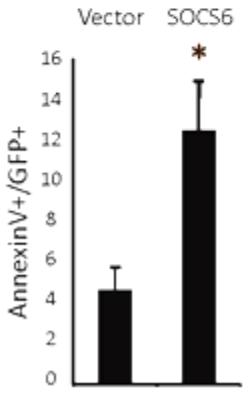
Vector
SOCS6
*
AnnexinV+/GFP+
16
14
12
10
8
6
4
2
0

C

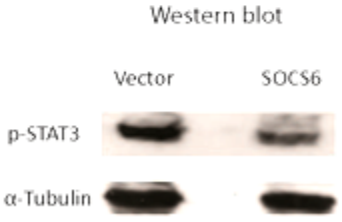
Western blot
Vector
SOCS6
p-STAT3
α-Tubulin

Figure 3-14: Ectopic expression of SOCS6 induces apoptosis in NK cell lines with STAT3 mutations.

(A)A representative plot for AnnexinV-PE staining on GFP gated cells is shown for empty vector or SOCS6 transduced YT cells 3 days post-transduction. (B) Quantification of the % of AnnexinV+/GFP+ population in YT cells transduced with empty vector or SOCS6 3 days post-transduction. Each data point represents a combination of biological replicate with two technical replicates (n=4). *=p= 0.001. (C) NKYS cells were transduced twice with empty vector or SOCS6 and GFP+ cells were sorted with FACS two or four days post-transduction. Western blot was performed on GFP sorted vector or SOCS6 transduced cells using P-STAT3 antibody. α-Tubulin was used as a loading control to ensure equal loading.

Chapter IV

Role of Blimp1 in NK cells homeostasis and function

Introduction

Extranodal NK/T- cell lymphoma is an aggressive lymphoma with poor prognosis. Studies revealed that this type of lymphoma is derived from cytotoxic lymphocytes of both NK- and T-cell lineages. Nasal NK-cell lymphomas are either CD3-CD56+ or CD3+(cytoplasmic),CD56+ and lack T cell receptor (TCR)γ and immunoglobulin heavy chain gene (IgH) clonal rearrangement, whereas nasal T-cell lymphomas are either sCD3+CD56+ or sCD3+CD56- with clonally rearranged TCRγ and germ-line IgH(Metgud et al., 2011). Even though its molecular background has been investigated in the last few years, the pathogenesis of NK/T cell lymphoma is still largely unknown. A distinctive feature of this disease is the strong association with Epstein–Barr virus infection; EBV is positive in 100% of NKCL cases by *in situ* hybridization for EBV-encoded small non-polyadenylated RNAs (EBER) (Chiang et al., 1996). However, the role of EBV infection in the pathogenesis of NKTCL is still not clear; the EBV-infected cells frequently express latent membrane protein 1 (LMP1), which activate several downstream signaling pathways such as NF-*κ*B pathway that are likely involved in NK/T-cell activation and proliferation(Chen, 2012). These LMP1-expressing proliferating cells are able to escape from elimination by host cytotoxic T- lymphocytes (CTLs)(Young et al., 1989). Other proteins that are expressed include Epstein–Barr virus nuclear antigen 1

(EBNA1) and latent membrane protein 2 (LMP2), and they may also be involved in NKTCL (Ian et al., 2008, Fox et al., 2010).Genetic abnormalities leading to the activation of oncogenes and inactivation of tumor suppressor genes likely play an important role in NK/T cell malignant transformation.

In our previous studies, we found that PR domain zinc finger protein 1 (PRDM1) was inactivated in NKTCL by the combination of chromosomal deletion and promoter hypermethylation in 44% of NKTCL cases, and in vitro studies demonstrated that

PRDM1 is a tumor suppressor gene in NKTCL(Kucuk et al., 2011). The encoded protein, PRDM1, also known as B lymphocyte-induced maturation protein 1(Blimp1), is a transcriptional repressor that has various effects on the function and homeostasis of B cells and T cells(Martins and Calame, 2008) and is frequently inactivated in B-cell malignancies such as diffuse large B cell lymphoma (DLBCL)(Pasqualucci et al., 2006).In B cells, Blimp-1 is expressed in plasmablasts and all plasma cells, and is a master regulator of the differentiation of B cells into immunoglobubin secreting cells(Savitsky and Calame, 2006). Conditional knockout of Blimp1 using cre-loxp system in the mouse resulted in the development of lymphoproliferative disorder including DLBCL (Mandelbaum et al., 2010). In T cells, Blimp1 expression increases in antigen-activated CD8+ and CD4+ T-cells and some CD25+ regulatory T-cells(Ozaki et al., 2004, Kallies et al., 2006) , and is important for T cell homeostasis and effector functions. Expression of Blimp1 was upregulated upon TCR stimulation. Blimp1-deficient T cells proliferated more and produced excess IL2 and IFNγ. Mice lacking Blimp1 in their T cells had more peripheral effector T cells and developed an inflammatory disease (Ozaki et al., 2004, Kallies et al., 2006).

Unlike in T and B cells, Blimp1 is expressed in NK cells in all stages and upregulated in mature or activated NK cell subsets. In our previous study, we observed an increase in PRDM1 expression in activated NK cells, and knocking down PRDM1 resulted in a positive selection of NK cells. Whereas ectopic PRDM1 expression in PRDM1-null NK cell lines resulted in G2/M cell cycle arrest, increased apoptosis, and a strong negative selection. These finding, along with the observation that PRDM1 was inactivated in NKTCL, indicated that PRDM1 is a potential tumor suppressor gene in NKTCL. A recent study using chimeric mice reconstituted with *Rag2*$^{-/-}$*Blimp1*$^{gfp/gfp}$ fetal liver cells showed that Blimp1 is required for NK cell maturation and homeostasis

(Kallies et al., 2011). Blimp1 was induced by IL15 in NK cells, and highly expressed in the most mature NK cell subsets. The reconstituted chimeric mice had reduced NK cells in peripheral and NK cell maturation was partially impaired in the transition from CD27+KLRG1- to the CD27-KLRG1+ stage. However, due to lack of B cells and T cells, this model cannot fully reflect the interaction of NK cells and other lymphocytes.

Therefore, we generated a NK-cell lineage conditional Blimp1 knockout mouse model to study the effect of BLIMP1 in NK cell maturation and homeostasis, as well as the possibility of development of NKTCL. In addition, we evaluated the phenotypic changes in mice with NK-cell lineage-specific deletion of Blimp1 and coexpression of EBV oncoprotein LMP1.

Results

Establish a NK-lineage specific Blimp1 knock out mouse model

Ncr1-cre mice previous generated by Dr. Alexander Tarakhovsky's lab, which express Cre recombinase under control of Ncr1 promoter, were crossed to Blimp1f/f mice, previous generated in Dr.Veronika Sexl's lab' in which the exon encoding the DNA binding domain was flanked by two loxP sites ("floxed"), resulted in Blimp1 knockout in NK cells from the pro-NK cell stage (Fig. 4-1). The function and lineage specificity of Ncr1-cre were tested by crossing Ncr1-cre mice with Cre reporter Cag-GFP $^{f/stop}$ mice, previously generated in Dr. Kay-Uwe Wagner's lab. The offspring express green fluorescence protein upon Cre-mediated deletion of a loxP-flanked stop cassette. As expected, Ncr1-dependent Cre-mediated GFP expression was restricted to the NK compartment, as more than 90% of the GFP+ cells were NK cells (CD3-NK1.1+) in blood and spleen (Fig. 4-2A). On average, 40% of the CD3-NKp46+ NK cells were GFP positive in blood and spleen (Fig. 4-2B). No *GFP* expression was detected in T-lymphoid cells, as analyzed by CD3, CD4, and CD8 staining, and B-lymphoid cells stained by CD45R (B220) and CD19 (Fig. 4-2C).

To confirm Cre-mediated Blimp1 deletion in Blimp1f/f mouse NK cells, NK cells were isolated from spleen using a negative selection NK cell isolation kit (Miltenyi Biotec). Genomic DNA was extracted from both NK cells and the rest of the splenocytes. Primers spanning the deleted region were used to amplify the genomic DNA. The band indicating Cre-mediated recombination was only observed in Ncr1-cre, Blimp1f/f NK cells, and a remaining floxed blimp1 band indicated incomplete deletion. To quantify the Cre-mediated Blimp1 deletion in Ncr1-cre, Blimp1f/f NK cells, primers within the deleted region were use for quantitive PCR on genomic DNA and revealed 90% deletion efficiency, which was higher than the efficiency we detected in Cre-reporter mice (Fig. 4-

3). Since GFP expression in NK cells does not affect NK cell function and homeostasis, we speculated that the Blimp1 knockout in NK cell might have a positive selection on NK cell function and homeostasis. However it might also due to the difference of accessibility between different loxP sequences.

Blimp1 has an effect on NK cell homeostasis and maturation in vivo

Ncr1-cre, Blimp1f/f mice were born at the expected Mendelian ratio. Hematopoietic organs displayed no gross abnormalities; weight and cellularity of spleens and cellularity of the lymph nodes and bone marrow were unaltered in Ncr1-cre, Blimp1f/f mice compared with Blimp1f/f littermate controls. Analysis of $CD3^{-}NK1.1$ cells in the peripheral blood and spleens revealed a reduction of the percentage of NK cells in the total lymphocyte gate and their absolute number in Ncr1-cre, Blimp1f/f mice (Fig. 4-4A). However, the NK cell frequency and number were unaltered in lymph nodes and were higher in bone marrow in Ncr1-cre, Blimp1f/f mice (Fig. 4-4A). T lymphocytes were analyzed by staining with CD3, CD4 and CD8 antibodies; B lymphocytes were stained with CD45R (B220) antibody. The numbers of total CD3+ cells, $CD4^{+}$ and $CD8^{+}$ T lymphocytes and CD45R+ B lymphocytes were largely unchanged in peripheral blood, spleen, lymph node and bone marrow (Fig. 4-4B).

NK cell maturation is a multi-step process; the mature subsets are mainly distributed in the peripheral lymphoid organs or tissues whereas the immature subsets are largely contained in the primary lymphoid organ such as bone marrow. Since NK cell frequency and number were decreased in peripheral blood and spleen and increased in bone marrow, we next investigated whether lack of Blimp1 could affect NK cell maturation. In mice, NK cells can be divided into immature and mature populations by expression of CD11b. CD11b- NK cells compose most of the NK cell population in fetal

mice. In the adult, CD11b- NK cells are found mostly in the bone marrow and primary lymphoid sites such as lymph nodes. CD11b+ NK cells are mostly found in peripheral sites such as peripheral blood mononuclear cells (PBMCs) and can also be found in spleen. CD11b+ NK cells can be further divided into 2 populations by the expression of CD27. NK cell differentiation follows the pathway CD27-CD11b- (referred as DN for double negative), CD27+CD11b-, CD27+CD11b+ (referred as DP for double positive) and CD27-CD11b+. Different subsets have different features; DN NK cells display an immature phenotype and highest potential for proliferation; $CD27^{+}$ $CD11b^{-}$ and DP NK cells show the best ability to secrete cytokines, whereas CD27-CD11b+NK cells are the most mature subset exhibiting highest cytotoxicity.

In adult mice, relatively immature NK subsets (DP and CD27+CD11b-) were present in lymph nodes (50.18± 1.87 % in control mice, 59.42 ± 1.90 % in Ncr1-cre,Blimp1f/f mice) and bone marrow (60.1±1.45% in control mice, 82.17 ± 1.60 % in Ncr1-cre,Blimp1f/f mice), mature NK subsets (DP and CD27-CD11b+) were found to predominate in spleen (76.80 ± 4.09 % in control mice, 60.82 ± 2.29 % in Ncr1-cre,Blimp1f/f mice) and PBMC (77.60 ± 4.25 % in control mice, 57.73 ± 4.95 % in Ncr1-cre,Blimp1f/f mice). The frequency of mature CD11b+ NK cell subsets was reduced in all the lymphoid sites, with a significant decrease from 39.93 ± 1.43% to 17.83 ± 1.61% in bone marrow in Ncr1-cre, Blimp1f/f mice (Fig. 4-5A). Further analysis of subsets distribution by staining CD27 and CD11b revealed that CD27+CD11b- NK cells were significantly increased in peripheral blood, lymph nodes and bone marrow and the most mature CD27-CD11b+ subset was decreased in all the lymphoid sites in the Ncr1-cre,Blimp1f/f mice compared to the control mice (Fig. 4-5B). These results indicated that Blimp1 has an effect on NK cell maturation and homeostasis.

Blimp1 has an effect on NK cell proliferation and survival

In our previous study, we identified Blimp1 as a tumor suppressor gene in NKTCL, as Blimp1 was silenced by the combination of allelic deletion and promoter methylation, and knockdown of Blimp1 in human primary NK cells resulted in enhanced proliferation and decreased apoptosis in vitro. To determine the proliferative potential of NK cells in the absence of Blimp1, freshly isolated splenic Ncr1-cre, Blimp1f/f and wild-type NK cells were cultured in media containing IL-2. Live cells were counted under the microscope as death cells were excluded by staining with trypan blue. In another experiment, NK cells were expanded in IL2 for 4 days followed by culturing in media containing IL15. Blimp1-deficient NK cells exhibited enhanced growth in vitro compared with wild-type controls (Fig. 4-6A). Wild-type NK cells started expanding 5 days after in vitro culture whereas Blimp1-deficient NK cells expansion started 3 days after culture. Blimp1-deficient NK cells proliferated more rapidly than wild-type cells when cultured in IL15 after initial stimulation in IL2 for 4 days (Fig. 4-6A, right panel).

To test the survivability of NK cells, Day 4 NK cells were cultured in media with or without IL2 for 24 hours; early and late apotosis was analyzed by staining with early apoptosis marker Annexin V and cell viability dye 7-AAD. Under normal IL2 condition, Ncr1-cre, Blimp1f/f and wild-type NK cells had similar baseline apoptosis (Fig. 4-6B). Withdrawal of IL2 for 24 hours resulted in significant cell death and cell apoptosis. Ncr1-cre, Blimp1f/f NK cells survived better (63.30 ± 0. 42% Anexin V-7-AAD- cells) than wild-type NK cells (42.10 ± 3.81 % Anexin V-7-AAD- cells) (Fig. 4-6B). Even though Ncr1-cre, Blimp1f/f NK cells had defective maturation in vivo, the in vitro experiment indicated that IL2 stimulation might contribute to the more potent proliferation and survival ability of Ncr1-cre, Blimp1f/f NK cells. In our previous study, we identified IL2Ra (CD25) as a direct target of Blimp1 in human NK cells.IL2Ra is the high affinity subunit of IL2

receptor, it promotes cell proliferation and survival upon upregulation.As expected, IL2Ra was expressed at a low level in freshly isolated NK cells and upregulated upon IL2 stimulation; the increase was more significant in Ncr1-cre, Blimp1f/f NK cells (Fig. 4-6C).

Since Ncr1-cre, Blimp1f/f NK cells grew faster when activated by IL2, we speculate that activated Ncr1-cre, Blimp1f/f NK cells might proliferate better in the mouse when stimulated in vivo. To test our hypothesis, Ncr1-cre, Blimp1f/f and control mice were injected with polyinosinic-polycytidylic acid (poly I:C), a dsRNA analog that induces antiviral activity in vivo by activating NK cells and CD8+ T cells, either one time as acute polyIC stimulation, or every other day for 4 weeks as chronic polyIC stimulation. Peripheral blood was collected 1 day and 3 days after polyIC injection during acute stimulation, and the lymphocyte profile was evaluated by FACS. While NK cell frequency in control mice showed little change, NK cell frequency in Ncr1-cre, Blimp1f/f mice increased 4-fold and 5-fold at day 1 and day 3 post injections, respectively (Fig. 4-7A), whereas T cells and B cells remained at the same level (Fig. 4-7B,C). NK cell subset distribution was similar in peripheral blood of control and Ncr1-cre, Blimp1f/f mice after acute polyIC stimulation, however compare to unstimulated mice, stimulated mice had more CD27+CD11b- subsets (less than 20% in unstimulated mice of both genotypes, 45.9% in polyIC stimulated control mice and 55.2% in polyIC stimulated Ncr1-cre, Blimp1f/f mice) (Fig. 4-7B). After 4 weeks of chronic polyIC stimulation, spleens of both groups were slightly enlarged to the same extent. NK cell frequency and NK cell number were increased both in control and Ncr1-cre, Blimp1f/f mice; the increase in Ncr1-cre, Blimp1f/f mice was greater (1.47 fold in control mice, 2.5 folds in Ncr1-cre, Blimp1f/f mice) (Fig. 4-8A, B). There were more activated NK cells stained as CD69+ in Ncr1-cre, Blimp1f/f mice (Fig. 4-8C). Similar to acute polyIC stimulation, NK cell subsets were

distributed with a similar pattern as the percentage of CD27+CD11b- NK cells were significanted increased (less than 30% in unstimulated mice of both genotypes, 69.8% in polyIC stimulated control mice and 75.8% in polyIC stimulated Ncr1-cre, Blimp1f/f mice) (Fig. 4-8D). Both in vitro and in vivo studies showed that Ncr1-cre, Blimp1f/f NK cells had better proliferation potential.

Blimp1 has an effect on NK cell cytotoxicity

Our previous study demonstrated that PRDM1 was upregulated upon IL2 stimulation and suppressed the expression of IFN γ and TNFa by directly binding to specific regions on their promoters. mRNA isolated from resting NK cells and day 8 NK cells cultured in the presence of IL2 were analyzed by real-time quantitative RT-PCR. Consistent with our finding in human NK cells, TNFα and TNFβ (Lta) were expressed at low level in the resting NK cells and unregulated upon IL2 stimulation. Expression of TNFα was higher in resting and IL2 stimulated Ncr1-cre, Blimp1f/f NK cells. TNFβ was expressed at a low level in both resting Blimp1f/f NK cells and wild-type NK cells, whereas its expression significantly increased in Blimp1f/f NK cells upon IL2 stimulation (Fig. 4-9A). Since TNFs are associated with NK cell cytotoxicity, we further tested the cytotoxic properties of Blimp1-deficient NK cells. NK cells isolated from spleen of control and Ncr1-cre, Blimp1f/f mice were expanded in IL2-containing media for 8 days. NK cells were then cocultured with CFSE-labeled YAC-1 target cells at different effector to target ratios for 4 hours; killed target cells were stained with cell viability dye 7-AAD and quantified by flow cytometry as CFSE+7-AAD+ cells. Ncr1-cre, Blimp1f/f NK cells showed greater cytotoxic activity than the wild-type NK cells (Fig. 4-8B), which was different from the results found using human NK cells, where Blimp1 did not affect NK cell cytotoxicity.

Establish a NK-lineage specific Lmp1 knock in Blimp1 knock out double transgenic mouse model

Although Blimp1 has been identified as a tumor suppressor gene in NKTCL, we have not observed the development of NKTCL in mice with Blimp1 knock out alone . As tumorgenesis is a multifactorial process, it is worthwhile to combine genomic aberrations that would likely cooperate with blimp1 deficiency. EBV infection is highly associated with NKTCL lymphoma, Epstein-Barr virus latent membrane protein 1(Lmp1) is the major oncoprotein in B-cell transformation and is expressed in NK lymphoma cells. It is a six-span transmembrane protein belonging to the TNF family. It functions as an activator of both the alternative and canonical NFκB pathways in B-cell transformation and may play an important role in NK cell activation as well. Thus we proceeded to evaluate the effect of simultaneously loss of tumor suppressor gene Blimp1 and expression of oncogenic Lmp1 on NKTCL development.

Ncr1-cre, Blimp1f/f or Ncr1-cre, Blimpf/- mice were crossed to $Lmp1^{stopf/-}$ mice to generate Ncr1-cre, $Lmp1^{stopf/-}$ and Ncr1-cre, Blimp1f/f, $Lmp1^{stopf/-}$ mice. Ncr1-cre, Blimp1f/f, $Lmp1^{stopf/-}$ mice have *Lmp1* coding sequence inserted into the *Gt(ROSA)26Sor* locus, along with a loxP flanked stop fragment placed between the promoter and LMP1 coding sequence. Expression of the *Lmp1* gene is blocked by the *loxP*-flanked STOP fragment, but upon Ncr1-dependent cre-mediated excision of the stop cassette, Lmp1 is expressed in NK cells. As mentioned above Blimp1 is deleted simultaneously (Fig. 4-10)

NK cells were severely reduced in Ncr1-cre, Blimp1f/f, Lmp1$^{stopf/-}$ mice

Ncr1-cre, Blimp1f/f, Lmp1$^{stopf/-}$ mice was born at the expected Mendelian ratio. Hematopoietic organs displayed no gross abnormalities; weight and cellularity of spleens and bone marrow were unaltered in Ncr1-cre, Blimp1f/f, Lmp1stopf$^{/-}$ mice compared with Blimp1f/f, Lmp1$^{stopf/-}$ littermate controls, however the lymph nodes were smaller in Ncr1-cre, Blimp1f/f, Lmp1$^{stopf/-}$ mice. Analysis of CD3^{-}NK1.1 cells in the different lymphoid sites revealed severe reduction of NK cell percentage and number in all the sites. The frequency of NK cells was most significantly decreased in peripheral blood, as a 16 fold (3.60 ± 0.37 % to 0.22 ± 0.05 %) decrease of NK cell was observed in Ncr1-cre, Blimp1f/f, Lmp1$^{stopf/-}$ mice compared to the control mice (Fig. 4-11A). A 10- fold decrease in NK cell frequency was observed is lymph nodes and bone marrow as well, whereas a 6-fold decrease in NK cell frequency was observed in spleen (Fig. 4-11A, upper panel). The decrease in NK cell number was consistent with the decrease in NK cell frequency as NK cell number was most significantly reduced in peripheral blood followed by bone marrow, lymph nodes and spleen (Fig. 4-11A, lower panel). The decrease of NK cell frequency and number was also more significant in Ncr1-cre, Blimp1f/f, Lmp1$^{stopf/-}$ mice than that in Ncr1-cre, Blimp1f/f mice which showed a defect in NK cell maturation. We were not able to evaluate the absolute number of NK cells in lymph nodes due to the small size of the lymph nodes in Ncr1-cre, Blimp1f/f, Lmp1$^{stopf/-}$ mice. The frequency of total CD3+ cells and CD45R+ B lymphocytes were largely unchanged in peripheral blood, spleen, lymph nodes and bone marrow (Fig. 4-11B).

Lmp1 expression altered NK cell subsets distribution

As we showed in the previous study, Blimp1 knockout in NK cells resulted in defective NK cell maturation, we next tested if Lmp1 could alter the NK cell subset distribution. NK cells subsets were analyzed for expression of CD27 and CD11b. The fraction of NK cells in relatively mature CD11b+ subsets was markedly decreased while the percentage of the immature CD11b- subsets increased in all the lymphoid sites (Fig. 4-12A). Compare to other lymphoid sites, spleen had a less signification NK cell reduction ($2.23\pm 0.32 \times 10^5$ /spleen in Blimp1f/f, $Lmp1^{stopf/-}$ mice, $0.8 \pm 0.09 \times 10^5$/spleen in Ncr1-cre, Blimp1f/f, $Lmp1^{stopf/-}$ mice) and was the largest NK cell pool in mice, 95% of NK cells were CD11b- in Ncr1-cre, Blimp1f/f, $Lmp1^{stopf/-}$ mice but only 35% of NK cells were CD11b- in control Blimp1f/f, $Lmp1^{stopf/-}$ mice (Fig. 4-12A). In control mice, the percentage of CD11b+ NK cell was higher in peripheral blood and spleen and lower in lymph nodes and bone marrow. In Ncr1-cre, Blimp1f/f, $Lmp1^{stopf/-}$ mice, CD11b+ NK cells were severely reduced in all the lymphoid sites compare to control mice (4.52 folds decrease in blood, 5.44 folds decrease in lymph nodes, 4.97 folds decrease in bone marrow and 13 folds decrease in spleen). When the subsets distribution was more specifically evaluated, the percentage of DN NK cell subset increased in all secondary lymphoid sites but remained the same in bone marrow. The increased fraction of CD11b- NK cells in bone marrow was mostly due to the increase of the CD27+CD11b- subset (Fig. 4-12B).

The decrease in NK cells in Ncr1-cre, Blimp1f/f, $Lmp1^{stopf/-}$ mice was due to Immunosurveillance

Lmp1 is an EBV encoded protein that may be strongly immunogenic. It is possible that NK cells expressing Lmp1 were recognized by the immune system as virus infected cells and subsequently destroyed by T-cells despite of their presence throughout

hematopoiesis. This speculation was also supported by a study in B cell-specific Lmp1 mice showing that, T cells were activated by lmp1-expressing B cells, and these activated CD8 T cells killed lmp1-expressing B cells. This indicated that Lmp1-expressing NK cells were killed by activated T cells, and the CD11b- NK cell subsets proliferate to compensate for the loss of NK cells. During NK cell maturation, NK progenitor cells gain NK1.1 first immediately followed by NKp46. More than 99% CD3-NK1.1+ NK cells are CD3-NKp46 cells (Walzer et al., 2007). Thus it is likely most of these CD11b- NK cells still express Lmp1 but they are able to escape immunosurviliance due to their potent proliferation ability.

In order to study the property of simultaneous Blimp1 knockout and lmp1 expressing NK cells without the interference of T cell-mediated cell killing. We depleted T cells in Ncr1-cre, Blimp1f/f, Lmp1$^{stopf/-}$ and control mice by injecting blocking CD3 antibodies. The blocking monoclonal CD3 antibodies are known to cause cytokine storm both in human and mice (Ferran et al., 1990). After anti-CD3 injection, mice loss body weight immediately in the first week. Then body weight started increasing until returning to normal in another week. NK cells and T cells in anti-CD3 injected mice were monitored at week 2, 3 and 4. At week 2, T cell depletion in control mice was more efficient as all three mice had less than 20% T cells, whereas only one Ncr1-cre, Blimp1f/f, Lmp1$^{stopf/-}$ mouse had less than 20% T cells (Fig. 4-13A). The NK cell percentage increased in both Ncr1-cre, Blimp1f/f, Lmp1$^{stopf/-}$ mice and control mice, and the increase was higher in the two Ncr1-cre, Blimp1f/f, Lmp1$^{stopf/-}$ mice with better T cell depletion (<30% in total lymphocytes) (Fig. 4-13A).

To exclude the interference of T cells, NK cell percentage and number were analyzed only using mice with less than 30% T cells (3 mice in control group, 2 mice in Ncr1-cre, Blimp1f/f, Lmp1$^{stopf/-}$ group). The NK cell number increased rapidly 2 weeks

after anti-CD3 injection in Ncr1-cre, Blimp1f/f, Lmp1$^{stopf/-}$, indicating a better proliferation capacity of these NK cells(Fig. 4-13B). This was also supported by the observation that the percentage of CD27+ CD11b- NK cell was higher in Ncr1-cre, Blimp1f/f, Lmp1$^{stopf/-}$ mice than in control mice (Fig. 4-1C). However, after week 2, T cells increased dramatically in two of the Ncr1-cre, Blimp1f/f, Lmp1$^{stopf/-}$ mice even though T cell depletion was still efficient in control mice (Fig. 4-13A). As T cells increased in Ncr1-cre, Blimp1f/f, Lmp1$^{stopf/-}$ mice, NK cells dropped back to a low level (Fig. 4-13A). Two months of anti-CD3 injections depleted most of the T cells in control mice in all the lymphoid sites, but failed to persistently deplete T cells in Ncr1-cre, Blimp1f/f, Lmp1$^{stopf/-}$ mice (Fig. 4-14). This finding supported our hypothesis that, Lmp1 expressing NK cells could stimulate T cells, and as Lmp1-specific CD8+ T cell expanded, LMP+ NK cells were eliminated. Intriguingly, although NK cells in Ncr1-cre, Blimp1f/f, Lmp1$^{stopf/-}$ mice remained at a low level in bone marrow , the percentage of NKT cells (CD3+, NK1.1+) increased dramatically (from 0.001% to 12.9% in bone marrow, 0.0008% to 13.06% in spleen) (Fig. 4-15). T cells upon stimulation, can acquire NK markers such as CD16, NK1.1 and NKp46. If these CD3+NK1.1+ positive cells also express NKp46 (Ncr1), then they may also express Lmp1, therefore further experiment are needed to address whether these NKT cells express Lmp1.

Discussion

In this study, we showed that Blimp1 plays an important role in NK cell homoeostasis and functions. A previous study using Blimp1$^{GFP/GFP}$, Rag2-/-γc-/- reconstituted chimeric mice showed that Blimp1 is a important player in the transcription network controlling NK cell maturation. However in their study, Blimp1 was deleted in all hematopoietic cells, which is not the case in real NKTCL cases, where Blimp1 deletion is NK cell specific. In addition, chimeric mice lack other lymphocytes such as T cells and B cells. NK cells depend on cytokines from the microenvironment, IL2; a cytokine primarily secreted by CD4+ T cells has long been used for NK cell culture in vitro, suggesting an interaction of NK cells and other lymphocytes. Therefore chimeric mice cannot fully reflect the interaction of NK cells and their microenvironment. Thus in our study, we established a NK-lineage specific Blimp1 knockout mouse model.

NK cells are believed to develop from common lymphoid progenitors (CLP) in bone marrow or other extramedullary sites such as lymph nodes and thymus (Kondo et al., 2001)[14,15]. In mouse, CLP develop into NK progenitors (NKP) as they acquire IL2/IL-15 receptor beta chain (CD122), identified as Lin-CD122+ cells(Di Santo, 2006). NKPs then express functional receptors following the order NK1.1, CD94/NKG2A, NKp46, Ly49 receptors, DX5, CD43 and Mac-1 (CD11b) (Kim et al., 2002), and become functional mature. In our study, the cre-mediated Blimp deletion was under the control of the Ncr1 (NKp46) promoter, thus Blimp1 was knocked out starting after the NKP stage. Consistent to the finding in the chimeric mice study, NK cell maturation was disrupted in Ncr1-cre, Blimp1f/f mice. Peripheral maturation of NK cells is known to be a 4-stage process marked by the expression of CD27, a member of the TNF-receptor superfamily, and CD11b, a protein subunit of integrin alpha-M beta-2 ($\alpha_M\beta_2$). NK cells were reduced in peripheral lymphoid sites such as peripheral blood and spleen. In contrast, NK cells

were increased in bone marrow. This was in agreement with the finding that Ncr1-cre, Blimp1f/f NK cells were impaired in the transition from relatively immature CD11b- subsets to the mature CD11b+ subsets. CD11b, also known as macrophage-1 antigen (Mac-1), along with common integrin β_2 subunit (CD18), forms the heterodimer integrin $\alpha_M\beta_2$. Integrin $\alpha_M\beta_2$ is expressed on the surface of many innate immune leukocytes, such as neutrophils,macrophages and NK cells, and regulates their adhesion and migration. Therefore, the lower number and frequency of NK cells in peripheral sites might due to the impairment of NK cell migration.

Moreover, CD11b- NK cells consist of DN NK subsets and CD27+ CD11b- subsets. These two subsets are known to have greatest proliferative potential and superior effector potential. This was supported by the finding that Ncr1-cre, Blimp1f/f NK cells proliferated better in the presence of IL2 and IL15 in vitro and upon polyIC stimulation in vivo. The better proliferation and survival of Ncr1-cre, Blimp1f/f NK cells might be associated with the dysregulation of IL2Ra (CD25), a direct target of Blimp1 in human NK cells. As we demonstrated, CD25 was transcribed at a detectable level in resting NK cells. Upon stimulation with IL2, CD25 was upregulated in both Ncr1-cre,Blimp1f/f NK cells and wild-type NK cells, however, the increase in Ncr1-cre,Blimp1 NK cells was about 2-fold higher. CD25 is the alpha chain of the IL-2 receptor and it can associate with CD122 to form a high affinity IL2 receptor. CD25 is expressed in diffuse large B-cell lymphoma (DLBCL) and follicular lymphoma (FL), and high expression of CD25 in the two types of lymphoma is correlated with a poor prognosis (Fujiwara et al., 2014). Expression of high affinity IL2 receptor allows Ncr1-cre, Blimp1f/f NK cells to survive in IL2 limiting conditions.

In contrast to the finding in experiments using chimeric mice, Ncr1-cre, Blimp1f/f NK cells exhibited better cytotoxic function in vitro. This can be explained by the

upregulation of Blimp1 targets involved in NK cell cytotoxicity such as TNFα and TNFβ, as both genes were upregulated upon IL2 stimulation and a 5-fold increase in TNFβ was observed in Ncr1-cre, Blimp1f/f NK cells compare to wild-type NK cells. Another possibility is the formation of CD25+ cytokine induced memory-like (CIML) NK cells. It has been show that brief preactivation with IL-12, IL15 and IL18 generated CIML NK cells that expressed CD25 and later exhibit enhanced proliferation, cytokine secretion and cytotoxicity via its high affinity αβγ IL2 receptor(Leong et al., 2014). Therefore, deletion of Blimp1 might promote generation of CD25+ memory-like NK cells though IL2 alone.

Even though PRDM1 silencing is one of the major genetic alterations in NKTCL, Blimp1 knockout alone was not sufficient to cause NKTCL in mice in steady state; moreover, it impaired NK cell maturation. However, the accumulated Blimp1-knockout NK cells exhibited potent proliferative and functional ability, which represent the highly activated feature of malignant NK cells, in the presence of cytokine stimulation. Thus the development of NKTCL may need another factor(s) that causes dysregulated NK cell activation. Lmp1 is the major oncoprotein of EBV, which isdetected in 99% of NKTCL. It activates the signaling pathways of nuclear factor-κB (NF-κB) and signal transducer and activator of transcription (STAT), which is also activated upon IL2 stimulation. However, the role of Lmp1 in NKTCL development was not studied as Lmp1-expressing Ncr1-cre, Blimp1f/f NK cells were killed by immunesurveiliance. Prolonged anti-CD3 injection resulted in a selection of Lmp1-specific cytotoxic T cells, as T cell depletion was complete in control mice but got worse in Ncr1-cre, Blimp1f/f, Lmp1stopf$^{/-\ mice.}$ However we observed a transient rapid growth of Lmp1-expressing Ncr1-cre, Blimp1f/f NK cells in the first two weeks, when T cell depletion was optimal and Lmp1- specific T cells were

not expanded. An alternative method needs to be applied to achieve a complete T cell deletion in Ncr1-cre, Blimp1f/f, Lmp1stopf$^{/-\ mice}$ in future experimental studies.

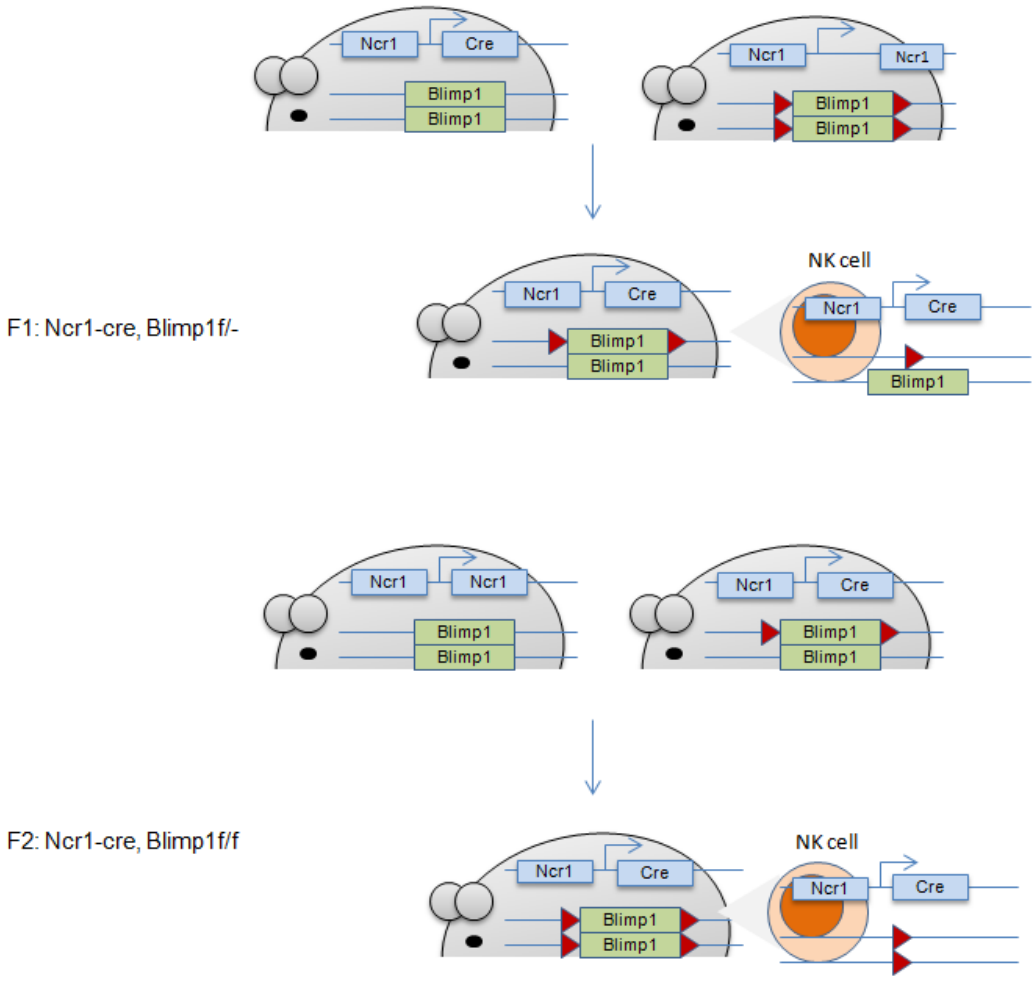

F1: Ncr1-cre, Blimp1f/-

F2: Ncr1-cre, Blimp1f/f

Figure 4-1: Strategy for breeding NK-lineage specific Blimp 1 knockout mice

Ncr1-cre mice were crossed with Blimp1f/f mice to generate heterozygous Ncr1-cre, Blimp1f/- mice in thefirst generation. Ncr1-cre, Blimp1f/- mice were crossed with Blimp1f/f mice to generate homozygous Ncr1-cre, Blimp1f/f mice.

A

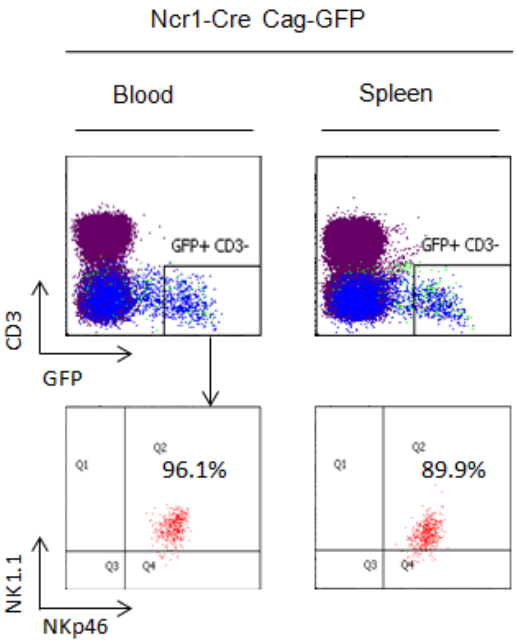
Ncr1-Cre Cag-GFP
Blood
Spleen
GFP+ CD3-
GFP+ CD3-
CD3
GFP
Q1
Q2
96.1%
Q3
Q4
Q1
Q2
89.9%
Q3
Q4
NK1.1
NKp46

B

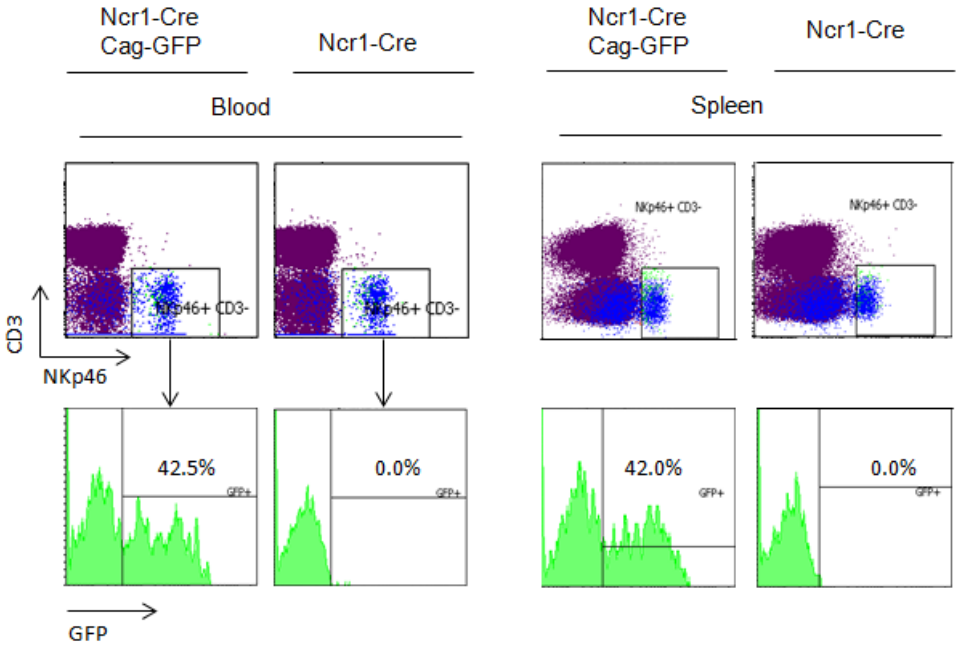
Ncr1-Cre Cag-GFP
Ncr1-Cre
Ncr1-Cre Cag-GFP
Ncr1-Cre
Blood
Spleen
NKp46+ CD3-
NKp46+ CD3-
NKp46+ CD3-
NKp46+ CD3-
CD3
NKp46
42.5%
GFP+
0.0%
GFP+
42.0%
GFP+
0.0%
GFP+
GFP

C

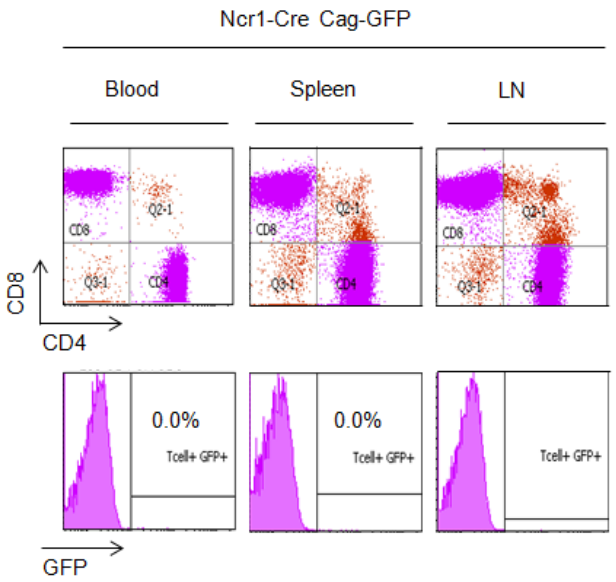
Ncr1-Cre Cag-GFP
Blood
Spleen
LN
CD8
CD4
Q2-1
Q3-1
0.0%
Tcell+ GFP+
GFP

D

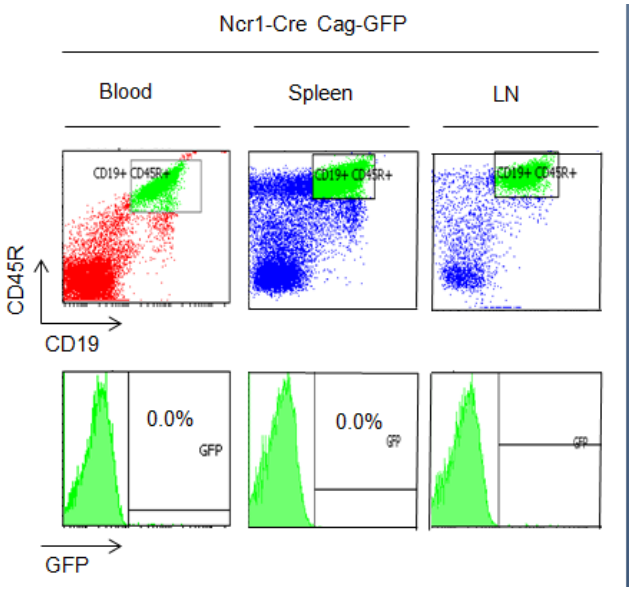
Ncr1-Cre Cag-GFP
Blood
Spleen
LN
CD19+ CD45R+
CD45R
CD19
0.0%
GFP

Figure 4-2: Ncr1-dependent Cre-mediated recombination was restricted to the NK cell compartment

(A) Cre-mediated GFP expression as shown by flow cytometry in Ncr1-cre, Cag-GFP report mice and littermate controls. Cells were analyzed within the lymphocyte gate (A) Most GFP+ cells were showed expression of NK cell markers NKp46 and NK1.1,thus most of the GFP+ cells were NK cells. (B) Percentage of GFP positive cells in NK cells (CD3-NKp46+) in blood and spleen. (C-D) Absence of GFP expression in T and B cells in different lymphoid sites. > 3 mice/genotype were used for analysis. LN, lymph nodes.

A

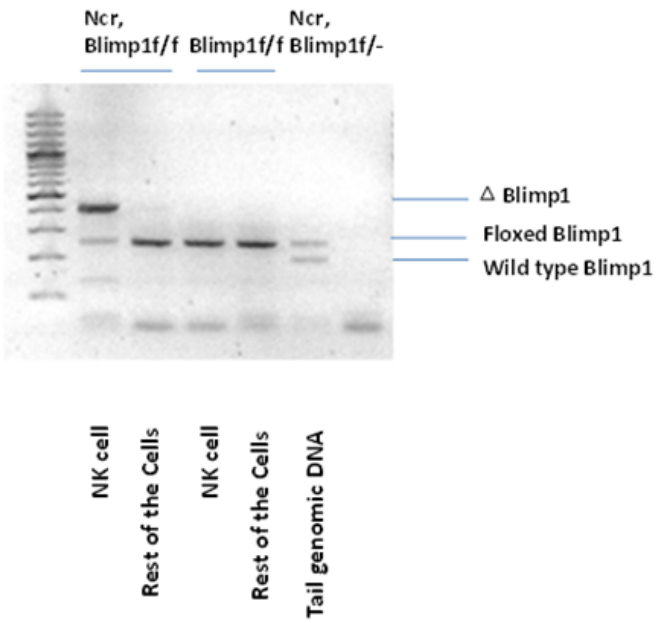
Ncr, Blimp1f/f
Blimp1f/f
Ncr, Blimp1f/-
Δ Blimp1
Floxed Blimp1
Wild type Blimp1
NK cell
Rest of the Cells
NK cell
Rest of the Cells
Tail genomic DNA

B

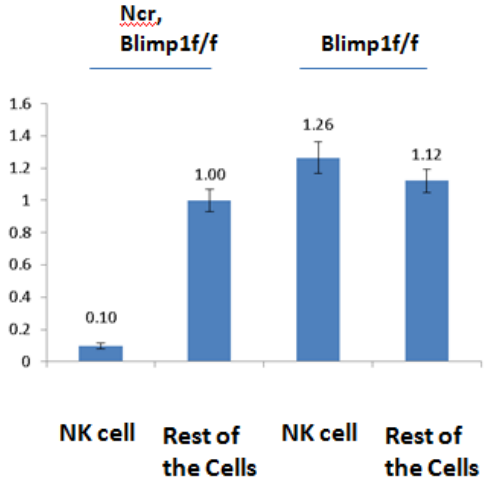
Ncr, Blimp1f/f
Blimp1f/f
1.6
1.4
1.2
1
0.8
0.6
0.4
0.2
0
0.10
1.00
1.26
1.12
NK cell
Rest of the Cells
NK cell
Rest of the Cells

Figure 4-3: Cre-mediated Blimp1knockout in mice

NK cells were isolated from the spleens of Ncr1-cre, Blimp1f/f and control mice (3 mice/phenotype) using a negative selection NK cell isolation kit. DNA was extracted from isolated NK cells and attached remaining cells. (A) Blimp1 deletion was tested by PCR using genomic DNA. A 200bp band indicates wild type Blimp1, a 250bp band indicates floxed Blimp1, and a 400bp band indicates deleted Blimp1. The band indicating Blimp1 deletion was only detected in the Ncr1-cre, blimp1f/f NK cells. (B) Quantification of Blimp1 deletion by q-PCR using genomic DNA.

A

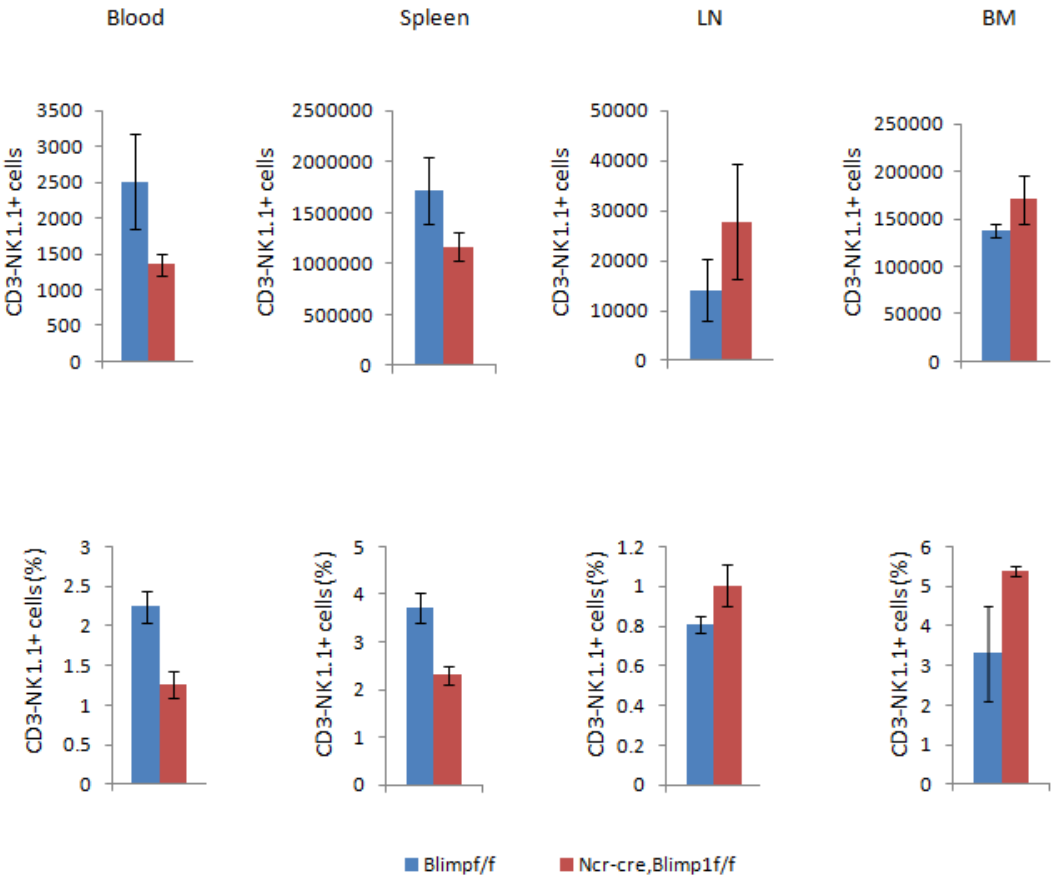
Blood
Spleen
LN
BM
CD3-NK1.1+ cells
CD3-NK1.1+ cells(%)
Blimpf/f
Ncr-cre,Blimp1f/f

B

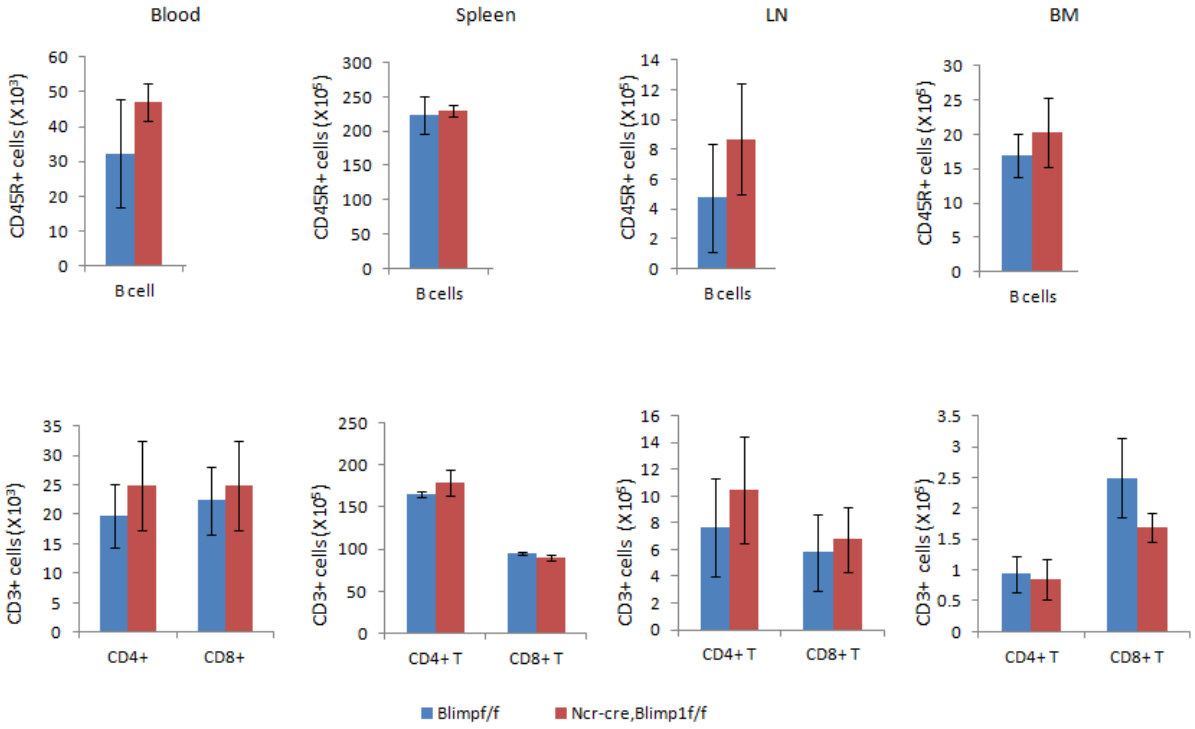
Blood
Spleen
LN
BM
CD45R+ cells (X10³)
CD45R+ cells (X10⁵)
B cell
B cells
CD3+ cells (X10³)
CD3+ cells (X10⁵)
CD4+
CD8+
CD4+ T
CD8+ T
Blimpf/f
Ncr-cre,Blimp1f/f

Figure 4-4: Blimp1 has an effect on NK cell homeostasis in vivo

Single cell suspensions were prepared from blood, spleen, lymph nodes and bone marrow in one femur. The lymphocyte profile was analyzed by FACS. NK cells were gated as CD3-NK1.1+, T cells were gated as CD3+ and different subsets were analyzed by CD4 and CD8 staining, B cells were gated as CD3-CD45R+.(A) Upper panel : absolute NK cell number in different lymphoid sites. Lower panel: percentage of NK cells in total lymphocytes in different lymphoid sites. (B) Absolute number of B cells, CD4+T cells and CD8+T cells in different lymphoid sites. LN: lymph node, BM: bone marrow

A

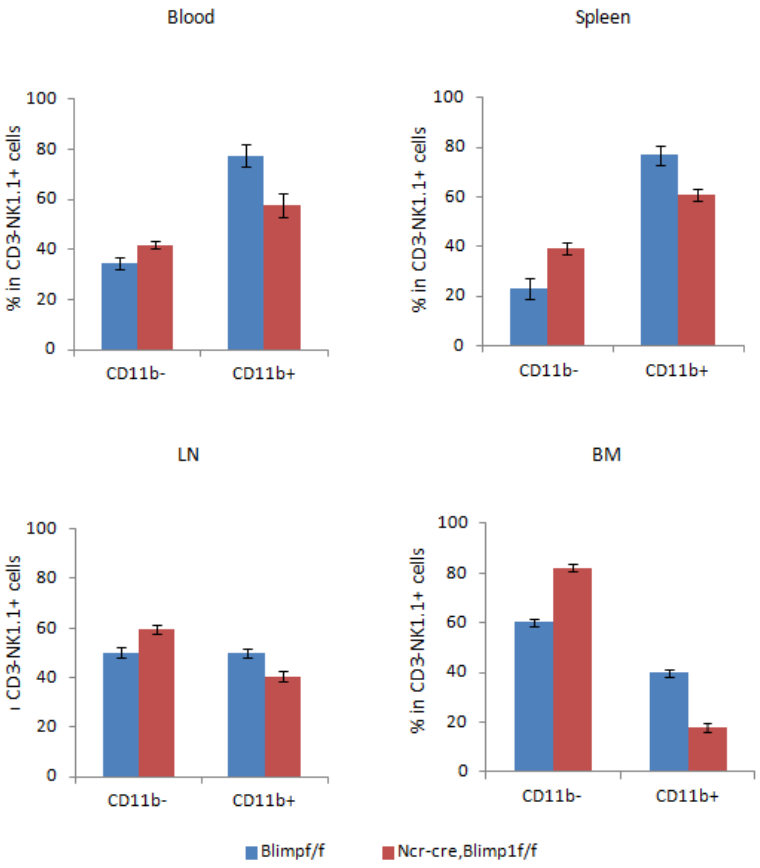
Blood
Spleen
LN
BM
% in CD3-NK1.1+ cells
100
80
60
40
20
0
CD11b-
CD11b+
Blimpf/f
Ncr-cre,Blimp1f/f

B

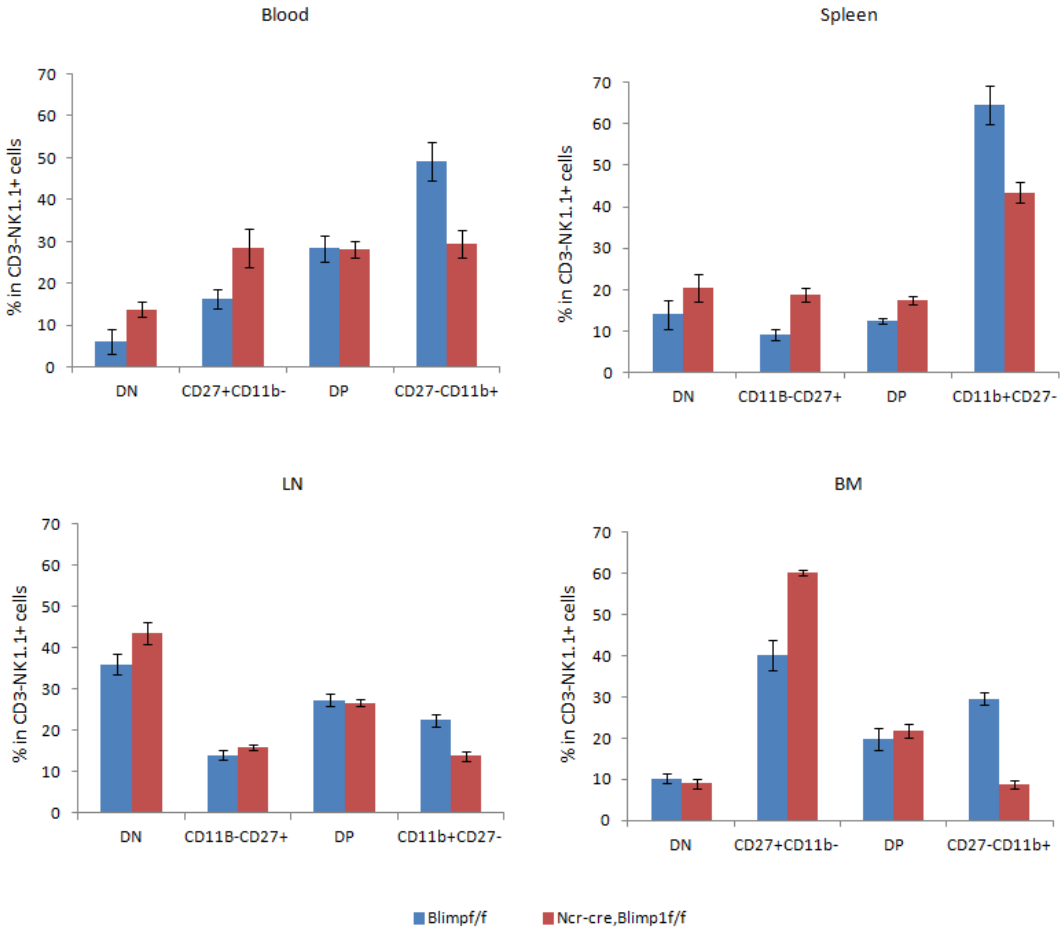
Blood
% in CD3-NK1.1+ cells
70
60
50
40
30
20
10
0
DN
CD27+CD11b-
DP
CD27-CD11b+
Spleen
% in CD3-NK1.1+ cells
DN
CD11B-CD27+
DP
CD11b+CD27-
LN
% in CD3-NK1.1+ cells
DN
CD11B-CD27+
DP
CD11b+CD27-
BM
% in CD3-NK1.1+ cells
DN
CD27+CD11b-
DP
CD27-CD11b+
Blimpf/f
Ncr-cre,Blimp1f/f

Figure 4-5: Blimp1 has an effect on NK cell maturation in vivo

NK cells were gated as CD3-NK1.1+. Different subsets were analyzed by the expression of CD27 and CD11b. (A) Comparison of the percentage of CD11b- and CD11b+ NK cells in different lymphoid sites in Ncr1-cre, Blimp1f/f mice and control mice. (B) NK cell subset distribution in different lymphoid sites in Ncr1-cre, Blimp1f/f mice and control mice.

A

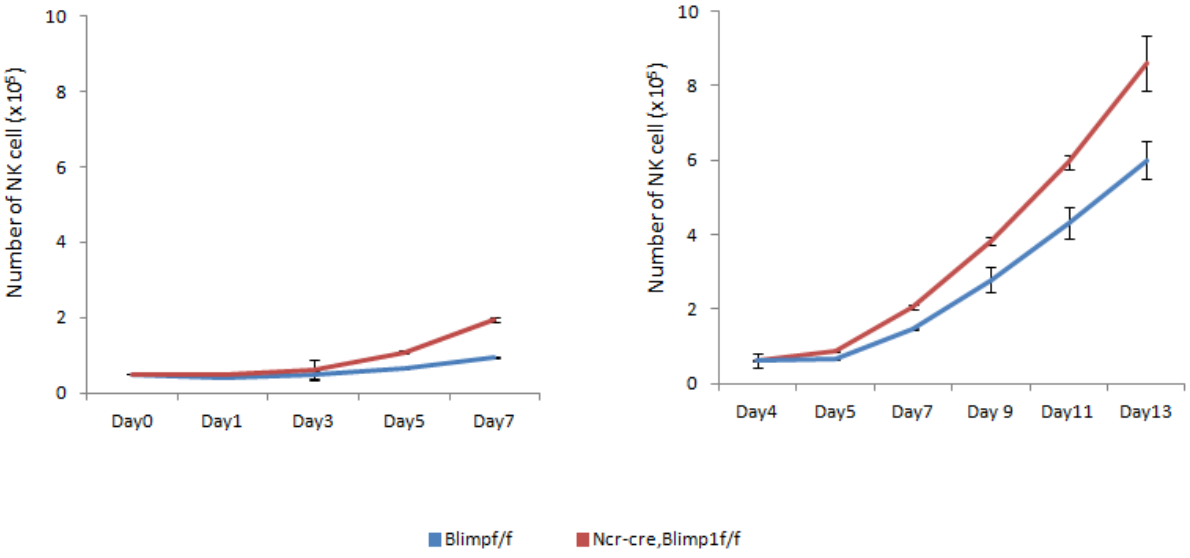
Number of NK cell (x10⁶)
10
8
6
4
2
0
Day0
Day1
Day3
Day5
Day7
Number of NK cell (x10⁶)
10
8
6
4
2
0
Day4
Day5
Day7
Day 9
Day11
Day13
Blimpf/f
Ncr-cre,Blimp1f/f

B

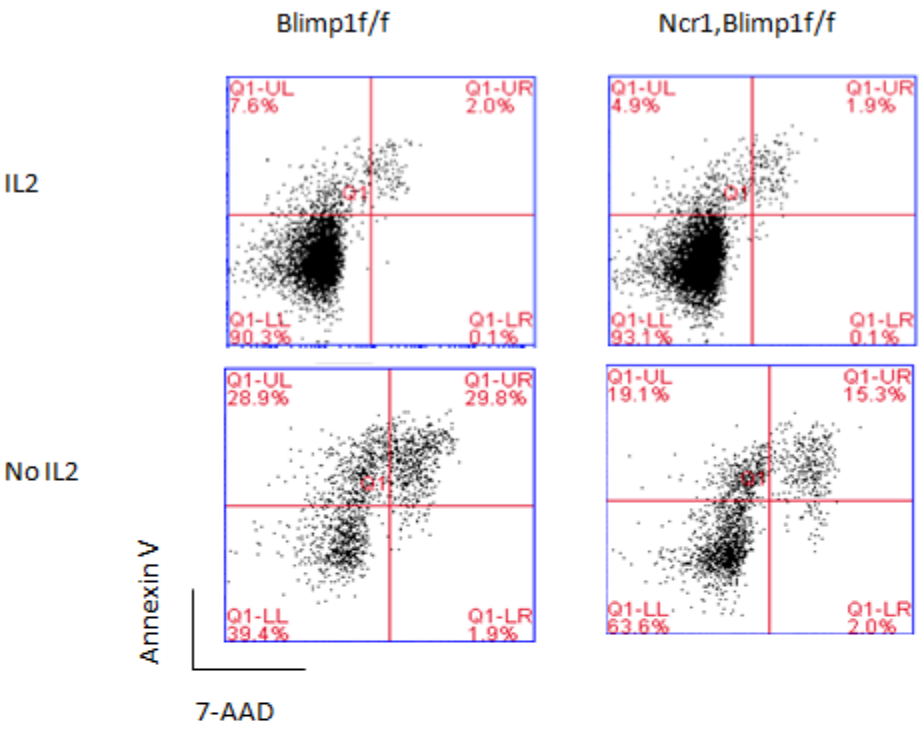
Blimp1f/f
Ncr1,Blimp1f/f
IL2
No IL2
Q1-UL 7.6%
Q1-UR 2.0%
Q1-LL 90.3%
Q1-LR 0.1%
Q1-UL 4.9%
Q1-UR 1.9%
Q1-LL 93.1%
Q1-LR 0.1%
Q1-UL 28.9%
Q1-UR 29.8%
Q1-LL 39.4%
Q1-LR 1.9%
Q1-UL 19.1%
Q1-UR 15.3%
Q1-LL 63.6%
Q1-LR 2.0%
Annexin V
7-AAD

C

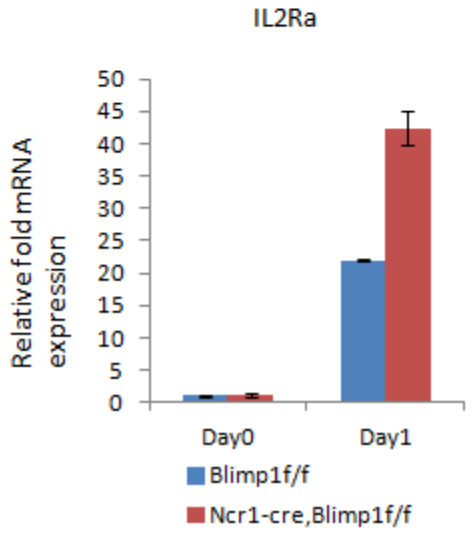
IL2Ra
Relative fold mRNA expression
50
45
40
35
30
25
20
15
10
5
0
Day0
Day1
Blimp1f/f
Ncr1-cre,Blimp1f/f

Figure 4-6: Blimp1 has an effect on NK cell proliferation and survival

(A)In vitro cultured NK cells were stained with 0.4% trypan blue and live cells were counted using an automated cell counter (Invitrogen). Right panel: 10^5 freshly isolated NK cells were seeded into a 24-well plate and cultured in medium containing 1000U/ml IL2. Live cells were counted at the indicated time points. (B) NK cells were expanded in media containing IL2 for 4 days; then 10^5 day4 NK cells were seeded into a 24-well plate and cultured in the medium containing 1000U/ml IL15. Live cells were counted at the indicated time points. (C) 10^5 day4 NK cells expanded in IL2 containing medium were seeded into plate bottom 96-well plate with or without IL2 for 24 hours. Apoptotic cells were stained with Annexin V and 7-AAD and analyzed by flow cytometry. (D) Expression of known Blimp1 target IL2Ra was tested by q-RT-PCR in resting NK cells and IL2 activated NK cells.

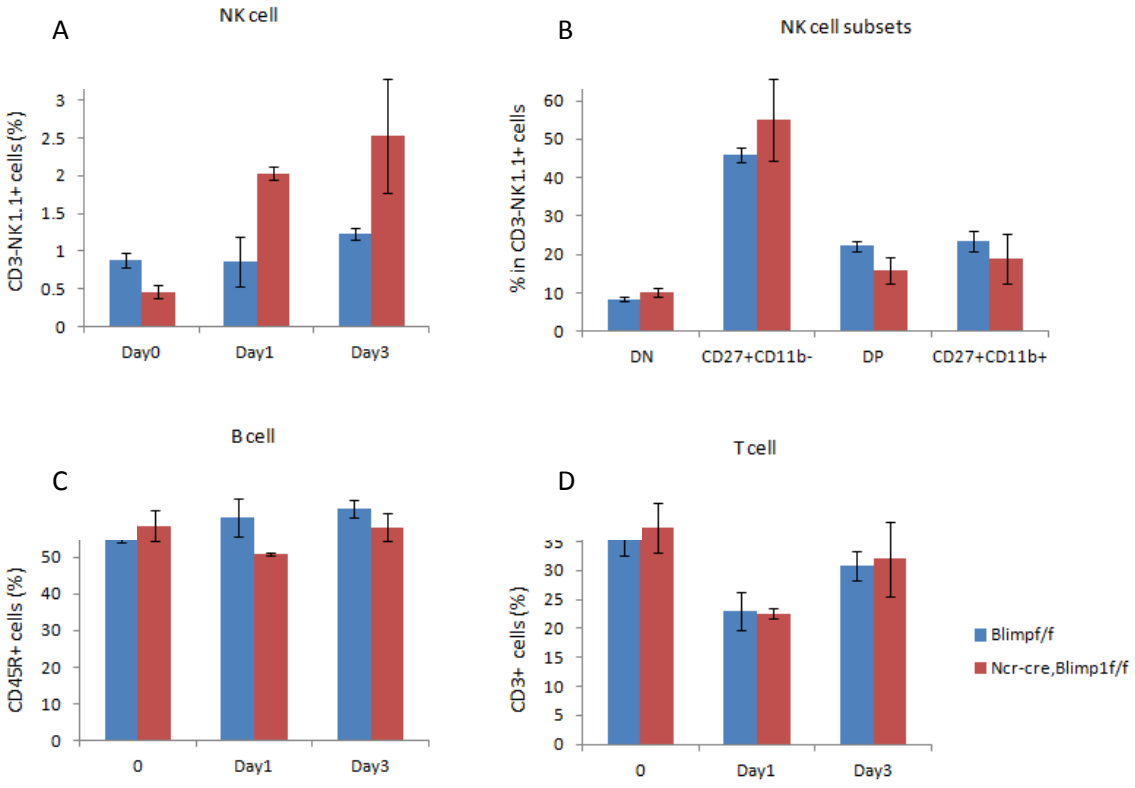
A
NK cell
CD3-NK1.1+ cells (%)
3
2.5
2
1.5
1
0.5
0
Day0
Day1
Day3
B
NK cell subsets
% in CD3-NK1.1+ cells
60
50
40
30
20
10
0
DN
CD27+CD11b-
DP
CD27+CD11b+
C
B cell
CD45R+ cells (%)
50
40
30
20
10
0
0
Day1
Day3
D
T cell
CD3+ cells (%)
30
25
20
15
10
5
0
0
Day1
Day3
Blimpf/f
Ncr-cre,Blimp1f/f

Figure 4-7: Acute PolyIC stimulation restores NK cells in peripheral blood

Mice were injected ip with 200µg polyIC. Peripheral blood samples were collected before and 1 day and 3 days after injection. NK cell frequency in peripheral blood (A), NK cell subset distribution (B) and B cell (C) and T cell (D) frequency in peripheral blood were analyzed by FACS (4 mice/ genotype).

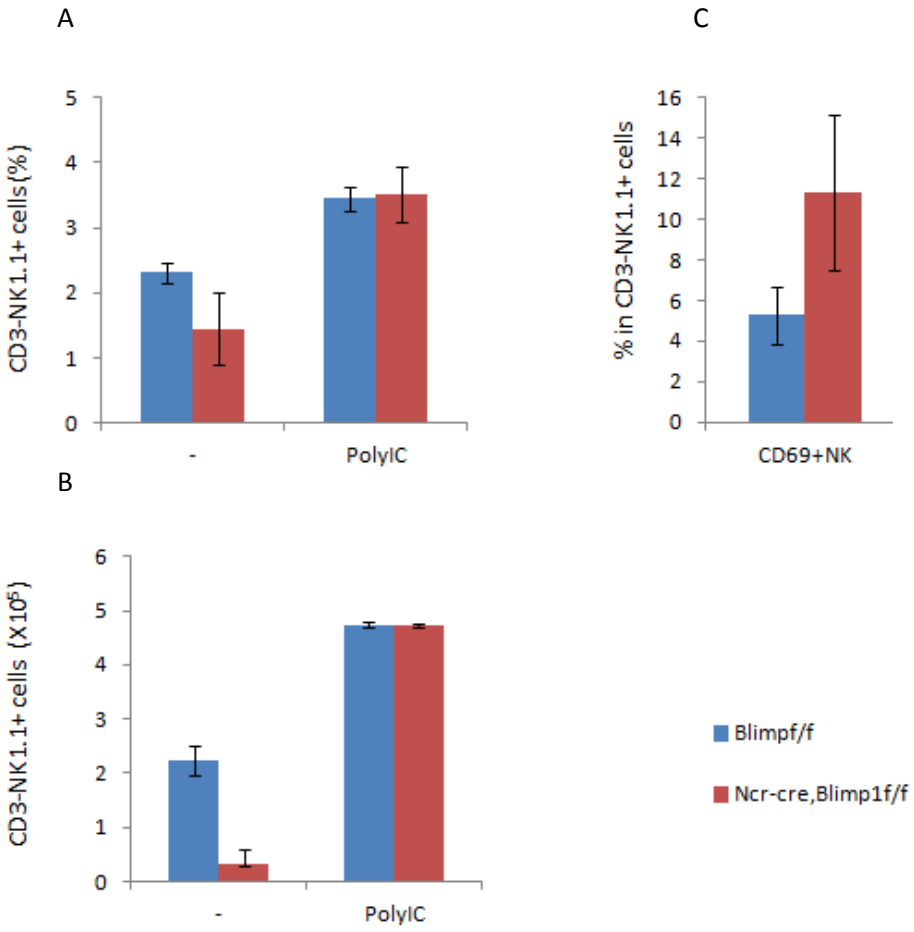
A
CD3-NK1.1+ cells(%)
5
4
3
2
1
0
-
PolyIC
C
% in CD3-NK1.1+ cells
16
14
12
10
8
6
4
2
0
CD69+NK
B
CD3-NK1.1+ cells (X10⁵)
6
5
4
3
2
1
0
-
PolyIC
Blimpf/f
Ncr-cre,Blimp1f/f

D

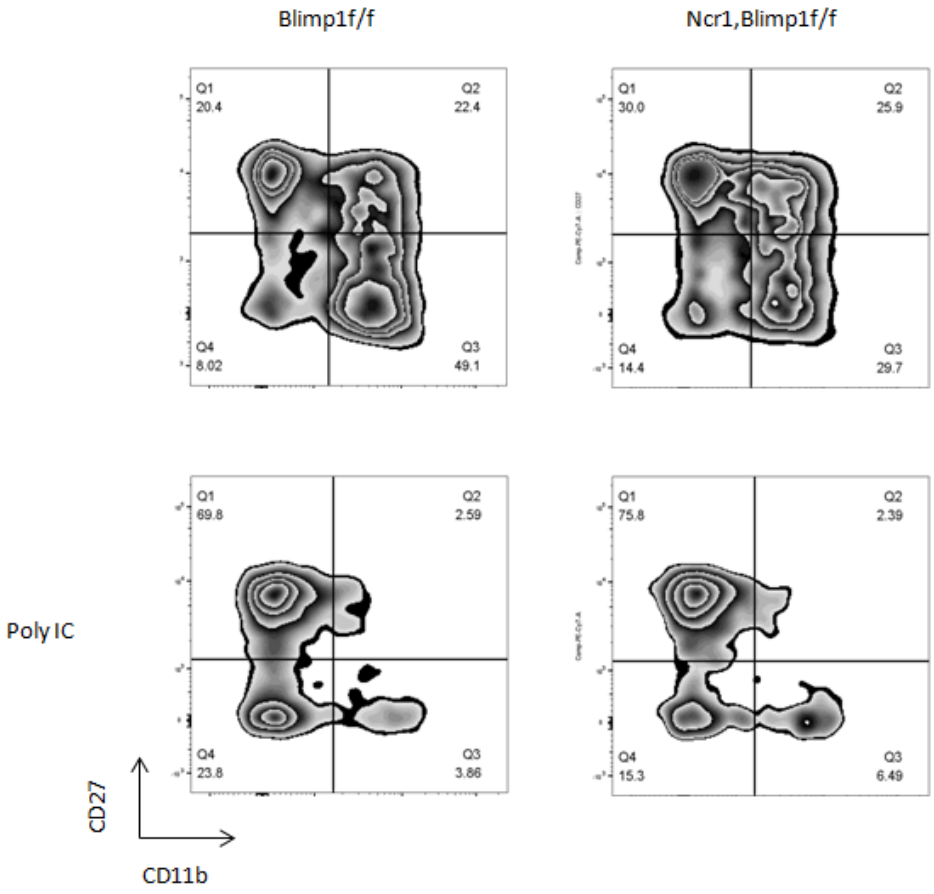
Blimp1f/f
Ncr1,Blimp1f/f
Q1
20.4
Q2
22.4
Q4
8.02
Q3
49.1
Q1
30.0
Q2
25.9
Q4
14.4
Q3
29.7
Poly IC
Q1
69.8
Q2
2.59
Q4
23.8
Q3
3.86
Q1
75.8
Q2
2.39
Q4
15.3
Q3
6.49
CD27
CD11b

Figure 4-8: Chronic PolyIC stimulation restores NK cells in spleen

4 mice/ phenotype were injected ip with 200µg poly IC every other day for 4 weeks. Spleens were harvested and lymphocyte profiles were analyzed by FACS. (A) Percentage of NK cells among total lymphocytes in spleen. (B) Absolute numbers of NK cells in spleen within the lymphocyte gate. (C) Comparison of the percentage of activated NK cells in Ncr1-cre, blimp1f/f and control mice. (D) Representative pattern of NK cell subsets distribution in Ncr1-cre, blimp1f/f and control mice.

A

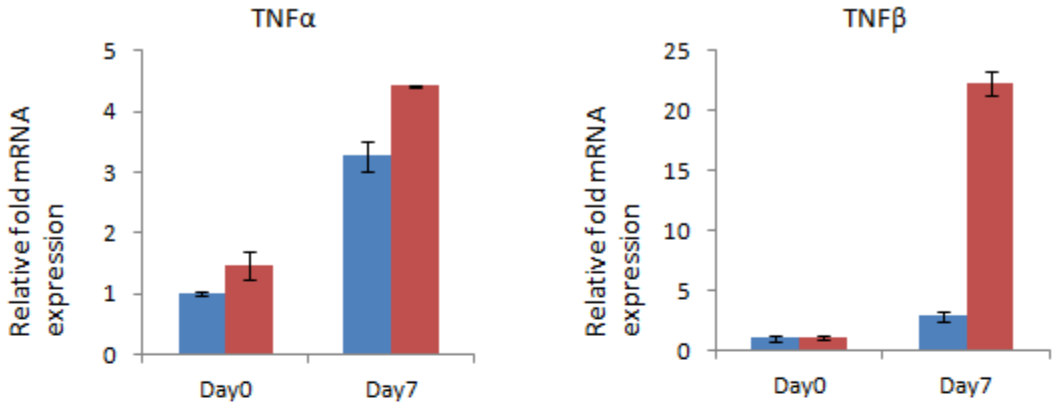
TNFα
Relative fold mRNA expression
5
4
3
2
1
0
Day0
Day7
TNFβ
Relative fold mRNA expression
25
20
15
10
5
0
Day0
Day7

B

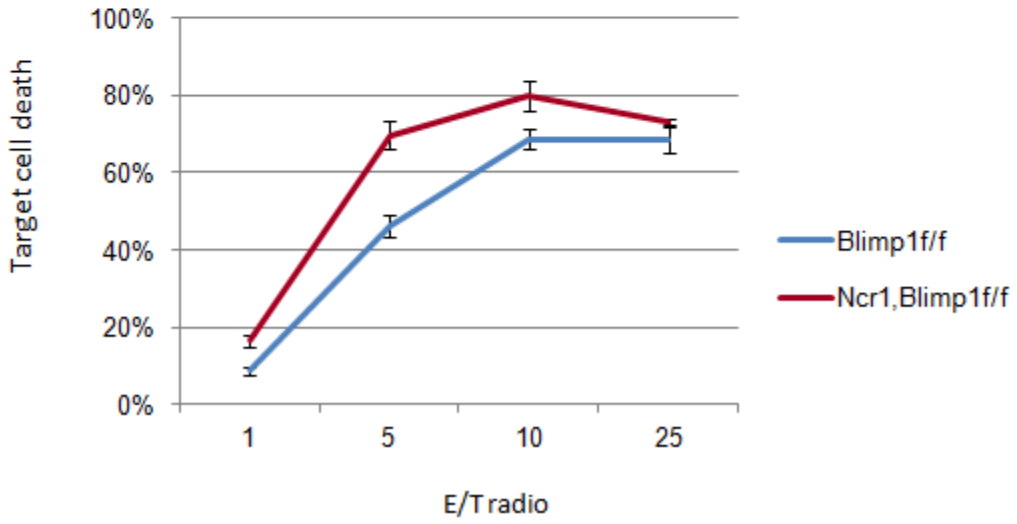
Target cell death
100%
80%
60%
40%
20%
0%
1
5
10
25
E/T radio
Blimp1f/f
Ncr1,Blimp1f/f

Figure 4-9: Blimp1 has an effect on NK cell cytotoxicity

(A) RNA was extracted from freshly isolated NK cells and IL2 expanded NKcells at day 7. Expression of known Blimp1 targets TNFα and TNFβ was tested by q-RT-PCR. (B) 1000 CFSE labeled YAC-cells were cocultured with day 7 NK cells at the indicated effector-target ratios in 200ul medium containing 1000U/ml IL2 in a round-bottom 96-well plate for 4 hours at 37°C. Killed cells were labeled with PI and analyzed by flow cytometry.

Ncr1-cre, Blimp1f/f,Lmp1$^{stopf/-}$

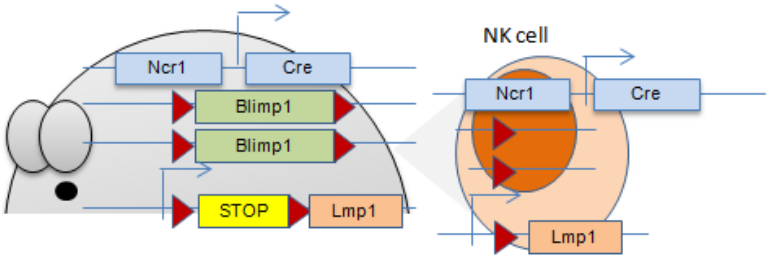

Figure 4-10: NK-lineage specific Blimp 1 knockout and Lmp1 knockin mice

Blimp1f/f,Lmp1$^{stopf/-}$ mice have *Lmp1* coding sequence inserted into the *Gt(ROSA)26Sor* locus. The transcription of lmp1 was blocked by a loxP-flanked STOP fragment placed between the ROSA26 promoter and the LMP1 coding sequences. When bred with Ncr1-cre mice, the offspring had the STOP fragment deleted in Cre expressing NK cells, resulting in expression of lmp1. At the same time, Cre-mediated deletion of Blimp1 resulted in Blimp1 knock out in NK cells.

A

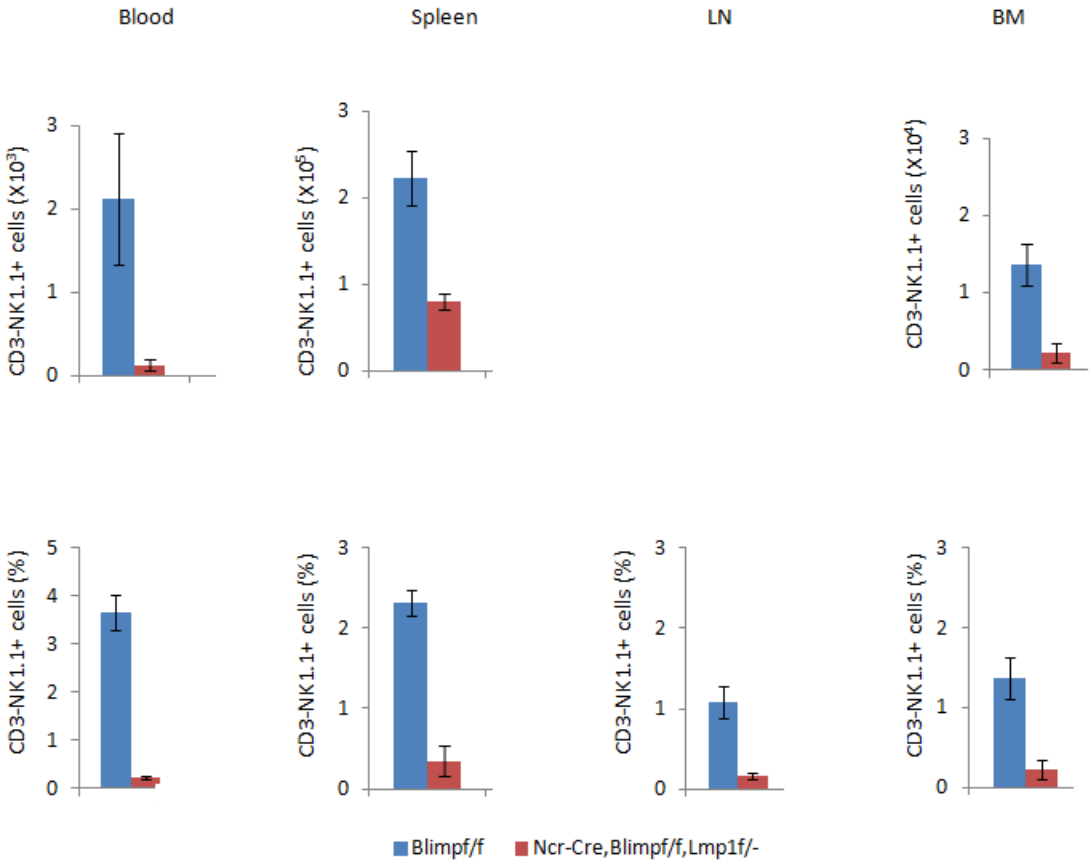
Blood
Spleen
LN
BM
CD3-NK1.1+ cells (X10³)
CD3-NK1.1+ cells (X10⁵)
CD3-NK1.1+ cells (X10⁴)
CD3-NK1.1+ cells (%)
CD3-NK1.1+ cells (%)
CD3-NK1.1+ cells (%)
CD3-NK1.1+ cells (%)
Blimpf/f
Ncr-Cre,Blimpf/f,Lmp1f/-

B

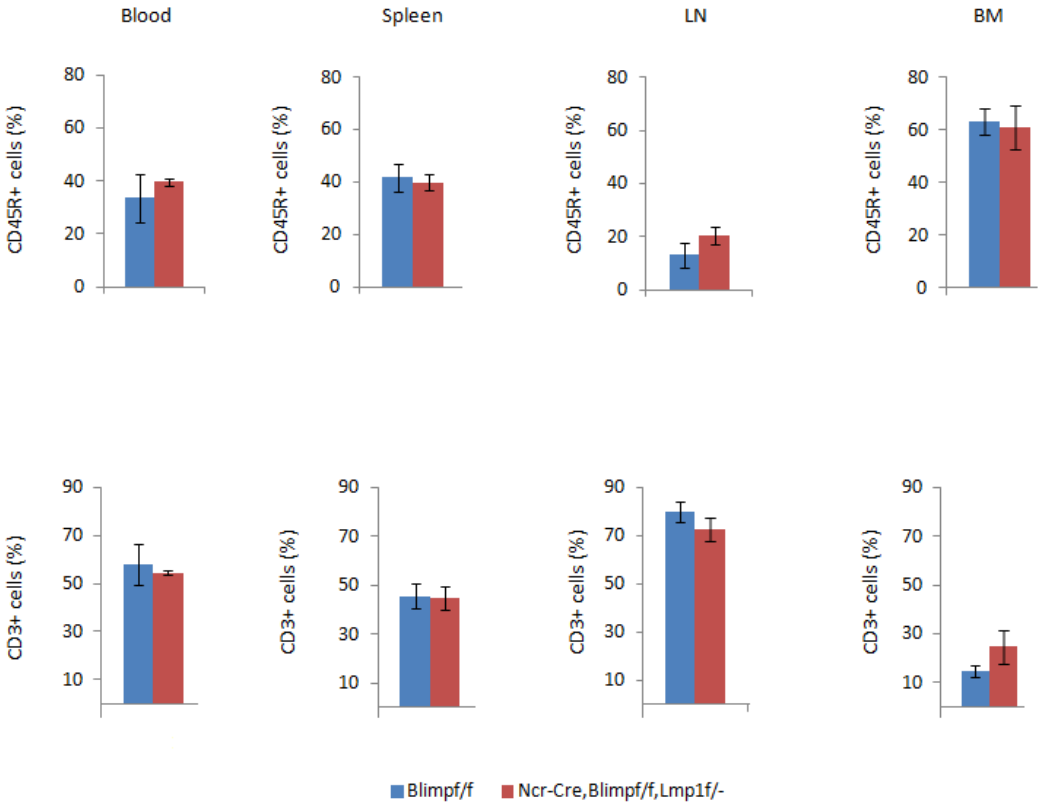
Blood
Spleen
LN
BM
CD45R+ cells (%)
CD3+ cells (%)
0
20
40
60
80
10
30
50
70
90
Blimpf/f
Ncr-Cre,Blimpf/f,Lmp1f/-

Figure 4-11: NK cells were reduced in Ncr1-cre, Blimp1f/f, Lmp1$^{stopf/-}$ mice

Single cell suspensions were prepared from blood, spleen, lymph nodes and the bone marrow in one femur. The lymphcyte profiles were analyzed by FACS. NK cells were gated as CD3-NK1.1+. T cells were gated as CD3+ and different subsets were analyzed by CD4 and CD8 staining. B cells were gated as CD3-CD45R+.(A) Upper panel: absolute NK cell number in different lymphoid sites. Lower panel: percentage of NK cells in total lymphocytes in different lymphoid sites. (B) Percentage of B cells (upper panel) and T cells (lower panel) in different lymphoid sites. LN: lymph node, BM: bone marrow. Absolute numbers of cells in lymph nodes could not be determined in Ncr1-cre, Blimp1f/f, Lmp1$^{stopf/-}$ mice due to their small size.

A

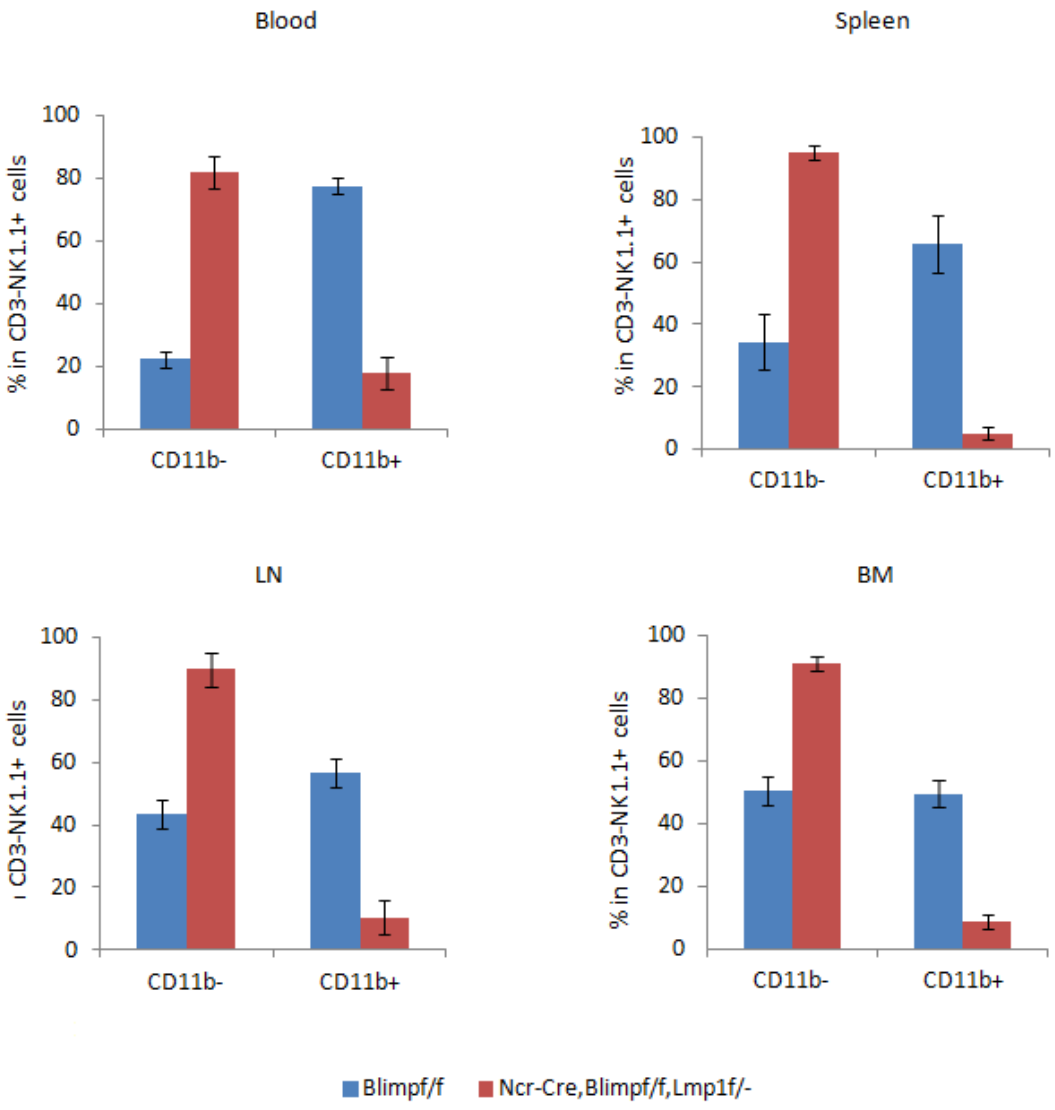
Blood
Spleen
LN
BM
% in CD3-NK1.1+ cells
100
80
60
40
20
0
CD11b-
CD11b+
Blimpf/f
Ncr-Cre,Blimpf/f,Lmp1f/-

B

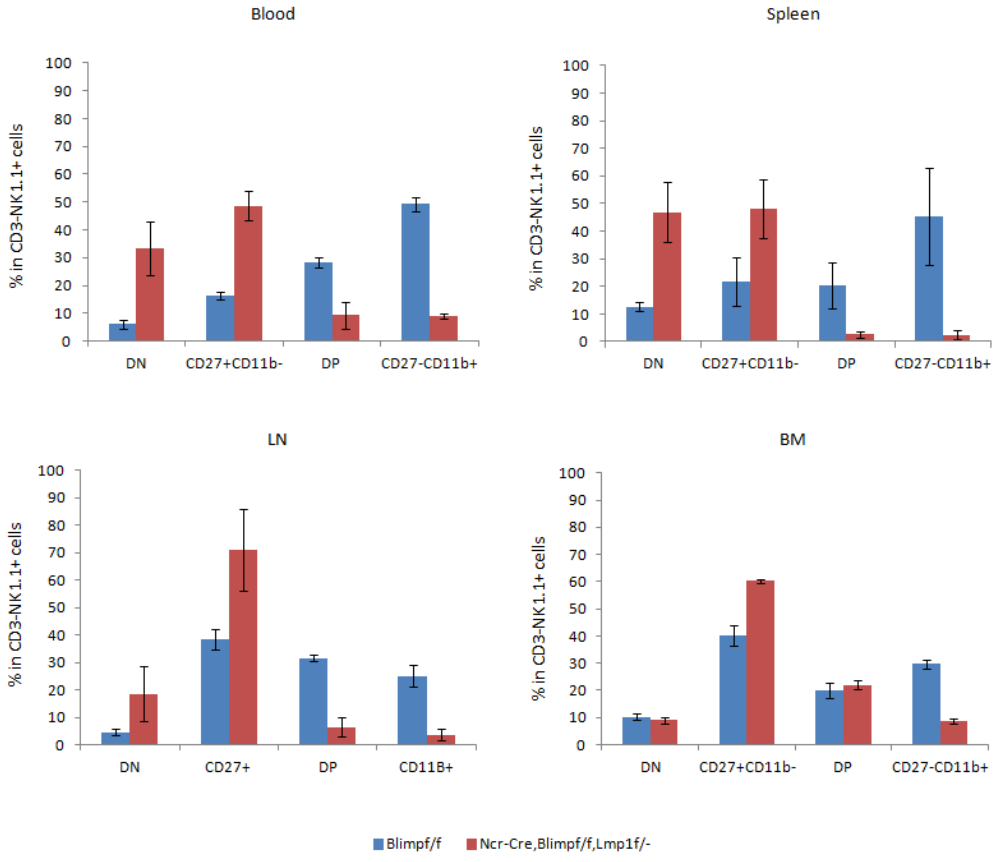
Blood
Spleen
LN
BM
% in CD3-NK1.1+ cells
100
90
80
70
60
50
40
30
20
10
0
DN
CD27+CD11b-
DP
CD27-CD11b+
CD27+
CD11B+
Blimpf/f
Ncr-Cre,Blimpf/f,Lmp1f/-

Figure 4-12: NK cell subsets distribution in Ncr1-cre, Blimp1f/f, Lmp1$^{stopf/-}$ mice

NK cells were gated as CD3-NK1.1+. Different subsets were analyzed by the expression of CD27 and CD11b. (A) Comparison of the percentage of CD11b- and CD11b+ NK cells in different lymphoid sites in Ncr1-cre, Blimp1f/f, Lmp1$^{stopf/-}$ mice and control mice. (B) NK cell subset distribution in different lymphoid sites in Ncr1-cre, Blimp1f/f, Lmp1$^{stopf/-}$ mice and control mice.

A

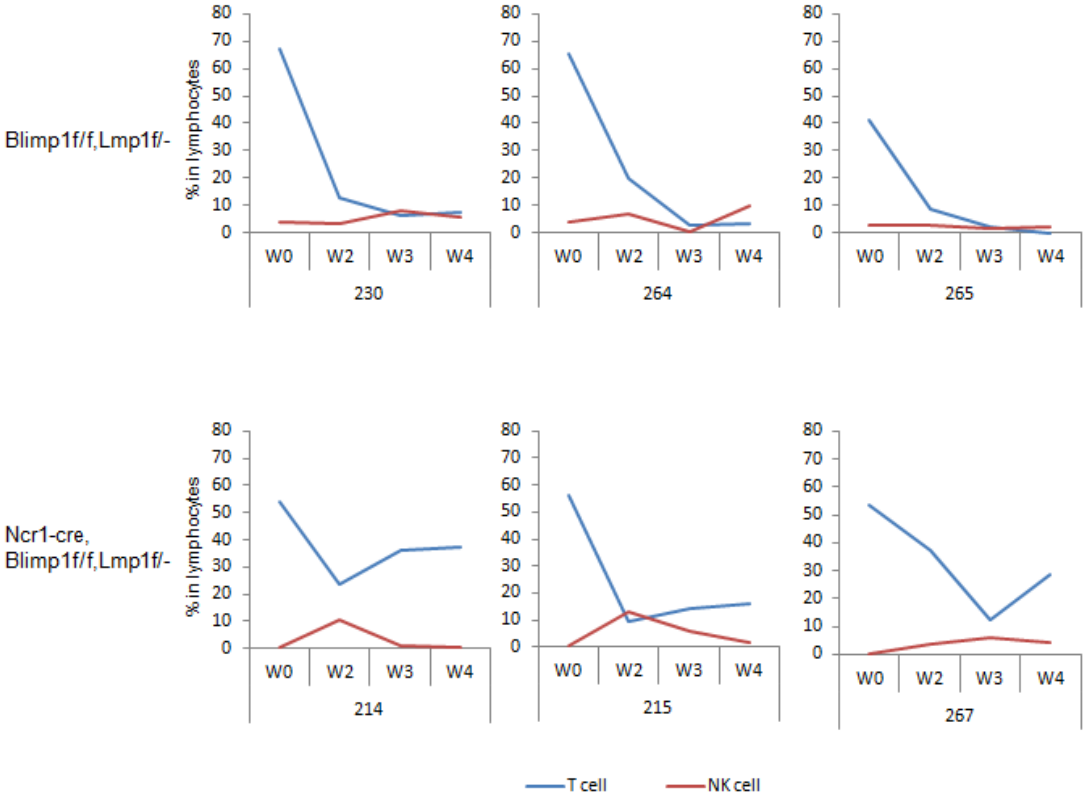
Blimp1f/f,Lmp1f/-
Ncr1-cre, Blimp1f/f,Lmp1f/-
% in lymphocytes
80
70
60
50
40
30
20
10
0
W0
W2
W3
W4
230
264
265
214
215
267
T cell
NK cell

B

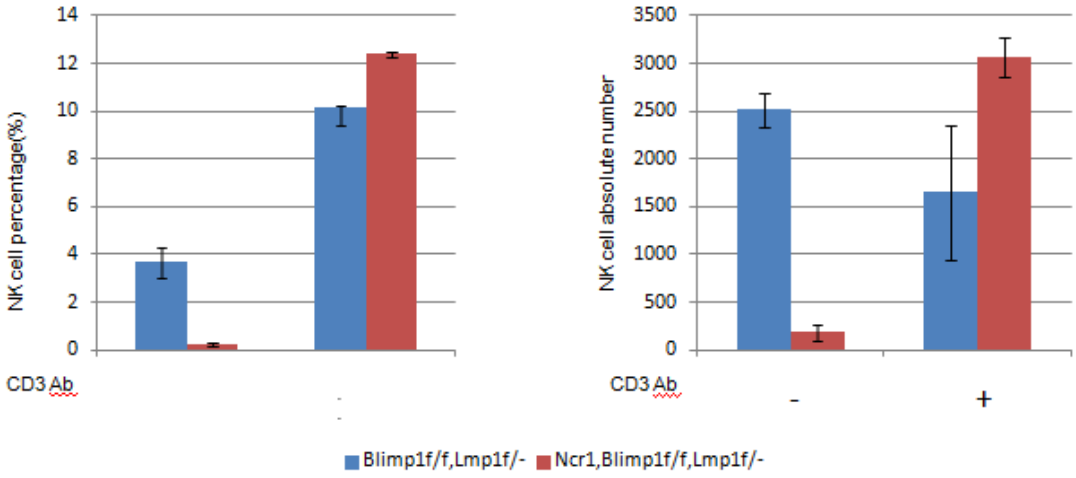
NK cell percentage(%)
14
12
10
8
6
4
2
0
CD3 Ab
NK cell absolute number
3500
3000
2500
2000
1500
1000
500
0
CD3 Ab
-
+
Blimp1f/f,Lmp1f/-
Ncr1,Blimp1f/f,Lmp1f/-

C

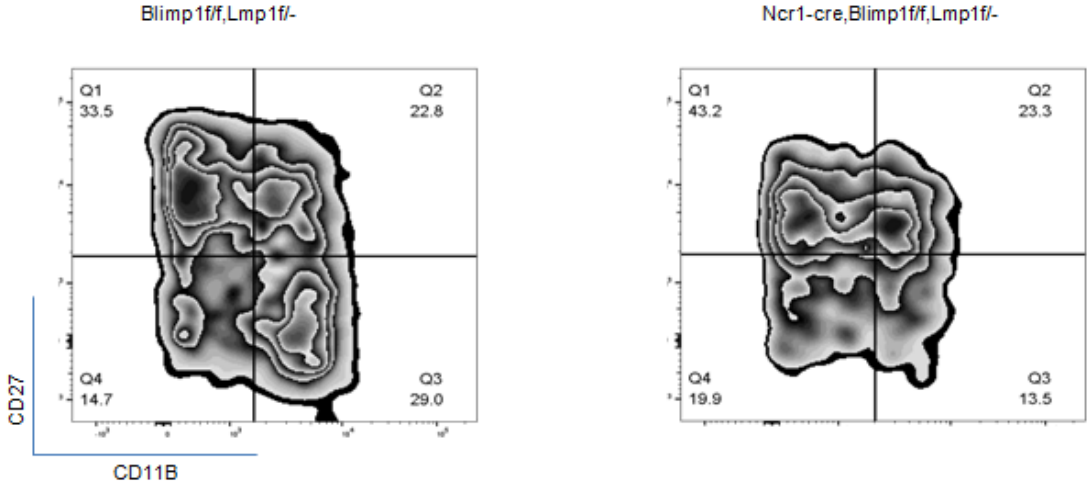
Blimp1f/f,Lmp1f/-
Q1
33.5
Q2
22.8
Q4
14.7
Q3
29.0
CD27
CD11B
Ncr1-cre,Blimp1f/f,Lmp1f/-
Q1
43.2
Q2
23.3
Q4
19.9
Q3
13.5

Figure 4-13: T cell depletion resulted in transient NK cell growth in Ncr1-cre, Blimp1f/f, Lmp1stopf/- mice

Mice were injected iv with 5mg/kg anti-CD3 antibodies once a week. Peripheral blood was collected retro-orbitally every week after the second week for 3 weeks. The lymphocyte profile was evaluated by FACS. (B) NK cells were analyzed using mice with optimal T cell depletion (< 30%). 3 mice in the control group, 2 mice in the Ncr1-cre, Blimp1f/f, $Lmp1^{stopf/-}$ group were used. Percentage of NK cells in total lymphocytes (Right panel) and absolute number of NK cells in peripheral blood are indicated as mean ± SEM. (C) Representative pattern of NK cell subsets distribution. NK cells were stained with CD3-NK1.1+. Subsets were analyzed by the expression of CD27 and CD11b.

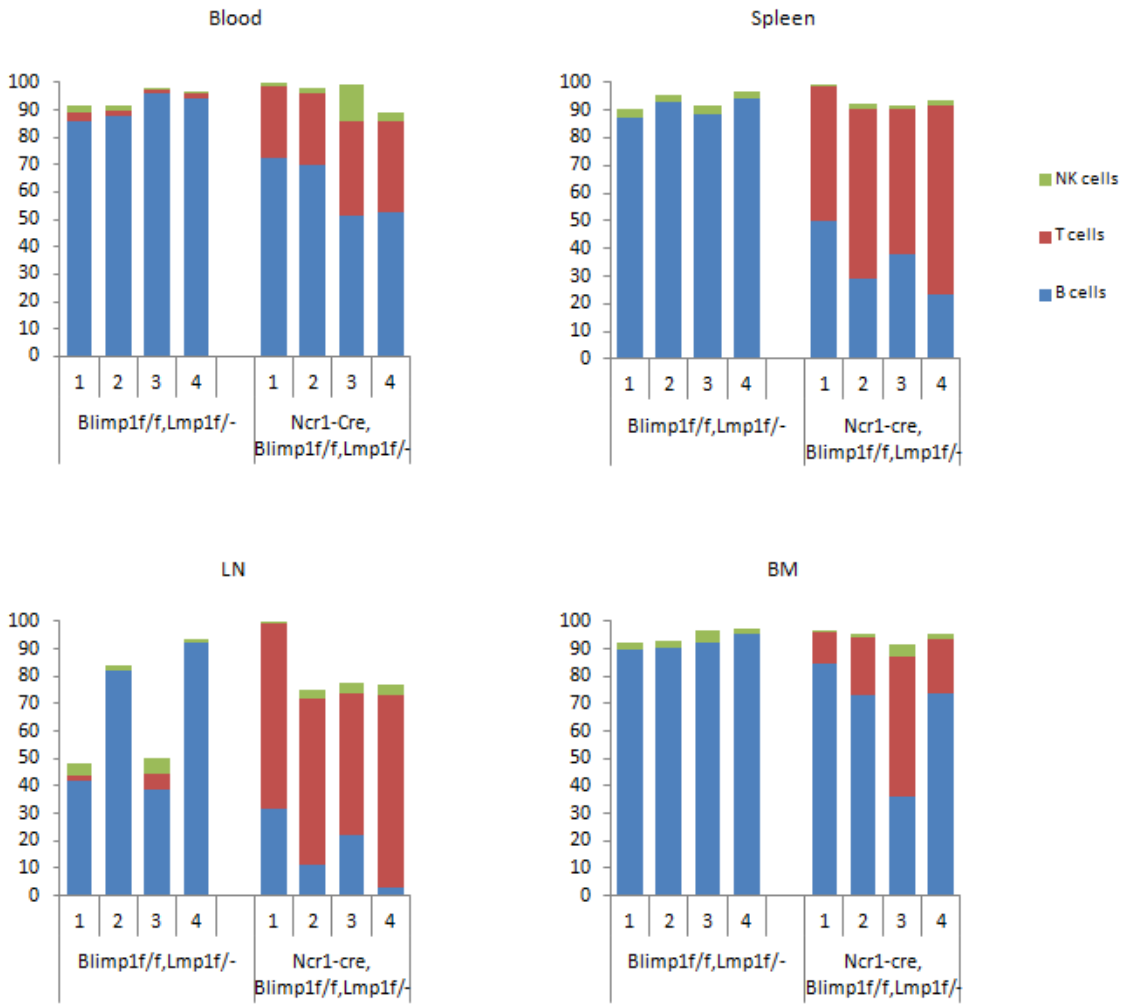
Blood
Spleen
LN
BM
100
90
80
70
60
50
40
30
20
10
0
1
2
3
4
Blimp1f/f,Lmp1f/-
Ncr1-Cre, Blimp1f/f,Lmp1f/-
Ncr1-cre, Blimp1f/f,Lmp1f/-
NK cells
T cells
B cells

Figure 4-14: T cell depletion in Ncr1-cre, Blimp1f/f, Lmp1stopf$^{/-}$ and control mice

Mice were injected ip with 40µg anti-CD3 antibodies daily for 5 consecutive days every other week for 2 months. 4 surviving mice in each group were then euthanized and their lymphocyte profile was evaluated in peripheral blood, spleen, lymph nodes and bone marrow. T cells were stained with CD3. B cells were stained with CD45R. NK cells were stained with CD3-NK1.1+. The percentage of T cells, B cells and NK cells is indicated for each mouse.

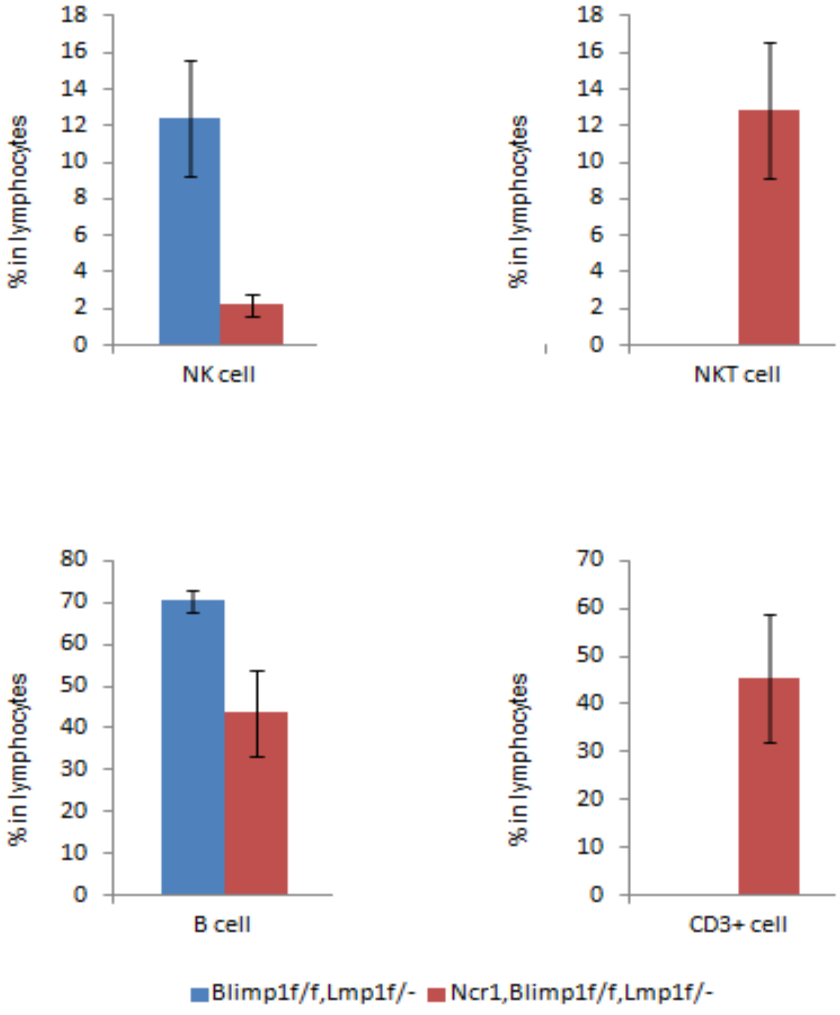
% in lymphocytes
NK cell
NKT cell
B cell
CD3+ cell
Blimp1f/f,Lmp1f/-
Ncr1,Blimp1f/f,Lmp1f/-

Figure 4-15: Occurrence of NKT cells in Ncr1-cre, Blimp1f/f, Lmp1$^{stopf/-}$ mice bone marrow after two months T cell depletion

Mice were injected ip with 40µg anti-CD3 antibodies daily for 5 consecutive days every other week for 2 months. 4 surviving mice in each group were then euthanized and their lymphocyte profile was evaluated in peripheral blood, spleen, lymph nodes and bone marrow. The frequency of NK cells (CD3-NK1.1+), NKT cells (CD3+NK1.1+) T cells (CD3+) and B cells (CD3-CD45R+) is indicated as mean ± SEM.

Chapter V

Summary and future directions

Global gene expression, methylation and mutation profile studies enable us to gain a better understanding of the changes in the comprehensive signaling network in NKTCL. In this summary, I will describe our major findings including activating STAT3 and STAT5B mutations and inactivation of Blimp1 in NKTCL.

Activating mutations in STAT3 and STAT5B were observed in lymphomas derived from NK cells and γδ-T cells. STAT3 mutations mainly were present in NKTCL cases and NK and γδ-T cell lines, whereas STAT5B mutations were frequently observed in γδ-T cell-derived lymphomas including PC- and HS-PTCL and enteropathy associated T-cell lymphoma (EATL) type II. All the mutations were present in the SH2 domain, which is required for STAT protein dimerization. Our experiments clearly showed that the mutated histidine within the SH2 domain of N642H STAT5B mutant bound to the phosphotyrosine of another STAT5B with a 5-fold higher affinity, resulting in a more stable N642H STAT5B homodimer or heterodimer that resistant to inactivation. Moreover, the mutant p-STAT5B dimers bound to their targets with higher occupancy and upregulated their expression. All of these resulted in the constitutive activation of the JAK-STAT pathway, which promoted NK cell proliferation, survival and transformation in NKTCL. The STAT3 and STAT5B proteins with activating mutations can still be regulated by upstream molecules. In our study we showed that JAK inhibitor treatment and SOCS6 overexpression can ablate the activating effect of mutant STAT3 and STAT5B in NK cells. The role of activating STAT5B mutation in NKTCL is summarized in Figure 5-1.

The question that arises after determining that mutant N642H STAT5B bound to certain known targets such as IL2Ra, Bcl-2, Bcl-XL and MIR155, with higher occupancy is whether the N642H STAT5B can bind to different targets. In the future, alterations in target genes and the activity of signaling pathways will be identified by CHIP-SEQ and

GEP analysis respectively. In order to distinguish the endogenous STAT5B and ectopic wild-type or mutant STAT5B, NK cell lines will be transduced with vector containing triple-flag tag labeled STAT5B. A triple-flag tag was fused to the C-terminus of WT or mutant STAT5B, and the entire sequence was inserted into PMIG vector. We already showed that fusion of triple-flag tag at its C-terminus did not affect STAT5B's phosphorylation and function. Western blot analysis showed that triple-flag wild-type and N642H STAT5B were phosphorylated upon IL2 stimulation (Fig 5-2A). CHIP-q-PCR using anti-flag antibody showed N642H STAT5B bound to its known target with higher occupancy (Fig 5-2B).

To help identify the direct target genes of STAT 5B employing GEPanalysis, it is important to capture the changes immediately after STAT5B activation, as prolonged activation may result in secondary signaling changes. Thus, we established a regulated STAT5B expression system for future application. In this system, triple-flag wild-type or N642H STAT5B was fused to an engineered Escherichia coli dihydrofolate reductase (DHFR) on its C-terminus, resulting in the rapid degradation of the entire fusion protein until stabilized by the small molecule trimethoprim (TMP) (Fig 5-3). This allows us to regulate the expression of STAT5B rapidly at the protein level.

As our in vitro experiments provided strong evidence to support our hypothesis that activating STAT3 and STAT5B mutations were driver mutations leading to the development of NKTCL, our next goal is to test our hypothesis in vivo. Conditional STAT5B N642H knock-in can be achieved using the Cre-loxP system. Using the CRISPR/Cas9 system, exon 16 of *STAT5B* will be replaced by a construct in which the sequence of WT-STAT5B followed by the inverted sequence of *STAT5B* N642H is flanked by two loxP sites with opposite orientation. We designed two sets of sgRNAs targeting regions within intron 15 and intron 17 of the *STAT5B* gene. The sgRNAs

should guide Cas9n nickase to the specific region and generate nicks on both DNA strands, in this case, resulted in cutting out *STAT5B* exon 16 with its flanking sequences. The double-strand break then can undergo homology-directed repair (HDR) in the presence of the template containing homology arm and loxP sites flanking WT STAT5B exon16- inverted STAT5B N642H exon 16 sequences, results in the replacement STAT5B exon 16 with the loxP sites flanked WT STAT5B exon16- inverted STAT5B N642H exon 16 sequence (Fig 5-4). The targeting donor vector WT STAT5B exon16-inverted STAT5B N642H exon 16- Bluescript was generated using Gibson Assembly. In its natural state, STAT5B encodes WT STAT5B, but when the STAT5B N642H f/- mice were crossed with Cre mice, Cre mediated inversion of the WT STAT5B exon16 -inverted STAT5B N642H exon 16 sequence results in the expression of STAT5B N642H (Fig 5-5). SgRNAs were cloned into the PU57 vector for in vitro transcription using T7 promoter. SgRNAs, Cas9n protein and the targeting donor vector will be injected into one-cell C57/Bl6 embryos. Pups with correct targeting will be identified by PCR and Southern blotting. Knock-in mice will then be bred to Ncr1-cre mice to determine the phenotypic effects of mutant STAT5B in NK cells and whether NKTCL develops.

In vivo study of Blimp1 showed that loss of Blimp1 immediately after the pro-NK stage resulted in partial impairment of NK cell maturation. Compared to wild-type mice, NK cell frequency in Blimp1-deficient mice was higher in bone marrow but lower in peripheral blood, lymph nodes and spleen as the transition from immature CD11b- subsets to mature CD11b+ subsets was partially blocked. However, Blimp1-deficient NK cells had better proliferation, survival and cytotoxic ability than wild-type NK cells in vitro in medium containing IL2. Blimp1-deficient NK cells also proliferated better than wild-type NK cells upon stimulated with dsRNA analog polyIC in vivo. However, we did not observe tumor develop in Ncr1-cre, Blimp1f/f mice. Since the development of NKTCL is

a multifactorial process, additional genetic alternations are needed to establish a NKTCL mouse model. Based on our recent finding, activating STAT3 and STAT5B mutations are potential driver mutations in NKTCL. Given the observation that IL2 and IL15 activate STAT3 and STAT5B in NK cells, activating STAT3 and STAT5B mutations may provide the stimulation signal to NK cells as it in IL2 and IL15 stimulation in vitro. Therefore, we plan to cross Ncr1-cre, Blimp1f/f mice with STAT5B N642H knockin mice to generate a NK-lineage specific Blimp1 knockout STAT5B N642H knockin mouse model.

To study the role of EBV infection in NKTCL. We generated a NK-lineage specific Blimp1 knockout Lmp1 knockin mouse model. Lmp1-expressing NK cells were destroyed by T cells in the mouse model. NK cells were restored within two weeks in Ncr1-cre, Blimp1f/f, $Lmp1^{stopf/-}$ mice after T cell depletion. However, after two weeks, Lmp1-specific T cells started expending and destroyed Lmp1-expressing NK cells. In order to test whether the combination Lmp1 expression and Blimp1 inactivation lead to NKTCL development, we need to deplete T cells completely. Anti-CD3 blocking antibodies are known to be associated with cytokine-storm related side effects. Therefore, increasing anti-CD3 dose is not practical. Cyclosporin A, an immunosupression drug that selectively inhibits T cell function at least in part by suppressing transcription of NFAT target genes including IL2, can be used alone or with CD3 antibody to enhance T cell depletion. Alternatively, Ncr1-cre, Blimp1f/f, $Lmp1^{stopf/-}$ mice can be cross with $TCR\beta^{-/-};TCR\delta^{-/-}$ mice which lack T cells. To study the feature of NK cell subsets, each NK subsets will be sorted and injected into $Rag2^{-/-}\gamma c^{-/-}$ mice respectively. For in vitro functional study, NK cells will be isolated from $Lmp1^{stopf/-}$ and Blimp1f/f, $Lmp1^{stopf/-}$ mice and treated with a soluble TAT-Cre to create Cre-mediated deletion in vitro. As mentioned in the discussion section, a large portion of the remaining

CD3+ cells were CD3+NK1.1+ NKT cells in Ncr1-cre, Blimp1f/f, Lmp1$^{stopf/-}$ mice. A study showed that NKp46 is expressed on a minute fraction of NK-like T cells (Walzer et al., 2007), and these NKp46-expressing NKT cells have higher proliferation and survival ability and propensity to become leukemic in IL-15 transgenic mice (Yu et al., 2011). To address the increase in NKT cells is due to the antigenic stimulation of Lmp1-expressing NK cells or intrinsic oncogenic effect of Lmp1, it is important to determine whether these CD3+NK1.1 NKT cells express NKp46, since Lmp1 expression is regulated by Cre under the control of the NKp46 (Ncr1) promoter. NKp46 expression can be detected by FACS. Lmp1 expression will be determined by q-RT-PCR on sorted CD3+NK1.1+ T cells.

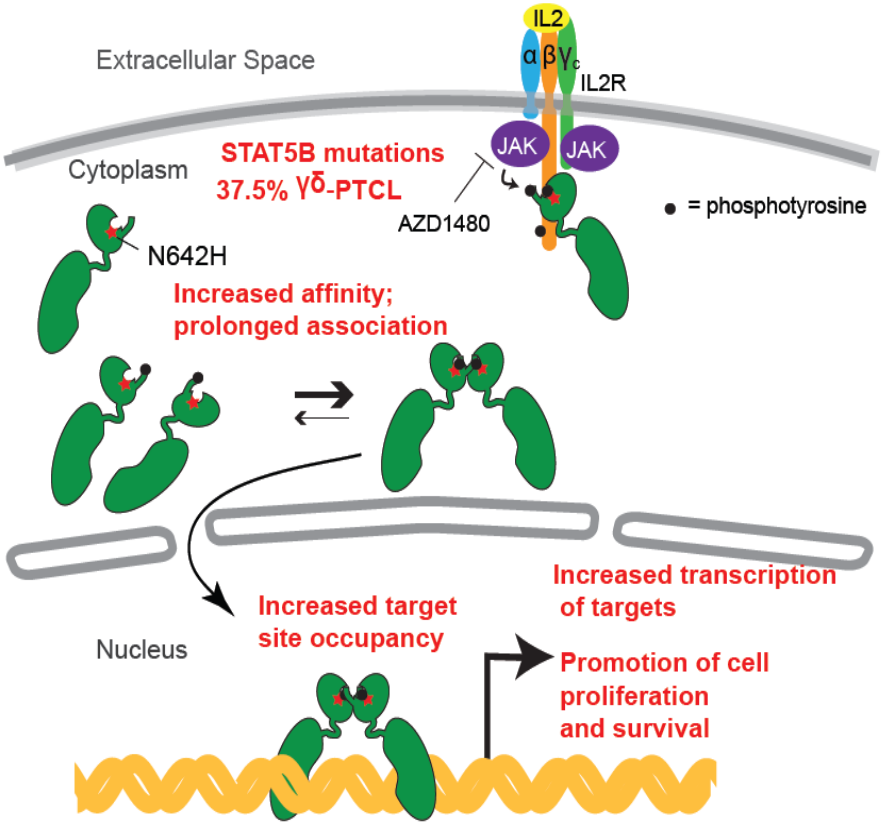
IL2
αβγc
IL2R
Extracellular Space
Cytoplasm
JAK
JAK
STAT5B mutations
37.5% γδ-PTCL
AZD1480
= phosphotyrosine
N642H
Increased affinity;
prolonged association
Increased target
site occupancy
Increased transcription
of targets
Nucleus
Promotion of cell
proliferation
and survival

Figure 5-1: Summary of the functional effects of activating STAT5B N642H mutation

STAT5B N642H mutation was frequently observed in γδ-PTCL. Mutant STAT5B, upon phosphorylation, can form a more stable dimer with prolonged activation. Mutant p-STAT5B bound to its target genes with increased occupancy and upregulated their expression, resulting in increased cell proliferation and survival.

A

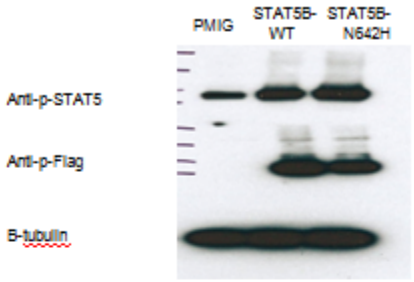
PMIG
STAT5B-WT
STAT5B-N642H
Anti-p-STAT5
Anti-p-Flag
B-tubulin

B

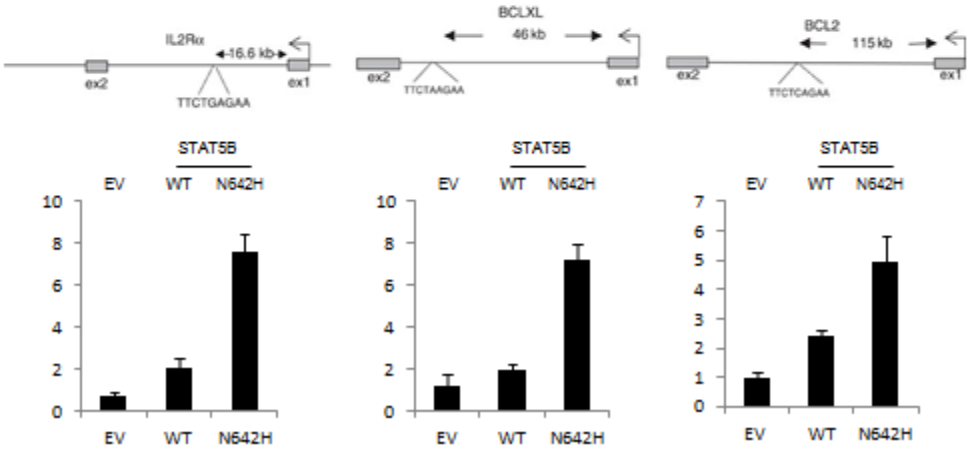
IL2Rα
16.6 kb
ex2
ex1
TTCTGAGAA
BCLXL
46 kb
ex2
TTCTAAGAA
ex1
BCL2
115 kb
ex2
TTCTCAGAA
ex1
STAT5B
EV
WT
N642H
10
8
6
4
2
0
STAT5B
EV
WT
N642H
10
8
6
4
2
0
STAT5B
EV
WT
N642H
7
6
5
4
3
2
1
0

Figure 5-2: Triple flag fusion does not alter STAT5B function

KAI3 cell were transduced with PMIG empty vector (EV) and vector containing wild-type STAT5B-triple flag or STAT5B N642H-triple flag construct. Western blot analysis of total STAT5 protein and STAT5B-triple flag fusion protein was performed using anti-STAT5 antibody and anti-flag antibody respectively. β-tubulin was used as loading control. (B) ChIP-q-PCR results for known STAT5 binding sites are shown for *IL2Rα, BCL-XL, and BCL2* in EV, STAT5B-WT-triple flag or STAT5B-N642H-triple flag transduced KAI3 cells. Anti-flag pull-down normalized to IgG control as a fold difference is shown in the y-axis using a log scale. STAT5B consensus sites and their approximate distance to the TSS sites are indicated.

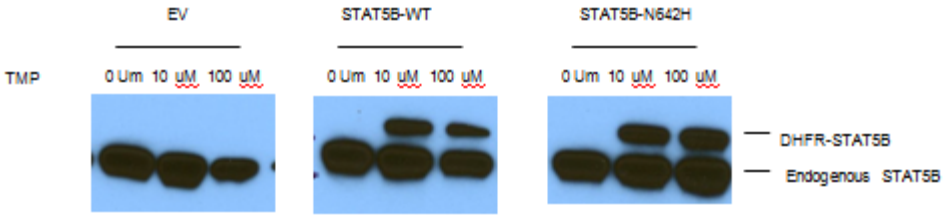
EV
STAT5B-WT
STAT5B-N642H
TMP
0 Um 10 uM 100 uM
0 Um 10 uM 100 uM
0 Um 10 uM 100 uM
DHFR-STAT5B
Endogenous STAT5B

Figure 5-3: TMP-mediated dose-dependent expression of STAT5B using DHFR vector

KAI3 cells were transduced with DHFR empty vector (EV) and vector containing wild-type STAT5B-triple flag or STAT5B N642H-triple flag construct. Cells were treated with TMP at indicated concentrations for 12 hours. Western blot analysis of endogenous p-STAT5 protein and DHFR-STAT5B-triple flag fusion protein was performed using anti p-STAT5 antibody. The ~120kDa band indicates DHFR-STAT5B-triple flag fusion protein, the ~90kDa bind indicates endogenous p-STAT5 protein.

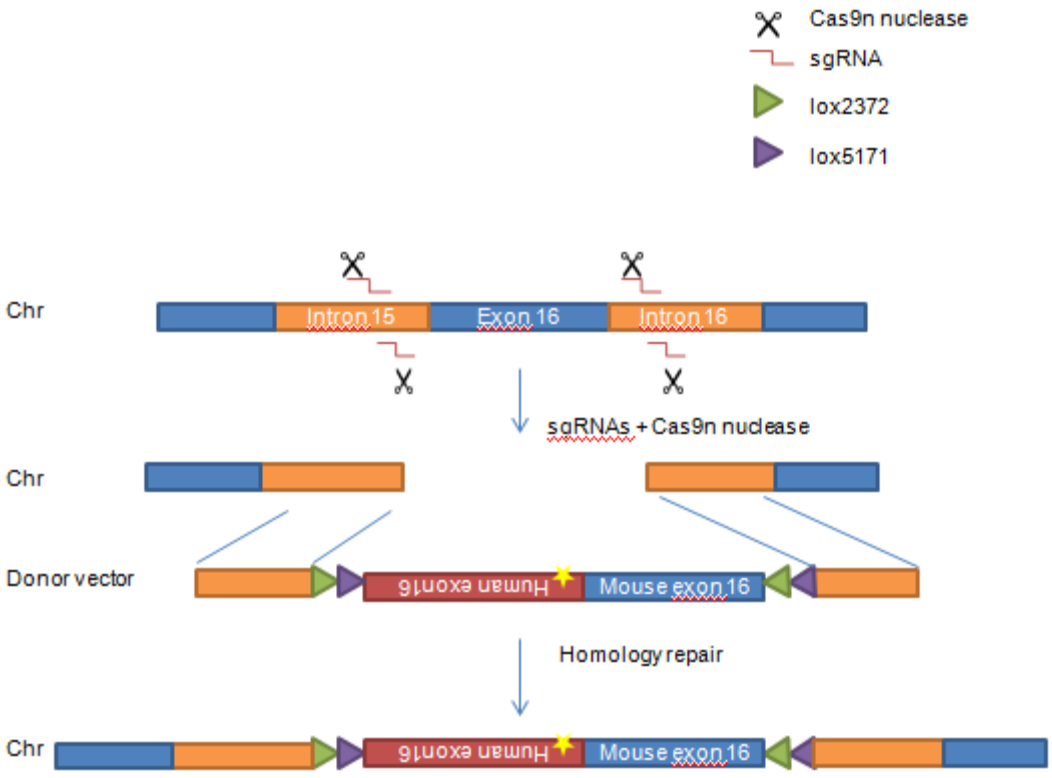
Cas9n nuclease
sgRNA
lox2372
lox5171
Chr
Intron 15
Exon 16
Intron 16
sgRNAs + Cas9n nuclease
Chr
Donor vector
Human exon16
Mouse exon 16
Homology repair
Chr
Human exon16
Mouse exon 16

Figure 5-4: Schematics of the donor plasmid and targeting strategy for HDR-mediated knock-in of loxP flanked WT STAT5B exon 16-inverted STAT5B N64H exon 16 sequences.

Two sets of sgRNAs were designed to target a region in intron 15 and intron 16, resulting in the deletion of the entire exon 16 and a portion of the flanking introns. The donor template consists of upstream homology arm, two loxP sites with a spacer, inverted human exon 16 with N642H mutation, mouse wild type exon 16, two loxP sites and a downstream homology arm. The mouse STAT5B exon 16 will be replaced by the construct after homology-directed repair.

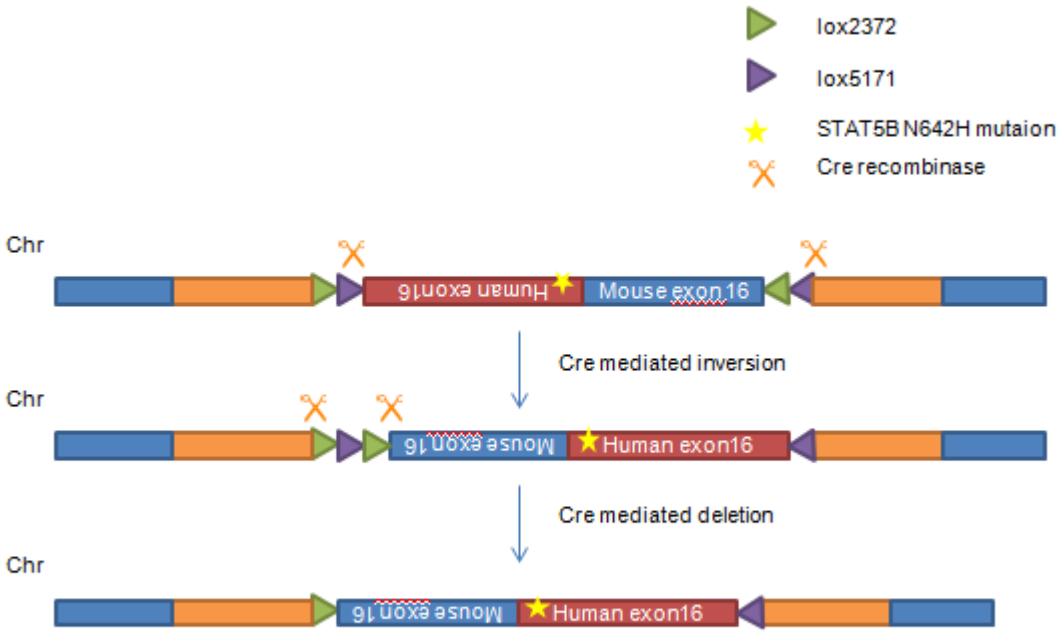
lox2372
lox5171
STAT5B N642H mutaion
Cre recombinase
Chr
Human exon16
Mouse exon16
Cre mediated inversion
Chr
Mouse exon16
Human exon16
Cre mediated deletion
Chr
Mouse exon16
Human exon16

Figure 5-5: Schematic representation of conditional STAT5B N642H knockin by Cre/loxP system.

The inverted mutant human exon 16 followed by mouse wild-type exon 16 was flanked by two pairs of loxP sites. Without Cre recombinase, wild type mouse exon16 will be transcripted. Two pairs of incompatible loxP sites were placed in head-to-head orientation. Cre-mediated recombination between either pair of loxP sites lead to an inversion resulted in transcription of mutant human exon 16. Another pair of loxP sites positioned in the same direction leading to the deletion of loxP sites within the flanked region so that the construct could no longer change.

Chapter VI

Reference

ABECASIS, G. R., AUTON, A., BROOKS, L. D., DEPRISTO, M. A., DURBIN, R. M., HANDSAKER, R. E., KANG, H. M., MARTH, G. T. & MCVEAN, G. A. 2012. An integrated map of genetic variation from 1,092 human genomes. *Nature,* 491**,** 56-65.

AOZASA, K., TAKAKUWA, T., HONGYO, T. & YANG, W. I. 2008. Nasal NK/T-cell lymphoma: epidemiology and pathogenesis. *Int J Hematol,* 87**,** 110-7.

ARIYOSHI, K., NOSAKA, T., YAMADA, K., ONISHI, M., OKA, Y., MIYAJIMA, A. & KITAMURA, T. 2000. Constitutive activation of STAT5 by a point mutation in the SH2 domain. *J Biol Chem,* 275**,** 24407-13.

AU, W. Y., WEISENBURGER, D. D., INTRAGUMTORNCHAI, T., NAKAMURA, S., KIM, W. S., SNG, I., VOSE, J., ARMITAGE, J. O. & LIANG, R. 2009. Clinical differences between nasal and extranasal natural killer/T-cell lymphoma: a study of 136 cases from the International Peripheral T-Cell Lymphoma Project. *Blood,* 113**,** 3931-7.

BALL, M. P., LI, J. B., GAO, Y., LEE, J. H., LEPROUST, E. M., PARK, I. H., XIE, B., DALEY, G. Q. & CHURCH, G. M. 2009. Targeted and genome-scale strategies reveal gene-body methylation signatures in human cells. *Nat Biotechnol,* 27**,** 361-8.

BECKNELL, B. & CALIGIURI, M. A. 2005. Interleukin-2, interleukin-15, and their roles in human natural killer cells. *Adv Immunol,* 86**,** 209-39.

BESSETTE, K., LANG, M. L., FAVA, R. A., GRUNDY, M., HEINEN, J., HORNE, L., SPOLSKI, R., AL-SHAMI, A., MORSE, H. C., 3RD, LEONARD, W. J. & KELLY, J. A. 2008. A Stat5b transgene is capable of inducing CD8+ lymphoblastic lymphoma in the absence of normal TCR/MHC signaling. *Blood,* 111**,** 344-50.

BEZMAN, N. A., KIM, C. C., SUN, J. C., MIN-OO, G., HENDRICKS, D. W., KAMIMURA, Y., BEST, J. A., GOLDRATH, A. W., LANIER, L. L. & IMMUNOLOGICAL GENOME PROJECT, C. 2012. Molecular definition of the identity and activation of natural killer cells. *Nat Immunol,* 13**,** 1000-9.

BOUCHEKIOUA, A., SCOURZIC, L., DE WEVER, O., ZHANG, Y., CERVERA, P., ALINE-FARDIN, A., MERCHER, T., GAULARD, P., NYGA, R., JEZIOROWSKA, D., DOUAY, L., VAINCHENKER, W., LOUACHE, F., GESPACH, C., SOLARY, E. & COPPO, P. JAK3 deregulation by activating mutations confers invasive growth advantage in extranodal nasal-type natural killer cell lymphoma. *Leukemia*.

BRANDES, M., WILLIMANN, K. & MOSER, B. 2005. Professional antigen-presentation function by human gammadelta T Cells. *Science,* 309**,** 264-8.

BUZZA, M. S. & BIRD, P. I. 2006. Extracellular granzymes: current perspectives. *Biol Chem,* 387**,** 827-37.

CHAN, J. K., CHAN, A. C., CHEUK, W., WAN, S. K., LEE, W. K., LUI, Y. H. & CHAN, W. K. 2011. Type II enteropathy-associated T-cell lymphoma: a distinct aggressive lymphoma with frequent gammadelta T-cell receptor expression. *Am J Surg Pathol,* 35**,** 1557-69.

CHEN, J. 2012. Roles of the PI3K/Akt pathway in Epstein-Barr virus-induced cancers and therapeutic implications. *World J Virol,* 1**,** 154-61.

CHIANG, A. K., TAO, Q., SRIVASTAVA, G. & HO, F. C. 1996. Nasal NK- and T-cell lymphomas share the same type of Epstein-Barr virus latency as nasopharyngeal carcinoma and Hodgkin's disease. *Int J Cancer,* 68**,** 285-90.

CHIOSSONE, L., CHAIX, J., FUSERI, N., ROTH, C., VIVIER, E. & WALZER, T. 2009. Maturation of mouse NK cells is a 4-stage developmental program. *Blood,* 113**,** 5488-96.

COMEAU, S. R., GATCHELL, D. W., VAJDA, S. & CAMACHO, C. J. 2004. ClusPro: an automated docking and discrimination method for the prediction of protein complexes. *Bioinformatics,* 20**,** 45-50.

CONG, L. & ZHANG, F. 2015. Genome engineering using CRISPR-Cas9 system. *Methods Mol Biol,* 1239**,** 197-217.

DELABIE, J., HOLTE, H., VOSE, J. M., ULLRICH, F., JAFFE, E. S., SAVAGE, K. J., CONNORS, J. M., RIMSZA, L., HARRIS, N. L., MULLER-HERMELINK, K., RUDIGER, T., COIFFIER, B., GASCOYNE, R. D., BERGER, F., TOBINAI, K., AU, W. Y., LIANG, R., MONTSERRAT, E., HOCHBERG, E. P., PILERI, S., FEDERICO, M., NATHWANI, B., ARMITAGE, J. O. & WEISENBURGER, D. D. 2011. Enteropathy-associated T-cell lymphoma: clinical and histological findings from the international peripheral T-cell lymphoma project. *Blood,* 118**,** 148-55.

DEPRISTO, M. A., BANKS, E., POPLIN, R., GARIMELLA, K. V., MAGUIRE, J. R., HARTL, C., PHILIPPAKIS, A. A., DEL ANGEL, G., RIVAS, M. A., HANNA, M., MCKENNA, A., FENNELL, T. J., KERNYTSKY, A. M., SIVACHENKO, A. Y., CIBULSKIS, K., GABRIEL, S. B., ALTSHULER, D. & DALY, M. J. 2011. A framework for variation discovery and genotyping using next-generation DNA sequencing data. *Nat Genet,* 43**,** 491-8.

DERENZINI, E., LEMOINE, M., BUGLIO, D., KATAYAMA, H., JI, Y., DAVIS, R. E., SEN, S. & YOUNES, A. 2011. The JAK inhibitor AZD1480 regulates proliferation and immunity in Hodgkin lymphoma. *Blood Cancer J,* 1**,** e46.

DI SANTO, J. P. 2006. Natural killer cell developmental pathways: a question of balance. *Annu Rev Immunol,* 24**,** 257-86.

DONALDSON, J. M., ZER, C., AVERY, K. N., BZYMEK, K. P., HORNE, D. A. & WILLIAMS, J. C. 2013. Identification and grafting of a unique peptide-binding site in the Fab framework of monoclonal antibodies. *Proc Natl Acad Sci U S A,* 110**,** 17456-61.

DYBKAER, K., IQBAL, J., ZHOU, G., GENG, H., XIAO, L., SCHMITZ, A., D'AMORE, F. & CHAN, W. C. 2007. Genome wide transcriptional analysis of resting and IL2 activated human natural killer cells: gene expression signatures indicative of novel molecular signaling pathways. *BMC Genomics,* 8**,** 230.

FATRAI, S., WIERENGA, A. T., DAENEN, S. M., VELLENGA, E. & SCHURINGA, J. J. 2011. Identification of HIF2alpha as an important STAT5 target gene in human hematopoietic stem cells. *Blood,* 117**,** 3320-30.

FAURIAT, C., LONG, E. O., LJUNGGREN, H. G. & BRYCESON, Y. T. 2010. Regulation of human NK-cell cytokine and chemokine production by target cell recognition. *Blood,* 115**,** 2167-76.

FERRAN, C., SHEEHAN, K., DY, M., SCHREIBER, R., MERITE, S., LANDAIS, P., NOEL, L. H., GRAU, G., BLUESTONE, J., BACH, J. F. & ET AL. 1990. Cytokine-related syndrome following injection of anti-CD3 monoclonal antibody: further evidence for transient in vivo T cell activation. *Eur J Immunol,* 20**,** 509-15.

FOUROUCLAS, N., LI, J., GILBY, D. C., CAMPBELL, P. J., BEER, P. A., BOYD, E. M., GOODEVE, A. C., BAREFORD, D., HARRISON, C. N., REILLY, J. T., GREEN, A. R. & BENCH, A. J. 2008. Methylation of the suppressor of cytokine signaling 3 gene (SOCS3) in myeloproliferative disorders. *Haematologica,* 93**,** 1635-44.

FOX, C. P., HAIGH, T. A., TAYLOR, G. S., LONG, H. M., LEE, S. P., SHANNON-LOWE, C., O'CONNOR, S., BOLLARD, C. M., IQBAL, J., CHAN, W. C., RICKINSON, A. B., BELL, A. I. & ROWE, M. 2010. A novel latent membrane 2 transcript expressed in Epstein-Barr virus-positive NK- and T-cell lymphoproliferative disease encodes a target for cellular immunotherapy. *Blood,* 116**,** 3695-704.

FREUD, A. G., YOKOHAMA, A., BECKNELL, B., LEE, M. T., MAO, H. C., FERKETICH, A. K. & CALIGIURI, M. A. 2006. Evidence for discrete stages of human natural killer cell differentiation in vivo. *J Exp Med,* 203**,** 1033-43.

FUJIWARA, S., MUROI, K., TATARA, R., MATSUYAMA, T., OHMINE, K., SUZUKI, T., MORI, M., NAGAI, T., TANAKA, A. & OZAWA, K. 2014. Clinical features of de novo CD25-positive follicular lymphoma. *Leuk Lymphoma,* 55**,** 307-13.

GALM, O., YOSHIKAWA, H., ESTELLER, M., OSIEKA, R. & HERMAN, J. G. 2003. SOCS-1, a negative regulator of cytokine signaling, is frequently silenced by methylation in multiple myeloma. *Blood,* 101**,** 2784-8.

GRAHAM, J. P., ARCIPOWSKI, K. M. & BISHOP, G. A. 2010. Differential B-lymphocyte regulation by CD40 and its viral mimic, latent membrane protein 1. *Immunol Rev,* 237**,** 226-48.

GREGOIRE, C., CHASSON, L., LUCI, C., TOMASELLO, E., GEISSMANN, F., VIVIER, E. & WALZER, T. 2007. The trafficking of natural killer cells. *Immunol Rev,* 220**,** 169-82.

HAYAKAWA, Y. & SMYTH, M. J. 2006. CD27 dissects mature NK cells into two subsets with distinct responsiveness and migratory capacity. *J Immunol,* 176**,** 1517-24.

HE, B., YOU, L., UEMATSU, K., ZANG, K., XU, Z., LEE, A. Y., COSTELLO, J. F., MCCORMICK, F. & JABLONS, D. M. 2003. SOCS-3 is frequently silenced by hypermethylation and suppresses cell growth in human lung cancer. *Proc Natl Acad Sci U S A,* 100**,** 14133-8.

HUANG, Y., DE REYNIES, A., DE LEVAL, L., GHAZI, B., MARTIN-GARCIA, N., TRAVERT, M., BOSQ, J., BRIERE, J., PETIT, B., THOMAS, E., COPPO, P., MARAFIOTI, T., EMILE, J. F., DELFAU-LARUE, M. H., SCHMITT, C. & GAULARD, P. 2010. Gene expression profiling identifies emerging oncogenic pathways operating in extranodal NK/T-cell lymphoma, nasal type. *Blood,* 115**,** 1226-37.

IAN, M. X., LAN, S. Z., CHENG, Z. F., DAN, H. & QIONG, L. H. 2008. Suppression of EBNA1 expression inhibits growth of EBV-positive NK/T cell lymphoma cells. *Cancer Biol Ther,* 7**,** 1602-6.

IQBAL, J., KUCUK, C., DELEEUW, R. J., SRIVASTAVA, G., TAM, W., GENG, H., KLINKEBIEL, D., CHRISTMAN, J. K., PATEL, K., CAO, K., SHEN, L., DYBKAER, K., TSUI, I. F., ALI, H., SHIMIZU, N., AU, W. Y., LAM, W. L. & CHAN, W. C. 2009. Genomic analyses reveal global functional alterations that promote tumor growth and novel tumor suppressor genes in natural killer-cell malignancies. *Leukemia,* 23**,** 1139-51.

IQBAL, J., WEISENBURGER, D. D., CHOWDHURY, A., TSAI, M. Y., SRIVASTAVA, G., GREINER, T. C., KUCUK, C., DEFFENBACHER, K., VOSE, J., SMITH, L., AU, W. Y., NAKAMURA, S., SETO, M., DELABIE, J., BERGER, F., LOONG, F., KO, Y. H., SNG, I., LIU, X., LOUGHRAN, T. P., ARMITAGE, J. & CHAN, W. C. Natural killer cell lymphoma shares strikingly similar molecular features with a group of non-hepatosplenic gammadelta T-cell lymphoma and is highly sensitive to a novel aurora kinase A inhibitor in vitro. *Leukemia,* 25**,** 348-58.

JACCARD, A., GACHARD, N., MARIN, B., ROGEZ, S., AUDRAIN, M., SUAREZ, F., TILLY, H., MORSCHHAUSER, F., THIEBLEMONT, C., YSEBAERT, L., DEVIDAS, A., PETIT, B., DE LEVAL, L., GAULARD, P., FEUILLARD, J., BORDESSOULE, D., HERMINE, O., GELA & INTERGROUP, G. 2011. Efficacy of L-asparaginase with methotrexate and dexamethasone (AspaMetDex regimen) in patients with refractory or relapsing extranodal NK/T-cell lymphoma, a phase 2 study. *Blood,* 117**,** 1834-9.

JAFFE, E. S. 2009. The 2008 WHO classification of lymphomas: implications for clinical practice and translational research. *Hematology Am Soc Hematol Educ Program***,** 523-31.

JEREZ, A., CLEMENTE, M. J., MAKISHIMA, H., KOSKELA, H., LEBLANC, F., PENG NG, K., OLSON, T., PRZYCHODZEN, B., AFABLE, M., GOMEZ-SEGUI, I., GUINTA, K., DURKIN, L., HSI, E. D., MCGRAW, K., ZHANG, D., WLODARSKI, M. W., PORKKA, K., SEKERES, M. A., LIST, A., MUSTJOKI, S., LOUGHRAN, T. P. & MACIEJEWSKI, J. P. 2012. STAT3 mutations unify the pathogenesis of chronic lymphoproliferative disorders of NK cells and T-cell large granular lymphocyte leukemia. *Blood,* 120**,** 3048-57.

JIANG, L., GU, Z. H., YAN, Z. X., ZHAO, X., XIE, Y. Y., ZHANG, Z. G., PAN, C. M., HU, Y., CAI, C. P., DONG, Y., HUANG, J. Y., WANG, L., SHEN, Y., MENG, G., ZHOU, J. F., HU, J. D., WANG, J. F., LIU, Y. H., YANG, L. H., ZHANG, F., WANG, J. M., WANG, Z., PENG, Z. G., CHEN, F. Y., SUN, Z. M., DING, H., SHI, J. M., HOU, J., YAN, J. S., SHI, J. Y., XU, L., LI, Y., LU, J., ZHENG, Z., XUE, W., ZHAO, W. L., CHEN, Z. & CHEN, S. J. 2015. Exome sequencing identifies somatic mutations of DDX3X in natural killer/T-cell lymphoma. *Nat Genet,* 47**,** 1061-6.

JOHNSTON, J. A., BACON, C. M., FINBLOOM, D. S., REES, R. C., KAPLAN, D., SHIBUYA, K., ORTALDO, J. R., GUPTA, S., CHEN, Y. Q., GIRI, J. D. & ET AL. 1995. Tyrosine phosphorylation and activation of STAT5, STAT3, and Janus kinases by interleukins 2 and 15. *Proc Natl Acad Sci U S A,* 92**,** 8705-9.

JOHNSTON, J. A., BACON, C. M., RIEDY, M. C. & O'SHEA, J. J. 1996. Signaling by IL-2 and related cytokines: JAKs, STATs, and relationship to immunodeficiency. *J Leukoc Biol,* 60**,** 441-52.

KALLIES, A., CAROTTA, S., HUNTINGTON, N. D., BERNARD, N. J., TARLINTON, D. M., SMYTH, M. J. & NUTT, S. L. 2011. A role for Blimp1 in the transcriptional network controlling natural killer cell maturation. *Blood,* 117**,** 1869-79.

KALLIES, A., HAWKINS, E. D., BELZ, G. T., METCALF, D., HOMMEL, M., CORCORAN, L. M., HODGKIN, P. D. & NUTT, S. L. 2006. Transcriptional repressor Blimp-1 is essential for T cell homeostasis and self-tolerance. *Nat Immunol,* 7**,** 466-74.

KANAI, T., SEKI, S., JENKS, J. A., KOHLI, A., KAWLI, T., MARTIN, D. P., SNYDER, M., BACCHETTA, R. & NADEAU, K. C. 2014. Identification of STAT5A and STAT5B target genes in human T cells. *PLoS One,* 9**,** e86790.

KIM, S., IIZUKA, K., KANG, H. S., DOKUN, A., FRENCH, A. R., GRECO, S. & YOKOYAMA, W. M. 2002. In vivo developmental stages in murine natural killer cell maturation. *Nat Immunol,* 3**,** 523-8.

KIMURA, H., KARUBE, K., ITO, Y., HIRANO, K., SUZUKI, M., IWATA, S. & SETO, M. 2014. Rare occurrence of JAK3 mutations in natural killer cell neoplasms in Japan. *Leuk Lymphoma,* 55**,** 962-3.

KOBOLDT, D. C., CHEN, K., WYLIE, T., LARSON, D. E., MCLELLAN, M. D., MARDIS, E. R., WEINSTOCK, G. M., WILSON, R. K. & DING, L. 2009. VarScan: variant detection in massively parallel sequencing of individual and pooled samples. *Bioinformatics,* 25**,** 2283-5.

KOMABAYASHI, Y., KISHIBE, K., NAGATO, T., UEDA, S., TAKAHARA, M. & HARABUCHI, Y. Downregulation of miR-15a due to LMP1 promotes cell proliferation and predicts poor prognosis in nasal NK/T-cell lymphoma. *Am J Hematol*.

KONDO, M., SCHERER, D. C., KING, A. G., MANZ, M. G. & WEISSMAN, I. L. 2001. Lymphocyte development from hematopoietic stem cells. *Curr Opin Genet Dev,* 11**,** 520-6.

KONG, Y., CAO, W., XI, X., MA, C., CUI, L. & HE, W. 2009. The NKG2D ligand ULBP4 binds to TCRgamma9/delta2 and induces cytotoxicity to tumor cells through both TCRgammadelta and NKG2D. *Blood,* 114**,** 310-7.

KOO, G. C., TAN, S. Y., TANG, T., POON, S. L., ALLEN, G. E., TAN, L., CHONG, S. C., ONG, W. S., TAY, K., TAO, M., QUEK, R., LOONG, S., YEOH, K. W., YAP, S. P., LEE, K. A., LIM, L. C., TAN, D., GOH, C., CUTCUTACHE, I., YU, W., NG, C. C., RAJASEGARAN, V., HENG, H. L., GAN, A., ONG, C. K., ROZEN, S., TAN, P., TEH, B. T. & LIM, S. T. Janus kinase 3-activating mutations identified in natural killer/T-cell lymphoma. *Cancer Discov,* 2**,** 591-7.

KOO, G. C., TAN, S. Y., TANG, T., POON, S. L., ALLEN, G. E., TAN, L., CHONG, S. C., ONG, W. S., TAY, K., TAO, M., QUEK, R., LOONG, S., YEOH, K. W., YAP, S. P., LEE, K. A., LIM, L. C., TAN, D., GOH, C., CUTCUTACHE, I., YU, W., NG, C. C., RAJASEGARAN, V., HENG, H. L., GAN, A.,

ONG, C. K., ROZEN, S., TAN, P., TEH, B. T. & LIM, S. T. 2012. Janus kinase 3-activating mutations identified in natural killer/T-cell lymphoma. *Cancer Discov,* 2**,** 591-7.

KOPP, K. L., RALFKIAER, U., GJERDRUM, L. M., HELVAD, R., PEDERSEN, I. H., LITMAN, T., JONSON, L., HAGEDORN, P. H., KREJSGAARD, T., GNIADECKI, R., BONEFELD, C. M., SKOV, L., GEISLER, C., WASIK, M. A., RALFKIAER, E., ODUM, N. & WOETMANN, A. 2013. STAT5-mediated expression of oncogenic miR-155 in cutaneous T-cell lymphoma. *Cell Cycle,* 12**,** 1939-47.

KOSKELA, H. L., ELDFORS, S., ELLONEN, P., VAN ADRICHEM, A. J., KUUSANMAKI, H., ANDERSSON, E. I., LAGSTROM, S., CLEMENTE, M. J., OLSON, T., JALKANEN, S. E., MAJUMDER, M. M., ALMUSA, H., EDGREN, H., LEPISTO, M., MATTILA, P., GUINTA, K., KOISTINEN, P., KUITTINEN, T., PENTTINEN, K., PARSONS, A., KNOWLES, J., SAARELA, J., WENNERBERG, K., KALLIONIEMI, O., PORKKA, K., LOUGHRAN, T. P., JR., HECKMAN, C. A., MACIEJEWSKI, J. P. & MUSTJOKI, S. Somatic STAT3 mutations in large granular lymphocytic leukemia. *N Engl J Med,* 366**,** 1905-13.

KREBS, D. L. & HILTON, D. J. 2001. SOCS proteins: negative regulators of cytokine signaling. *Stem Cells,* 19**,** 378-87.

KUCUK, C., HU, X., IQBAL, J., GAULARD, P., KLINKEBIEL, D., CORNISH, A., DAVE, B. J. & CHAN, W. C. 2013. HACE1 is a tumor suppressor gene candidate in natural killer cell neoplasms. *Am J Pathol,* 182**,** 49-55.

KUCUK, C., IQBAL, J., HU, X., GAULARD, P., DE LEVAL, L., SRIVASTAVA, G., AU, W. Y., MCKEITHAN, T. W. & CHAN, W. C. 2011. PRDM1 is a tumor suppressor gene in natural killer cell malignancies. *Proc Natl Acad Sci U S A,* 108**,** 20119-24.

KWONG, Y. L. 2005. Natural killer-cell malignancies: diagnosis and treatment. *Leukemia,* 19**,** 2186-94.

LAI, R. H., HSIAO, Y. W., WANG, M. J., LIN, H. Y., WU, C. W., CHI, C. W., LI, A. F., JOU, Y. S. & CHEN, J. Y. SOCS6, down-regulated in gastric cancer, inhibits cell proliferation and colony formation. *Cancer Lett,* 288**,** 75-85.

LAM, L. T., WRIGHT, G., DAVIS, R. E., LENZ, G., FARINHA, P., DANG, L., CHAN, J. W., ROSENWALD, A., GASCOYNE, R. D. & STAUDT, L. M. 2008. Cooperative signaling through the signal transducer and activator of transcription 3 and nuclear factor-{kappa}B pathways in subtypes of diffuse large B-cell lymphoma. *Blood,* 111**,** 3701-13.

LANIER, L. L. 2008. Up on the tightrope: natural killer cell activation and inhibition. *Nat Immunol,* 9**,** 495-502.

LEONG, J. W., CHASE, J. M., ROMEE, R., SCHNEIDER, S. E., SULLIVAN, R. P., COOPER, M. A. & FEHNIGER, T. A. 2014. Preactivation with IL-12, IL-15, and IL-18 induces CD25 and a functional high-affinity IL-2 receptor on human cytokine-induced memory-like natural killer cells. *Biol Blood Marrow Transplant,* 20**,** 463-73.

LI, G., MISKIMEN, K. L., WANG, Z., XIE, X. Y., BRENZOVICH, J., RYAN, J. J., TSE, W., MORIGGL, R. & BUNTING, K. D. 2010. STAT5 requires the N-domain for suppression of miR15/16, induction of bcl-2, and survival signaling in myeloproliferative disease. *Blood,* 115**,** 1416-24.

LI, H. & DURBIN, R. 2009. Fast and accurate short read alignment with Burrows-Wheeler transform. *Bioinformatics,* 25**,** 1754-60.

LONG, E. O. 2008. Negative signaling by inhibitory receptors: the NK cell paradigm. *Immunol Rev,* 224**,** 70-84.

MANDELBAUM, J., BHAGAT, G., TANG, H., MO, T., BRAHMACHARY, M., SHEN, Q., CHADBURN, A., RAJEWSKY, K., TARAKHOVSKY, A., PASQUALUCCI, L. & DALLA-FAVERA, R. 2010.

BLIMP1 is a tumor suppressor gene frequently disrupted in activated B cell-like diffuse large B cell lymphoma. *Cancer Cell,* 18**,** 568-79.

MARKS, J. L., GONG, Y., CHITALE, D., GOLAS, B., MCLELLAN, M. D., KASAI, Y., DING, L., MARDIS, E. R., WILSON, R. K., SOLIT, D., LEVINE, R., MICHEL, K., THOMAS, R. K., RUSCH, V. W., LADANYI, M. & PAO, W. 2008. Novel MEK1 mutation identified by mutational analysis of epidermal growth factor receptor signaling pathway genes in lung adenocarcinoma. *Cancer Res,* 68**,** 5524-8.

MARTINS, G. & CALAME, K. 2008. Regulation and functions of Blimp-1 in T and B lymphocytes. *Annu Rev Immunol,* 26**,** 133-69.

MEINHARDT, K., KROEGER, I., ABENDROTH, A., MULLER, S., MACKENSEN, A. & ULLRICH, E. 2012. Influence of NK cell magnetic bead isolation methods on phenotype and function of murine NK cells. *J Immunol Methods,* 378**,** 1-10.

METGUD, R. S., DOSHI, J. J., GAURKHEDE, S., DONGRE, R. & KARLE, R. 2011. Extranodal NK/T-cell lymphoma, nasal type (angiocentric T-cell lymphoma): A review about the terminology. *J Oral Maxillofac Pathol,* 15**,** 96-100.

MORETTA, A., BOTTINO, C., VITALE, M., PENDE, D., CANTONI, C., MINGARI, M. C., BIASSONI, R. & MORETTA, L. 2001. Activating receptors and coreceptors involved in human natural killer cell-mediated cytolysis. *Annu Rev Immunol,* 19**,** 197-223.

NAGATA, H., KONNO, A., KIMURA, N., ZHANG, Y., KIMURA, M., DEMACHI, A., SEKINE, T., YAMAMOTO, K. & SHIMIZU, N. 2001. Characterization of novel natural killer (NK)-cell and gammadelta T-cell lines established from primary lesions of nasal T/NK-cell lymphomas associated with the Epstein-Barr virus. *Blood,* 97**,** 708-13.

NAGY, Z. S., LEBARON, M. J., ROSS, J. A., MITRA, A., RUI, H. & KIRKEN, R. A. 2009. STAT5 regulation of BCL10 parallels constitutive NFkappaB activation in lymphoid tumor cells. *Mol Cancer,* 8**,** 67.

NG, S. B., SELVARAJAN, V., HUANG, G., ZHOU, J., FELDMAN, A. L., LAW, M., KWONG, Y. L., SHIMIZU, N., KAGAMI, Y., AOZASA, K., SALTO-TELLEZ, M. & CHNG, W. J. Activated oncogenic pathways and therapeutic targets in extranodal nasal-type NK/T cell lymphoma revealed by gene expression profiling. *J Pathol,* 223**,** 496-510.

O'SHEA, J. J., GADINA, M. & SCHREIBER, R. D. 2002. Cytokine signaling in 2002: new surprises in the Jak/Stat pathway. *Cell,* 109 Suppl**,** S121-31.

ODEJIDE, O., WEIGERT, O., LANE, A. A., TOSCANO, D., LUNNING, M. A., KOPP, N., KIM, S., VAN BODEGOM, D., BOLLA, S., SCHATZ, J. H., TERUYA-FELDSTEIN, J., HOCHBERG, E., LOUISSAINT, A., DORFMAN, D., STEVENSON, K., RODIG, S. J., PICCALUGA, P. P., JACOBSEN, E., PILERI, S. A., HARRIS, N. L., FERRERO, S., INGHIRAMI, G., HORWITZ, S. M. & WEINSTOCK, D. M. 2014. A targeted mutational landscape of angioimmunoblastic T-cell lymphoma. *Blood,* 123**,** 1293-6.

OHGAMI, R. S., MA, L., MERKER, J. D., MARTINEZ, B., ZEHNDER, J. L. & ARBER, D. A. 2013. STAT3 mutations are frequent in CD30+ T-cell lymphomas and T-cell large granular lymphocytic leukemia. *Leukemia,* 27**,** 2244-7.

OHGAMI, R. S., MA, L., MONABATI, A., ZEHNDER, J. L. & ARBER, D. A. 2014. STAT3 mutations are present in aggressive B-cell lymphomas including a subset of diffuse large B-cell lymphomas with CD30 expression. *Haematologica*.

OZAKI, K., SPOLSKI, R., ETTINGER, R., KIM, H. P., WANG, G., QI, C. F., HWU, P., SHAFFER, D. J., AKILESH, S., ROOPENIAN, D. C., MORSE, H. C., 3RD, LIPSKY, P. E. & LEONARD, W. J. 2004. Regulation of B cell differentiation and plasma cell generation by IL-21, a novel inducer of Blimp-1 and Bcl-6. *J Immunol,* 173**,** 5361-71.

PAIK, P. K., ARCILA, M. E., FARA, M., SIMA, C. S., MILLER, V. A., KRIS, M. G., LADANYI, M. & RIELY, G. J. 2011. Clinical characteristics of patients with lung adenocarcinomas harboring BRAF mutations. *J Clin Oncol,* 29**,** 2046-51.

PARDANANI, A. 2008. JAK2 inhibitor therapy in myeloproliferative disorders: rationale, preclinical studies and ongoing clinical trials. *Leukemia,* 22**,** 23-30.

PASQUALUCCI, L., COMPAGNO, M., HOULDSWORTH, J., MONTI, S., GRUNN, A., NANDULA, S. V., ASTER, J. C., MURTY, V. V., SHIPP, M. A. & DALLA-FAVERA, R. 2006. Inactivation of the PRDM1/BLIMP1 gene in diffuse large B cell lymphoma. *J Exp Med,* 203**,** 311-7.

PERUSSIA, B., CHEN, Y. & LOZA, M. J. 2005. Peripheral NK cell phenotypes: multiple changing of faces of an adapting, developing cell. *Mol Immunol,* 42**,** 385-95.

PETERMANN, F., ROTHHAMMER, V., CLAUSSEN, M. C., HAAS, J. D., BLANCO, L. R., HEINK, S., PRINZ, I., HEMMER, B., KUCHROO, V. K., OUKKA, M. & KORN, T. 2010. gammadelta T cells enhance autoimmunity by restraining regulatory T cell responses via an interleukin-23-dependent mechanism. *Immunity,* 33**,** 351-63.

PIVA, R., AGNELLI, L., PELLEGRINO, E., TODOERTI, K., GROSSO, V., TAMAGNO, I., FORNARI, A., MARTINOGLIO, B., MEDICO, E., ZAMO, A., FACCHETTI, F., PONZONI, M., GEISSINGER, E., ROSENWALD, A., MULLER-HERMELINK, H. K., DE WOLF-PEETERS, C., PICCALUGA, P. P., PILERI, S., NERI, A. & INGHIRAMI, G. 2010. Gene expression profiling uncovers molecular classifiers for the recognition of anaplastic large-cell lymphoma within peripheral T-cell neoplasms. *J Clin Oncol,* 28**,** 1583-90.

QIU, Z. Y. & FAN, Y. 2016. [Large Granular Lymphocytic Leukemia and JAK/STAT Signaling Pathway--Review]. *Zhongguo Shi Yan Xue Ye Xue Za Zhi,* 24**,** 254-60.

RAJALA, H. L., ELDFORS, S., KUUSANMAKI, H., VAN ADRICHEM, A. J., OLSON, T., LAGSTROM, S., ANDERSSON, E. I., JEREZ, A., CLEMENTE, M. J., YAN, Y., ZHANG, D., AWWAD, A., ELLONEN, P., KALLIONIEMI, O., WENNERBERG, K., PORKKA, K., MACIEJEWSKI, J. P., LOUGHRAN, T. P., JR., HECKMAN, C. & MUSTJOKI, S. Discovery of somatic STAT5b mutations in large granular lymphocytic leukemia. *Blood,* 121**,** 4541-50.

RES, P., MARTINEZ-CACERES, E., CRISTINA JALECO, A., STAAL, F., NOTEBOOM, E., WEIJER, K. & SPITS, H. 1996. CD34+CD38dim cells in the human thymus can differentiate into T, natural killer, and dendritic cells but are distinct from pluripotent stem cells. *Blood,* 87**,** 5196-206.

RORING, M., HERR, R., FIALA, G. J., HEILMANN, K., BRAUN, S., EISENHARDT, A. E., HALBACH, S., CAPPER, D., VON DEIMLING, A., SCHAMEL, W. W., SAUNDERS, D. N. & BRUMMER, T. Distinct requirement for an intact dimer interface in wild-type, V600E and kinase-dead B-Raf signalling. *EMBO J,* 31**,** 2629-47.

SALI, A. & BLUNDELL, T. L. 1993. Comparative protein modelling by satisfaction of spatial restraints. *J Mol Biol,* 234**,** 779-815.

SAVITSKY, D. & CALAME, K. 2006. B-1 B lymphocytes require Blimp-1 for immunoglobulin secretion. *J Exp Med,* 203**,** 2305-14.

SCHILBACH, K. E., GEISELHART, A., WESSELS, J. T., NIETHAMMER, D. & HANDGRETINGER, R. 2000. Human gammadelta T lymphocytes exert natural and IL-2-induced cytotoxicity to neuroblastoma cells. *J Immunother,* 23**,** 536-48.

SCHMITZ, R., YOUNG, R. M., CERIBELLI, M., JHAVAR, S., XIAO, W., ZHANG, M., WRIGHT, G., SHAFFER, A. L., HODSON, D. J., BURAS, E., LIU, X., POWELL, J., YANG, Y., XU, W., ZHAO, H., KOHLHAMMER, H., ROSENWALD, A., KLUIN, P., MULLER-HERMELINK, H. K., OTT, G., GASCOYNE, R. D., CONNORS, J. M., RIMSZA, L. M., CAMPO, E., JAFFE, E. S., DELABIE, J., SMELAND, E. B., OGWANG, M. D., REYNOLDS, S. J., FISHER, R. I., BRAZIEL, R. M., TUBBS, R. R., COOK, J. R., WEISENBURGER, D. D., CHAN, W. C., PITTALUGA, S., WILSON, W.,

WALDMANN, T. A., ROWE, M., MBULAITEYE, S. M., RICKINSON, A. B. & STAUDT, L. M. 2012. Burkitt lymphoma pathogenesis and therapeutic targets from structural and functional genomics. *Nature,* 490**,** 116-20.

SHEN, B., ZHANG, W., ZHANG, J., ZHOU, J., WANG, J., CHEN, L., WANG, L., HODGKINS, A., IYER, V., HUANG, X. & SKARNES, W. C. 2014. Efficient genome modification by CRISPR-Cas9 nickase with minimal off-target effects. *Nat Methods,* 11**,** 399-402.

SHUKLA, N., AMEUR, N., YILMAZ, I., NAFA, K., LAU, C. Y., MARCHETTI, A., BORSU, L., BARR, F. G. & LADANYI, M. Oncogene mutation profiling of pediatric solid tumors reveals significant subsets of embryonal rhabdomyosarcoma and neuroblastoma with mutated genes in growth signaling pathways. *Clin Cancer Res,* 18**,** 748-57.

SILVA, M., BENITO, A., SANZ, C., PROSPER, F., EKHTERAE, D., NUNEZ, G. & FERNANDEZ-LUNA, J. L. 1999. Erythropoietin can induce the expression of bcl-x(L) through Stat5 in erythropoietin-dependent progenitor cell lines. *J Biol Chem,* 274**,** 22165-9.

SOMANCHI, S. S., SENYUKOV, V. V., DENMAN, C. J. & LEE, D. A. 2011. Expansion, purification, and functional assessment of human peripheral blood NK cells. *J Vis Exp*.

SONBOL, M. B., FIRWANA, B., ZARZOUR, A., MORAD, M., RANA, V. & TIU, R. V. 2013. Comprehensive review of JAK inhibitors in myeloproliferative neoplasms. *Ther Adv Hematol,* 4**,** 15-35.

SUN, J. C., MA, A. & LANIER, L. L. 2009. Cutting edge: IL-15-independent NK cell response to mouse cytomegalovirus infection. *J Immunol,* 183**,** 2911-4.

SUN, L., ZHAO, Y., SHI, H., MA, C. & WEI, L. 2015. LMP1 promotes nasal NK/T-cell lymphoma cell function by eIF4E via NF-kappaB pathway. *Oncol Rep,* 34**,** 3264-71.

THOMSEN, R. & CHRISTENSEN, M. H. 2006. MolDock: a new technique for high-accuracy molecular docking. *J Med Chem,* 49**,** 3315-21.

VANHERBERGHEN, B., OLOFSSON, P. E., FORSLUND, E., STERNBERG-SIMON, M., KHORSHIDI, M. A., PACOURET, S., GULDEVALL, K., ENQVIST, M., MALMBERG, K. J., MEHR, R. & ONFELT, B. 2013. Classification of human natural killer cells based on migration behavior and cytotoxic response. *Blood,* 121**,** 1326-34.

VANTOUROUT, P. & HAYDAY, A. 2013. Six-of-the-best: unique contributions of gammadelta T cells to immunology. *Nat Rev Immunol,* 13**,** 88-100.

WALZER, T., BLERY, M., CHAIX, J., FUSERI, N., CHASSON, L., ROBBINS, S. H., JAEGER, S., ANDRE, P., GAUTHIER, L., DANIEL, L., CHEMIN, K., MOREL, Y., DALOD, M., IMBERT, J., PIERRES, M., MORETTA, A., ROMAGNE, F. & VIVIER, E. 2007. Identification, activation, and selective in vivo ablation of mouse NK cells via NKp46. *Proc Natl Acad Sci U S A,* 104**,** 3384-9.

WAN, P. T., GARNETT, M. J., ROE, S. M., LEE, S., NICULESCU-DUVAZ, D., GOOD, V. M., JONES, C. M., MARSHALL, C. J., SPRINGER, C. J., BARFORD, D. & MARAIS, R. 2004. Mechanism of activation of the RAF-ERK signaling pathway by oncogenic mutations of B-RAF. *Cell,* 116**,** 855-67.

WANG, K., LI, M. & HAKONARSON, H. 2010. ANNOVAR: functional annotation of genetic variants from high-throughput sequencing data. *Nucleic Acids Res,* 38**,** e164.

WU, Y. L., DING, Y. P., TANAKA, Y., SHEN, L. W., WEI, C. H., MINATO, N. & ZHANG, W. 2014. gammadelta T cells and their potential for immunotherapy. *Int J Biol Sci,* 10**,** 119-35.

XU, Z. G., IWATSUKI, K., OYAMA, N., OHTSUKA, M., SATOH, M., KIKUCHI, S., AKIBA, H. & KANEKO, F. 2001. The latency pattern of Epstein-Barr virus infection and viral IL-10 expression in cutaneous natural killer/T-cell lymphomas. *Br J Cancer,* 84**,** 920-5.

YOKOYAMA, W. M. & PLOUGASTEL, B. F. 2003. Immune functions encoded by the natural killer gene complex. *Nat Rev Immunol,* 3**,** 304-16.

YOSHIKAWA, H., MATSUBARA, K., QIAN, G. S., JACKSON, P., GROOPMAN, J. D., MANNING, J. E., HARRIS, C. C. & HERMAN, J. G. 2001. SOCS-1, a negative regulator of the JAK/STAT pathway, is silenced by methylation in human hepatocellular carcinoma and shows growth-suppression activity. *Nat Genet,* 28**,** 29-35.

YOUNG, L., ALFIERI, C., HENNESSY, K., EVANS, H., O'HARA, C., ANDERSON, K. C., RITZ, J., SHAPIRO, R. S., RICKINSON, A., KIEFF, E. & ET AL. 1989. Expression of Epstein-Barr virus transformation-associated genes in tissues of patients with EBV lymphoproliferative disease. *N Engl J Med,* 321**,** 1080-5.

YU, H., PARDOLL, D. & JOVE, R. 2009. STATs in cancer inflammation and immunity: a leading role for STAT3. *Nat Rev Cancer,* 9**,** 798-809.

YU, J., FREUD, A. G. & CALIGIURI, M. A. 2013. Location and cellular stages of natural killer cell development. *Trends Immunol,* 34**,** 573-82.

YU, J., MITSUI, T., WEI, M., MAO, H., BUTCHAR, J. P., SHAH, M. V., ZHANG, J., MISHRA, A., ALVAREZ-BRECKENRIDGE, C., LIU, X., LIU, S., YOKOHAMA, A., TROTTA, R., MARCUCCI, G., JR., BENSON, D. M., LOUGHRAN, T. P., JR., TRIDANDAPANI, S. & CALIGIURI, M. A. 2011. NKp46 identifies an NKT cell subset susceptible to leukemic transformation in mouse and human. *J Clin Invest,* 121**,** 1456-70.

ZHANG, T., MA, J., NIE, K., YAN, J., LIU, Y., BACCHI, C. E., QUEIROGA, E. M., GUALCO, G., SAMPLE, J. T., ORAZI, A., KNOWLES, D. M. & TAM, W. 2014. Hypermethylation of the tumor suppressor gene PRDM1/Blimp-1 supports a pathogenetic role in EBV-positive Burkitt lymphoma. *Blood Cancer J,* 4**,** e261.